Shaking loose mushy magma: the effect of seismic waves on magma mush bodies and the potential for triggering an eruption

SMART, ELEANOR,PAIGE

Shaking loose mushy magma: the effect of seismic waves on magma mush bodies and the potential for triggering an eruption

Eleanor Paige Smart

Masters by Research (Volcanology)

Supervisors: Dr Fabian Wadsworth & Professor Ed Llewellin

Department of Earth Sciences

University of Durham

December 2020

Shaking loose mushy magma: the effect of seismic waves on magma mush bodies and the potential for triggering an eruption

Eleanor Paige Smart

Abstract.

A central goal within volcanology is understanding how eruptions are triggered. Statistical analyses of earthquake and eruption data indicates that volcanoes show heightened activity after major earthquakes within ~750 km of the source, caused by transient (dynamic) and permanent (static) stress, particularly on gases within the reservoir, such as the accumulation of bubbles, and crustal extension and relaxation. Refinement of the volcanic plumbing structure via geophysical imaging reveals reservoirs are largely comprised of crystal mush, however the effect of earthquakes on crystal movement within this mush is unknown. This thesis explores whether seismic shaking encourages compaction and melt expulsion within mush, and whether energy produced by seismic waves is sufficient to form melt 'caps' at the top of mush columns, like in crystal-poor rhyolitic melts. Building on previous studies using saturated particle "packs" as synthesised mush, particle movement under oscillation is analysed using Stokes' Law, combined with the acceleration of waves via $\Gamma = A/g$, where Γ is the effective wave acceleration, A is the shaking parameters (amplitude and frequency) and $g = 9.81\, m/s^2$. Within a few hundred kilometres, accelerations (PGA) produced by seismic waves are sufficient to encourage compaction (i.e. $\Gamma > 1$), as applied to six case studies from locations such as Chile and Indonesia. However, not all volcanic bodies within these case studies fall within this effective distance, as waves decay over distance via an inverse square law. Γ at the volcanoes is < 1, but above $\Gamma = 0.2$, meaning minor compaction and expulsion from the mush may occur, but is not of significant volume. Hence, shaking alone may not be responsible for triggering volcanic activity, and melt segregation and dynamic stress work with other triggering mechanisms. Reservoirs must already be at a critical state of instability (within 99% of the maximum overpressure) if any process, including seismic forcing, is to affect the activity.

Table of Contents.

List of Figures.

Statement of Copyright.

Acknowledgements.

I would like to thank Dr Fabian Wadsworth and Professor Ed Llewellin, the primary and secondary supervisors for this project, for their endless support and guidance during the course of this past year. I would also like to thank the members of the Earth Sciences department at Durham University, for their advice, reassurance and all of the incredible work they have put in to keeping the department running and the students safe during a very difficult year.

COVID-19 Statement.

The methodology presented in this thesis is founded on re-analysis of data presented elsewhere (de Richter et al., 2015). The original methodological design for this thesis was to create primary data using new experiments in the laboratory. However, due to COVID-19 and laboratory closures in March, this was not possible.

Chapter 1. Introduction

The connection between earthquakes and volcanic eruptions, and whether one event causes the other, is not new (Eggert and Walter, 2009). However, despite repeated statistical and regional analyses, the question as to whether earthquakes can trigger volcanic activity or not remains unclear (Hill et al., 2002; Manga and Brodsky, 2006). This thesis aims to explore the effects of seismic waves on crystalline magma. In particular, this thesis will explore how a mush of packed crystals in a magmatic liquid (a 'crystal mush' or 'magma mush') is affected by a passing seismic wave. Crystal mush is a major feature of the volcanic reservoir and influences chemical and thermal evolution (Liao et al., 2018). Mush dynamics are thought to be key to controlling large eruptions (Cashman et al., 2017), as mush can store large volumes of melt and fluids within. Here, I will determine whether crystal mush compacts under dynamic stress, expelling melt from the interstitial space between crystals as they reorganise into a more efficiently packed structure, which can then erupt.

In this chapter, the introductory concepts are introduced: (1) the role that crystal mush plays in a magma chamber and why it is important, (2) previous work on seismically triggered volcanism and the stresses involved, (3) the mechanisms by which eruption results from mush compaction, and (4) the importance of chamber conditions at the time of seismic shaking. The lack of mush-centred study in previous work is also discussed. Finally, the path of action is outlined and the case studies to be involved in this study are introduced.

1.1 Redefining the magma chamber

The conceptual underpinnings of the 'magma chamber' (or 'magma storage regions') is the subject of debate (Cashman et al., 2017). While geochemical and geophysical evidence unequivocally confirms that there are regions of molten or partially molten rock collected in the Earth's crust at various levels (Lees, 2007; Lees and Crosson, 1989), the details of the microstructure, state, and organisation of the contents of these magma storage regions is contested hotly. Seismic tomography has been particularly successful in imaging the coarse size and shape of magma bodies accumulated in the upper crust at Mount St Helens (Lees and Crosson, 1989), Mount Rainier (Moran et al., 1999), Mount Pinatubo (Mori et al., 1996), and Long Valley caldera (Sanders et al., 1995), amongst other volcanoes. Despite these successes, ultimately, the resolution and detail that these observations can provide is low and provides little evidence for the physics of internal chamber processes.

The earliest conceptions of magma chambers were simplistic, and conceived of the entire oblate volume being filled with melt (visible in Figure 1 of Sparks et al. (2019)). At many volcanoes worldwide, the geochemistry of suites of erupted rock could be explained by suggesting that crystals had grown sequentially, but been left behind – settling out of suspension from the melt-rich magma chamber to be accumulated at the base (Jaupart and Tait, 1995; Klein and Philpotts, 2017; Marsh, 2015). More recently, this simplistic view of a melt pocket raining out crystals as they grow has been over-turned by what is generally referred to as the 'mush model' (Marsh, 2015; Sparks et al., 2019; Cashman et al., 2017). This thesis is founded on the mush model's framework for magma storage, and so here it is worth exploring that underpinning framework.

Geochemical insights are at the core of the mush model. For example, petrology and geochemistry of erupted products has led to the conclusion that magma storage at silicic volcanoes appears to be at relatively low temperatures and high average crystal content. For example at Soufriere Hills volcano a chamber has been identified at 5-7 km depth, with a temperature of ~850°C and a high crystal content of 60-65% (Paulatto et al., 2012). This body is clearly not a pond of pure melt, as in the old magma chamber model outlined above. However, erupted products can be crystal-poor despite silicic chambers apparently being crystal-rich. For crystal-poor (i.e. melt-dominated) magmas to erupt, removal of the crystals within the body of mushy magma must first occur via segregation, to be discussed further in this chapter. While the magma chamber model has moved away from melt-dominated bodies, it has in fact come full circle, with the refinement of how melt-dominant lenses form within partially molten, mushy columns, thereby showing how the old model has since evolved into a newer paradigm.

Observations are drawn from geochemical analyses and petrological studies to determine the composition and previous processes occurring within reservoirs (Cooper, 2017), which has led to the development of a newer chamber model largely comprised of crystal mush that is vertically expansive through the lithosphere. This new model, termed the trans-crustal magmatic system (TCMS) and summarised by Cashman et al. (2017), has become a basis for new chamber models being tested today. Crystal mush is a key feature, occupying around 40-50% of the reservoir (Sparks et al., 2019; Cooper, 2017; Bachmann and Bergantz, 2008), even at shallow depths, like at the Soufriere Hills volcano example described. This reservoir through which volcanic material ascends is permanently in a state of flux, with storage and differentiation occurring on all levels (Cashman et al., 2017). Melt is supplied at the base of the reservoir where it rises due to buoyant effect, before cooling and crystallising into mush. This mush will compact over time, with melt pushed upwards and continuing to rise, further encouraged by injections of molten material below, which supplies heat. This process happens continuously, evolving over time, until the highly evolved magma is closer to the surface, with the shallowest pre-eruptive chambers believed to be largely ephemeral, as illustrated in Figure 2.1 of this work. Crystal mush itself is largely uneruptible due to its high viscosity, on account of the high percentage of crystals compared to melt fraction contained within. With an approximate crystallinity of 50-60%, evolution of melt does not occur largely due to convection, but due to the segregation and continuous forcing of molten material upwards as described. This is true for silicic rocks such as rhyolite (e.g. Bachmann and Bergantz (2009)), with ignimbrite super-eruptions attributed to this method of magma migration and evolution (Cooper, 2017). Further discussion can be found in Section 1.5 and Chapter 2.

The TCMS paradigm and the compaction process as a mechanism for melt segregation also opens new questions about the timescale over which these mushy, expansive reservoirs persist, with compaction-driven melt migration gradually building towards a period at which the reservoir is “primed” for eruption (illustrated numerically by Khazan (2010)). Rhyolitic volcanic centres have been known to erupt massive volumes of material numerous times in relatively recent geological history (e.g. Laguna del Maule, Chile). To produce these volumes, often on the order of several hundred cubic kilometers, evolved magma must be accumulated and stored for a period of time in large systems, typically in molten lenses or ‘caps’ at the top of the chamber

system, which are crystal-poor (see Section 2.3). This storage period is thought to be between 10 and 10,000 years, depending on the size of the chamber, and is sustained from heat and injection of melt from below (Jellinek and DePaolo, 2003). Hence, large bodies of mush can persist for a long time, allowing segregation to a greater degree, so that evolved silicic melt rises and accumulates, and leaves the residual mush lower in the reservoir (Cashman et al., 2017). This further builds the reservoir upwards, where the same process can occur again, or contributes to the formation of evolved melt that can subsequently erupt.

Hence, both the new and old magma chamber models are not divorced from each other. Cashman and Giordano (2014) note that when determining the formation of the magma reservoir structure, the shallow chamber may be considered to function like the pond-like chamber featured in the previous model. This is evidenced by erupted products such as pumice clasts and melt inclusions within crystals, which show indication of forming from both a single chamber (previous model) and a multi-layered, highly evolved system (TCMS) through their compositions, such as whether the chamber from which they were sourced was homogenous or not (Cashman and Giordano, 2014; Gualda and Ghiorso, 2013). The next step is to determine how the segregation that forms these highly evolved melts, which go on to be erupted, occurs. Despite several mechanisms being put forward, such as settling of crystals out of melt and subsequent compaction (see Section 1.5.1), the timescale over which these mechanisms work is not known, and the compaction of mush is inefficient and unable to produce large quantities of melt on short timescales for eruption (Bachmann and Huber, 2019; Holness, 2018). The mechanisms also suffer from a lack of assessment. Hence, this thesis will explore how these inefficient mechanisms may be encouraged to work over shorter timescales via seismic forcing due to large magnitude earthquakes, a study on which has not yet been considered.

1.2 Previous work on volcanism associated with earthquakes

Volcanoes produce a wide spectrum of seismicity, particularly during magma migration, intrusion, and ascent, as well as gas pressure changes (Bullen and Bolt, 1985a; Gudmundsson, 2020). This spectrum includes various volcanic earthquake types, including 1) HF (high frequency, 5-15 Hz – also known as A-type) and LF (low frequency, 1-5 Hz – also known as B-type) events, which occur due to fault slip/shear and bubble or fluid pressure changes, respectively; 2) hybrid events, which are a combination of HF and LF; 3) volcanic tremors, which are continuous signals at the volcano that have long durations; and 4) VLPEs (very long period events), which have very low frequencies and are associated with large faults (McNutt and Roman, 2015). However, in this project the focus is on large-magnitude, tectonic earthquakes close to volcanoes.

The connection between large earthquakes and volcanic activity is not a new concept, but interest has increased following a landmark study by Linde and Sacks (1998), who proposed a correlation between large earthquakes and volcanic eruptions spanning several hundred kilometres by using a statistical analysis of global data. It was found that there were increased eruption events within ~750 km of an earthquake source, with a large proportion of eruptions occurring on the same day as the associated earthquake. Since then, there have been attempts to verify this analysis and test the correlation, with varying results. Examples include Manga and

Brodsky (2006) and Lemarchand and Grasso (2007). These authors agree that the paired earthquakes and successive volcanic eruptions occur within this 750 km distance and find that a stronger correlation can be drawn between events within 250 km. However, Lemarchand and Grasso (2007) indicates that the processes thought to occur as a result of a volcano being shaken (such as the dynamic micro-physical processes laid out in Sections 1.3 and 2.5) have poorly understood timescales over which they act. The time between the earthquake event and the eruption appears too short for the volcano to react, and they also note that some cases actually showed increased volcanic unrest before the earthquake events, meaning that there are many more processes at play and that the shaking alone was not the only trigger.

It is reiterated throughout the literature that there are a large number of variables at play when considering potentially-triggered volcanism, including the stress involved (i.e. static or dynamic), crustal deformation induced by tectonic earthquakes such as extension and compression, volcanic setting, volatile content and pressure in the reservoir at the time of shaking, earthquake magnitude, and distance between the earthquake source and the volcanic centre (Eggert and Walter, 2009; Hill et al., 2002; Bebbington and Marzocchi, 2011; Gomberg et al., 1997; Barrientos, 1994; Lemarchand and Grasso, 2007; Linde and Sacks, 1998). The relationship between an earthquake and the subsequent apparent triggering of an eruption is therefore a case-by-case basis, complicating the use of a statistical analysis across a global dataset. These variables include regional factors such as the geology of the area, which will alter the effects and attenuation of seismic waves, the energy released by the earthquake, as larger earthquakes will in turn produce more radiating energy that may come into contact with a volcanic body, and the conditions within the volcanic reservoir system at the time of the earthquake (Walter and Amelung, 2007). Because of this, comparing seismic records with coinciding eruptions produces little or a very weak correlation. Watt et al. (2009) notes that examining data globally may be counterintuitive, due to the sheer size of the records but also how local relationships may be lost, particularly in arc environments. Their approach was to study a single seismically active volcanic region, which allowed closer inspection of records from the Andean southern volcanic zone. Relationships could then be drawn from major earthquakes in this volcanic region, eliminating ‘noise’ from other global events, and creating a clearer picture of the correlation in that region. Those relationships may then be extrapolated to other settings, once the mechanics of how earthquakes affect volcanoes, and partially molten chamber systems, are better understood.

Clearly, there is some evidence that indeed there may be a correlation between large magnitude seismic events and volcanic eruptions, on a statistical basis. But the question remains as to what processes the seismicity may be activating that could in turn cause the eruption. In what follows, I will briefly introduce the dominant mechanisms by which studies have suggested a volcanic eruption could be triggered by a seismic event.

1.3 Mechanisms of triggered volcanism as a result of seismicity

Many processes have been proposed and modelled that are attributed to eruptive activity. The complexity of a volcano plumbing system, composed of the shallow sill-like chambers and melt channels such as dikes, the

deeper reservoir and the influx of material from the regional tectonic setting, e.g. the melting that occurs above a subducting plate in the continental crust, means that many of these processes may occur together. This complicates the exact mechanism by which a volcano erupts, and it is unlikely that only one single process is the cause. In this study, melt segregation as a mechanism will be proposed, but the common mechanisms already known must first be understood, so that a strong comparison can be made later. Further discussion of some of these mechanisms, in relation to seismic waves, can be found in Section 2.5.

Most mechanisms that work at the bubble- or crystal-scale are associated with increasing the pressure of the chamber to a critical level, where overpressure becomes great enough to rupture the chamber and cause an eruption. The proposed mechanisms which contribute towards overpressure, and used in this thesis for comparison to melt extraction with seismic influence, are:

1.3.1 Rectified diffusion:

Bubbles in a chamber expand and compress according to the pressure around them. This allows for volatile transfer in and out of the bubble – as the bubble expands volatiles diffuse in, and as it contracts volatiles are expelled into the surrounding melt. This process has many variables, including saturation, compressibility, and the initial overpressure of the chamber prior to the process. In it noted that the pressure fluctuations induced are quite small, and may only be significant enough to cause rupture if the chamber is already highly unstable (Brodsky et al., 1998; Ichihara and Brodsky, 2006; Manga and Brodsky, 2006).

1.3.2 Advective overpressure:

Bubbles are shaken free of their nucleating surfaces on crystals and within melt channels and will rise. If the bubble does not “leak” its’ internal pressure into the surrounding magma, it may carry that internal pressure to the top of the chamber, thereby increasing the overpressure. This may be particularly powerful if the bubble has risen from a point deep in the chamber, however there are issues with the speed at which the bubbles rise, and that other processes, such as rectified diffusion, may occur on the bubble as it does so, reducing the pressure that can be transported as the bubble equilibrates with the surroundings (Sahagian and Proussevitch, 1992; Pyle and Pyle, 1995; Manga and Brodsky, 2006).

1.3.3 Bubble nucleation:

Supersaturated magma will allow for the formation of gas bubbles if the supersaturation pressure is high enough to overcome the surface tension barrier. Passing seismic waves produce fluctuations in pressure, which may then allow increased nucleation. The supersaturation pressure required to create new bubbles can be lowered by the crystallisation of certain crystals (e.g. Fe-Ti oxides), increasing the water content, or decompressing the system. In high-viscosity magma, this process is slow and new bubbles are sensitive to pressure change, which means they may be absorbed back into the melt. However, once formed they can grow very quickly, due to the saturation and short diffusion lengths for volatiles into the bubble (Manga and Brodsky, 2006; Ripepe and Gordeev, 1999; Ittai et al., 2011).

1.4 The importance of the initial state of the chamber

When applying these mechanisms to a real-world chamber, the initial chamber conditions must first be considered. There is a general agreement in the literature that a chamber being influenced by seismic waves should already be in an agitated state, such as at a critical pressure, with a certain volatile balance and composition, as well as at a prone depth within the upper crustal reservoir (Walter and Amelung, 2007; Watt et al., 2009). Factors such as composition, storage depth and storage dimensions (Pyle and Pyle, 1995) can dictate what internal processes occur within a magma chamber, without seismic influence.

This critical overpressure is illustrated by Manga and Brodsky (2006), who calculate the excess pressure required for chamber failure via static and dynamic stresses, and find that the chamber in question must be at '99%-99.9% of the maximum overpressure' for these stresses to initiate activity. This results in a very small fraction of events where activity may be induced by seismic shaking. Watt et al. (2009) provides another illustration, where surpassing this critical overpressure leads to a chain of events: the already-unstable chamber is shaken via dynamic stress, and nucleation and ascension of volatiles occurs, followed by depressurization. Unstable mush material at the roof of the chamber may be excited and dislodged by the passing waves, leading to a subsequent rising plume of molten material as the mush sinks, further encouraging bubble growth (Manga and Brodsky, 2006; Walter and Amelung, 2007). Shaking itself does not directly cause the eruption of the chamber contents, but it initiates or encourages other processes, which work alongside each other (Hill et al., 2002).

This can be applied to a study of the Palermo earthquake in September 2002, where Walter et al. (2009) uses synthetic seismograms to model the event and finds pressure fluctuation on the order of ~20 kPa. This is a small value, as magmatic overpressure expected for rupturing events such as dike propagation and wall rupture are on the order of MPa. Hence, they conclude that the shaking itself may not be strong enough to cause outright eruptive activity but would influence other processes already occurring within the chamber, leading to activity later on. Furthermore, this provides an explanation for significant delays observed between shaking and eruptive events, which is often of days up to years, making it difficult to pair up the two events as one being the product of the other (Walter and Amelung, 2007).

1.5 Mechanisms of volcanic triggering without seismicity

In this thesis, two families of ignimbrites are mentioned: crystal-poor and crystal-rich (monotonous intermediates). As the focus is placed on large mush-dominated systems, it can be assumed that the composition of the mush and magmas involved are towards the silicic end of the compositional spectrum. In addition to this, mush zones are attributed to the formation of rhyolitic melt zones within them. While crystal-rich ignimbrites are explored due to their formation via mush breakage and remobilisation with the addition of heat and volatiles, such as via injection of new molten material at the base of the chamber, (Streck, 2014; Huber et al., 2012; Bachmann and Bergantz, 2008), the focus is placed on crystal-poor ignimbrites. This is

because their formation directly involves the melt segregation processes outlined previously: settling according to Stokes' Law, and compaction.

Removing seismic forcing from the equation, melt segregation occurs within mush bodies once the body has become rheologically locked, where it can no longer convect and settling processes take over (Bachmann and Bergantz, 2004; 2009). As crystals settle to form and add to mush zones, gravity causes these crystals to compact into a tighter formation, which expels interstitial melt towards the top of the chamber. This melt forms a rhyolitic 'cap', from which crystal-poor ignimbrites are sourced (Daines and Pec, 2015).

Shaking, according to Stokes' Law as explored in this thesis, should allow for particle (i.e. crystal) remobilisation and subsequent settling, reducing further the pore space within the lattice and expelling more melt (Section 2.2). There are several variables that should be considered: composition of the mush, including geochemical composition (e.g. silicic); viscosity and crystal size; crystallinity (%) of the mush as well as melt fraction stored within; strength of shaking and the types of waves and stresses involved (i.e. dynamic or static); and, when considering real-world case studies, the proximity between the source of the shaking (e.g. the earthquake rupture zone) and the mush body and volcano, as well as how this proximity relates to the fluctuation and decay of the seismic waves involved. These factors will be explored and analysed critically within this thesis, to understand whether seismic forcing encourages melt segregation processes, and how it links to increased eruption potential.

1.5.1 Melt segregation and micro-settling:

Micro-settling and melt segregation are two processes on a continuum. Micro-settling involves individual crystals settling to the base of melt pockets, displacing the melt out and upwards. This allows for particle reorganisation within a mushy pack on a very small scale without deforming the crystals or crystal-pack involved (Bachmann and Bergantz, 2004; Bachmann and Huber, 2019; Holness, 2018). Melt segregation is usually used to refer to the more wholesale compaction and melt expulsion, usually driven by deformation of the crystals.

Micro-settling: Crystals in a melt body will settle according to Stokes' Law, and form aggregates at the base of the body. While this process is often used in the context of single crystals in an infinite body of melt and the settling velocity of those crystals, the process is also attributed to several crystals clumping together and settling out under gravity as a unit. This process produces a loosely-packed mush at the base of the body, but other processes such as compaction are required to reduce the interstitial melt space and expel melt. Typically occurring in bodies of high melt content, convection disturbs the process until around 45% crystallinity, where rheological lock-up of the formed mush begins. Alone this process is not significant in melt segregation; it runs in tandem with processes like compaction (Holness, 2018; Bachmann and Huber, 2016; Bachmann and Huber, 2019).

Compaction due to gravity: This process is central to this project. Once a mush has been formed with a crystallinity of >45%, crystals will compact under gravity without deformation, pushing interstitial melt out. Alongside crystal reorganisation, the compaction process is optimal for melt expulsion and segregation

(Bachmann and Huber, 2019; Bachmann and Bergantz, 2004; Holness, 2018). In this project, we investigate how seismic waves can act in the role of crystal reorganisation, with the compaction of mush increased and melt expelled from the mush pack.

1.5.2 Regional tectonic changes in the crust around the chamber:

Another process by which melt can be segregated is via external forcing, e.g. tectonics. This mechanism is one of the most widely-studied (Eggert and Walter, 2009) and features two permanent deformation processes:

Extension: This is often attributed to subduction zones, where the volcanic arc of the continental crust is pulled towards the subduction zone, as the subducting plate moves in the opposite direction underneath, thereby extending the continental crust. Walter and Amelung (2007) present this in Figure 2 and 3 of their paper, with volumetric expansion recorded at several volcanoes after high magnitude earthquakes. This extension causes the reservoir to decompress, forming dikes and allowing injection from below, contributing to chamber overpressure (LaFemina, 2015).

Compression: This occurs when crust is compressed via faults and tectonic forces, causing a "toothpaste" effect where magma is physically squeezed out of the chamber. However, this mechanism is debated due to the volumes of magma involved (Eggert and Walter, 2009).

1.6 Have crystal mush shaking processes been overlooked?

Previous studies on the contents of the magma chamber, predominantly of liquid rheology, tend to focus on internal processes and dynamics of the chamber setting, rather than their connection to larger-scale, crustal processes. Furthermore, it is remarked that the role of mush in chamber evolution has not been subjected to systematic study. There are a myriad of ideas, but there is little way to properly test many of them (Liao et al., 2018). Indeed, Cashman et al. (2017) summarises that while the concept of a trans-crustal system and its processes are 'easy to conceptualise', they are hard to model in a numerical sense.

Previous studies on chamber-wide processes, such as overturning or remobilisation, leading to eruption, have mainly assumed that chambers are liquid in rheology. Particularly in instances of seismically-induced eruptions, most explanations involve 'interactions with crustal fluid movement, disruption or bubble growth through a variety of possible mechanisms' in the build-up towards magmatic overpressure (Watt et al., 2009), modelled with experiments that only use liquid synthetic magmas. The timescales over which these interactions work is still poorly understood (Watt et al., 2009; Ichihara and Brodsky, 2006). Many experimental studies consider injection of new magma at the base of the chamber to be a vital part of chamber disruption, particularly when remobilising mush, but focus on mafic compositions of both injected material and chamber, or injecting mafic material into relatively low density, sometimes rhyolitic, fluid. Where mush has been introduced, like in the experimental study of Girard and Stix (2009), it has been under the influence of this magma injection, resulting in 1) the lower-density injection rising through a mush "pack" to mingle with the overlying chamber contents, often displaying entrainment of mush particles in the flow and potentially leading to overpressure via the

resulting processes, or 2) sinking of an injected fluid that is too dense to rise, to produce a zone of accrued melt at the base of the chamber. However, it was noted that the internal processes of fluid movement through the mush could not be seen.

However, as the interest surrounding crystal mush has increased, more studies have been carried out on the internal relationships particles within a "pack" have under agitation. Davis et al. (2007) indicates that particle pressure and fluid pressure play a vital role when crystals in fluid are oscillated, specifically that a drop in fluid pressure could encourage the formation of gas bubbles, derived in the zone at the base of the chamber where oscillatory effect will be the highest. Authors agree that disturbance of mush and the production of gas bubbles go hand-in-hand, an idea revisited consistently when discussing the overpressure of the chamber system. Overpressure is thought to be a main factor in triggered eruptions, where seismic waves are included or not, but as noted, there are few studies that focus on mush and micro-scale interactions. While this initially may pose an issue when understanding the theoretical interactions, it provides a clear playing field to develop new or updated concepts surrounding particle interaction in mushes, and how seismic forcing influences those interactions, when studying the role of mush in seismically-triggered volcanic activity.

1.7 Target Case Studies for this thesis

There are five case studies that have been utilised in this project and are subjected to analysis within Chapter 5. They were chosen based on level of knowledge within the volcanology field, including the proposed mechanisms of triggering and the type of activity produced, the magnitude of the earthquakes involved, and the distance from earthquake rupture to the volcano in question. They are: the 2006 M_w 6.4 Java earthquake in relation to Mt. Merapi which erupted 72 hours after (Kawazoe and Koketsu, 2010; Tsuji et al., 2009; Walter et al., 2007; Harris and Ripepe, 2007; Elnashai et al., 2007; USGS, 2020a); the 1990 M_w 7.7 Luzon earthquake and the apparently delayed eruption of Mt. Pinatubo in 1991 (Yoshida and Abe, 1992; Velasco et al., 1996; Bautista et al., 1996; USGS, 2020c); the 2004 M_w 9.3 Sumatra-Andaman earthquake, alongside a M_w 8.7 aftershock in 2005 along the Sunda megathrust, in relation to the distant volcanoes of Barren Island and Mt. Talang (Walter and Amelung, 2007; Park et al., 2005; Ishii et al., 2007; Banerjee et al., 2005; Ammon et al., 2005; Lay et al., 2005; Sørensen et al., 2007; Briggs et al., 2006; Konca et al., 2007; Mishra et al., 2007; Sheth, 2014; Laluraj et al., 2006; Bebbington and Marzocchi, 2011; Fiantis et al., 2010; Cassidy, 2015; Kamesh Raju et al., 2012; USGS, 2020d; f); the 1992 M_w 7.3 Landers earthquake and triggered seismicity at Long Valley Caldera on the same day (Johnston, 1995; Hill et al., 1995; Hauksson et al., 1993; Sieh et al., 1993; Velasco et al., 1994; Wald and Heaton, 1994; Linde et al., 1994; USGS, 2020b); and the 1960 M_w 9.5 Great Chile earthquake with the 2010 M_w 8.8 Maule earthquake, and its effect on Cordon Caulle volcano after both events, as well as a comparison to neighbouring volcanoes Villarrica and Llaima (Elnashai et al., 2010; Lara et al., 2004; Barrientos and Ward, 1990; Plafker and Savage, 1970; Hicks et al., 2014; Vigny et al., 2011; Saragoni et al., 2010; Pritchard et al., 2013; Mora-Stock et al., 2014; USGS, 2020g; e).

Large magnitudes are the focus of this project, so that significant seismic energy, such as ground accelerations, can be used. The distance between the two or more localities for each case study also varies, from around 50 km (such as for the Java event) and over 1000 km (such as for the Sumatra-Andaman event). This is because seismic waves decay and attenuate as they propagate through the crust (Lay and Wallace, 1995a), which may reduce the dynamic stress acting on distant volcanoes. This is introduced and then explored in detail in Chapter 2 and 5.

1.8 Aims of this project

The goal of this study is to understand how crystal mush reacts to seismic waves and whether they will encourage melt segregation. The effectiveness of seismically induced particle mobilisation will be compared to other triggering mechanisms laid out in this chapter, to determine whether it is a realistic mechanism when applied to highly complex, real-world magma reservoirs.

This thesis will explore how chambers are constructed and the processes that occur within them, both with and without seismic forcing. Previous literature on particle settling and reorganisation will be evaluated, and a hypothesis constructed where seismic waves with a certain level of energy will cause crystals within a packet of mush to mobilise and resettle into a more efficiently packed structure, so that melt from between the crystals can be expelled. An experimental setup and resulting data will be sourced from the literature to calculate the significant threshold of this seismic energy.

Then, using the case studies outlined in this chapter, this energy as calculated from the acceleration of seismic ground motion of each earthquake will be critically analysed. Using these calculations, the distance at which shaking is significant will be plotted, as waves and the associated energy (e.g. acceleration) decay with distance. If the volcanoes featured within the case studies lie within this distance boundary, it can be implied that seismic waves may cause particle movement within these volcanic reservoirs, leading to increased melt expulsion and an influence on other chamber processes, as well as increased chances of an eruption.

Chapter 2. Solid crystals in magmatic liquids

While Chapter 1 gave a broad overview of the topics that are pertinent to this thesis, here a deeper dive into the life-cycle of crystals in magmatic systems is presented. The potential for links between crystal-scale processes and seismic waves is explored in the context of previous work, which is used to set up the methodology that follows.

Magmas contain a liquid, solid and gas phase in variable proportions. These proportions evolve from the region in the mantle where melt (liquid) is first generated, through buoyant percolative rise into the crust, accumulation in crustal magma reservoirs where crystals grow (solid), and eruption driving by the birth and growth of bubbles (gas). This picture of the phase changes that magma undergoes on its journey upward in the shallow Earth is a simplistic one, and in fact the phase proportions change in a far more complicated way. While this thesis is concerned with the way liquid can be liberated from the interstices of a pack of solid crystals, it is important to build a general picture of where this specific process sits in the full life cycle of crystals and melt in the crust. One reason that taking this wider view may be useful, is that while this thesis focusses on dynamics in relatively shallow magma reservoirs, the same physical processes may be operative elsewhere in the same system.

During the movement of melts and magmas from generation to eruption, the liquid phase variably crystallises. The growth of crystals in magmatic liquids affects the rheology (Lavallée et al., 2007; Cimarelli et al., 2011; Mueller et al., 2011), and therefore the ascent dynamics and gas movement (e.g. Degruyter et al. (2012)), the propensity for explosivity in the shallow conduit(s) (e.g. Arzilli et al. (2019)), and is one of the principal mechanisms by which melt compositions evolve and differentiate. Some magmas crystallise more readily than others. As a general rule, highly silicic peraluminous and metaluminous magmas (e.g. rhyolite) are less likely to crystallise on their pathway to the Earth's surface, than less silicic, more mafic magmas or peralkaline magmas. Here, it is summarised in a non-exhaustive manner the lifecycle of crystals in magmas and highlighted the importance of settling dynamics, mush formation, and mush evolution, thereby providing the motivation behind this thesis and work.

To understand crystal dynamics, we must first consider crystal formation and interactions, from point of crystallisation until they settle. Magma reservoirs themselves show long, dynamic histories, and are complex systems (Sparks et al., 2019; Bachmann and Bergantz, 2008; Cashman et al., 2017). The new paradigmatic view of a silicic magma reservoir is as a collection of successive sill-like magma chambers arranged in a trans-crustal array (e.g. Sparks et al. (2019)). At the base of this crustal system, melt enters from the mantle zone of melt formation, and on its journey through the crust it forms and interacts with crystals at different levels. In Figure 2.1, the generic and schematic view of this trans-crustal system is outlined.

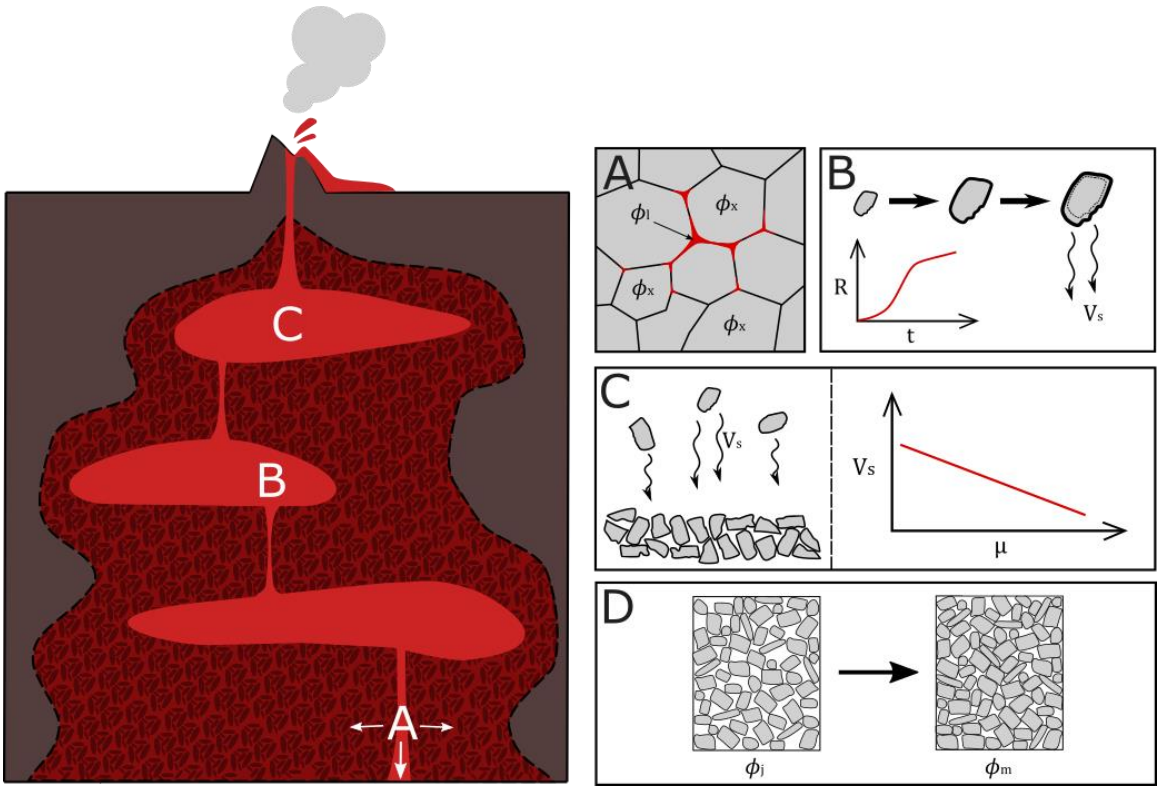

Figure 2.1 – A schematic diagram showing the 'life-cycle' of crystals within a trans-crustal magma system. General diagram adapted from Cashman et al. (2017). The red regions are melt-dominated lenses in the dark red halo of crustal mush. (A) Denotes the region of the system where melt is generated at volume fraction ϕ_l from an initially fully crystalline lower-crustal and mantle region where the crystals occupy a volume fraction ϕ_x. The melt percolates upwards into a partially molten system at increasing ϕ_l. (B) Shows schematically how crystal growth and eventual crystal settling occurs, with the crystal size (R), increasing over time (t). (C) Shows the accumulation of these settled crystals, which settle out from suspension – at steady state this settling velocity is v_s. See text for details. To the right of (C) is a schematic showing the relationship between settling velocity v_s and viscosity of the melt μ, where an increase in viscosity means a decrease in the settling velocity of crystals in the melt. (D) shows the densification of crystals within a mush from a jammed state (ϕ_j) to a maximum packing fraction (ϕ_m), allowing the expulsion of melt from between them. The mechanisms of how this occurs have yet to be explored.

2.1 The lower crust – phase separation of melt from crystals

The melt phase in magmas is generally first derived from melting of the mantle and the location of melting is controlled by plate tectonics (Sigurdsson, 2015). At divergent boundaries, decompression of the mantle below the point of extension occurs causing the interception of the solidus, while at convergent boundaries volatiles introduced by the subducting slab allow chemical composition changes in the mantle, so that the solidus for that altered composition is lowered (Grove and Till, 2015).

The details of how melt moves from the source of generation into the lower crust is still largely unknown. At the micro-scale, the fluid percolates according to Darcy's Law, i.e. the melt percolates through the granular pack of crystals (Daines and Pec, 2015). While the processes of migration are not fully understood, experimental and mathematical studies have shown that increased melt fraction, wider melt phase channel geometry, and larger crystal grain size encourages migration (Holtzman and Kohlstedt, 2007; McKenzie, 1984).

This portion of the system of crystal-melt will be revisited when discussing the application of the models explored in this thesis (see Chapters 4 and 5).

2.2 From the lower crust – transport and storage in dykes and sills

Percolating melt described briefly in Section 2.1 is thought to result in accumulations of melt into larger and larger channels at increasing vertical distances from the source of melt generation. However, there is something of a disconnect between our understanding of melt generation and the microphysics of melt-crystal phase separation (Section 2.1) and the next well-studied step in the system which is transport along dykes and sills – large intrusions in country rock. The details of how melt collects into regions of sufficient size to allow for elevated buoyancy and dyke propagation is poorly understood, but is undergoing some exploration, particularly relating to initial propagation, chamber overpressure and subsequent eruptive intensity (Caricchi et al., 2014; Costa et al., 2011; Maccaferri et al., 2011). Although the role that meso-scale crustal damage zones and tectonically-forced ruptures could play provides a tantalizing connection (Bercovici and Ricard, 2003), what is clear is that once collected in dykes and sills, much of the storage and propagation is thought to be without significant fractions of suspended crystals (Marsh, 1996). That is, while the liquid is mobile, it is nominally aphyric and single-phase. The next point at which crystals play a role in the dynamics of magma movement and storage is in the mid- or upper-crust where pressures are sufficiently low and storage times sufficiently long (Cashman et al., 2017) that crystallization *from* the melt can occur.

Part of the new paradigm of the trans-crustal magma system shown in Figure 2.1, is that magma reservoirs are thought of as accumulations of sill and dyke injections, rather than discrete and different bodies. Magma ascent via interconnected sills and dikes gradually build to form reservoirs; time allowed for the accumulation of material will decide the size of the chamber (Menand, 2011; Gudmundsson, 2012; Cashman and Giordano, 2014). Throughout the magmatic system, but notably in the mid- to upper crustal sills, compositional changes occur via several processes. Most commonly discussed is fractional crystallization – new crystals grow in the melt and then are incrementally removed from that parcel of crystallising melt by settling processes (Philpotts and Ague, 2009). The rate of sinking is dependent on the buoyant force acting on the crystal, which is proportional to the difference between the crystal density and the density of the melt, i.e. a higher density crystal of larger size will settle more quickly than smaller, less dense crystals (Jaupart and Mareschal, 2010). Jaupart and Mareschal (2010) note that smaller crystals may grow in glomerocrystic clots to produce a localised mush, which can then settle more rapidly.

Settling velocity here relates to the buoyancy forces acting on a particle as it descends through the suspending medium. We can define this using Stokes' Law for the settling velocity of spheres in a liquid, given as v_s:

$$v_s = \frac{2\Delta\rho g R^2}{9\mu} \qquad \text{[Eq. 2.1]}$$

where $\Delta\rho$ refers to the density difference between the melt phase and the crystal phase (i.e. $\Delta\rho = \rho_c - \rho_m$), g is the acceleration due to gravity (9.81 m/s^2), R is the radius of the crystal and μ is the viscosity of the melt. Eq. 2.1 is valid when the Reynolds number is low. Here we define the Reynolds number to be

$$\mathrm{Re} = \frac{\rho_m R v_s}{\mu} \qquad \text{[Eq. 2.2]}$$

such that the velocity defining the Reynolds number is approximately that of the particle relative to the fluid v_s. Because μ is typically large, for almost all conditions on the crystal scale $\mathrm{Re} \ll 1$, rendering Eq. 2.2 valid.

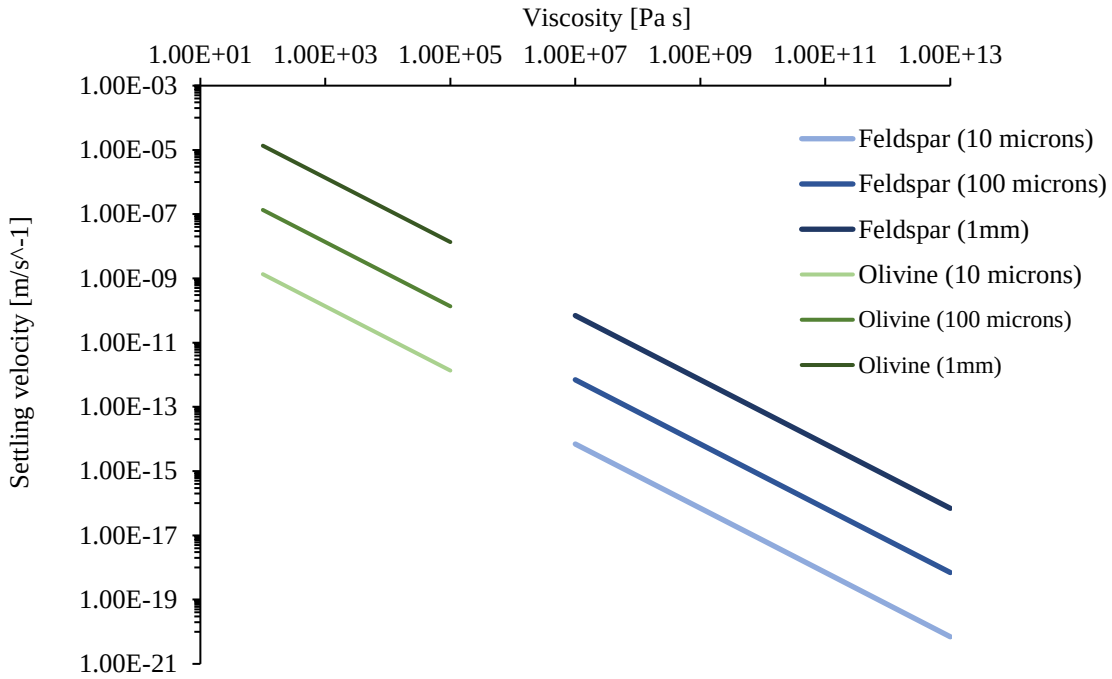

Figure 2.2 - Graph denoting the relationship between settling velocity of crystals (v_s) and the viscosity (μ) of melt. In this example, olivine within basaltic melt (green) and plagioclase feldspar within rhyolitic melt (blue) have been used, over a range of crystal sizes and melt viscosities. The trend shows that with increasing melt viscosity, the settling velocity of crystals within decreases. Hence, crystals within rhyolite take longer to settle.

It is noted that these relationships are idealised, and do not account for particle-particle interactions or non-spherical particles, which would require additional steps within the calculation regarding particle orientation and volume (Clift et al., 2013a; b). As the analysis here is a simple exploration of settling, this can be disregarded.

In the crystal settling model of magma reservoir evolution, the end-result is a pile of crystal-rich magma toward the base of a melt-rich region: a crystal mush (Cashman and Giordano, 2014; Bachmann and Bergantz, 2008). Given sufficient time, the reservoir would be completely mushified. Another model for magma mush formation is that crystals do not settle but rather grow from the sill and dyke or chamber walls inward. Both formations are shown schematically in Figure 1 of Marsh (1996). In either case, the combination of field evidence for

eroded mushy zones recorded in plutons, and geochemical evidence for the presence of mush via, for example, erupted cumulates representing mush fragments, such as Picrite Hill in Cyprus (Bromiley and Law, 2020) and within Snake River Plain in the United States (Ellis et al., 2014), or erupted products holding the geochemical signature of a highly crystalline environment (Sliwinski et al., 2015), has led to the crystal mush concept being a mainstay of the trans-crustal magmatic system paradigm.

2.3 Storage of melt in magma mush

As illustrated in Figure 2.1, the trans-crustal magma model features a vertically extensive reservoir with several sill-steps leading to the surface, providing a network of accumulated melt and mush. As outlined by de Saint Blanquat et al. (2011), there are 'active' and 'passive' phases in magma chamber construction: the dike/sill system is active when new molten material is injected, and becomes passive during the periods of hiatus between these injections. The injected material may enter a previously emplaced sill body if the system has remained hot enough to stay at least partially molten. The added volume and the influx of heat causes the sill to increase in size, typically by lateral expansion, accommodated by deformation of the rock around it, with a more stable rounded or elliptical chamber geometry achieved over time, such as recorded in large plutons (Gudmundsson, 2011; 2012; Biggs and Annen, 2019). Accretion of sills can occur above and below a previously emplaced intrusion, so reservoir geometry is variable (Gudmundsson, 2012; Menand, 2011).

The critical control on sill growth - and therefore the formation of shallow reservoirs in the mid to upper crust - is the rate of cooling of the injecting melt, as well as the rate of supply. When magma is intruded, heat is lost to the surrounding country rock. Long hiatuses between active phases produce clustered zones of sills, as the intrusions have solidified during the passive phase, disallowing melt input and expansion of those sills already established or requiring brittle fracturing to re-open the sill system. In systems where the intrusions remain at sufficient temperature (i.e. the rate of cooling is slow or injection rate is high), sills can expand into chamber-like reservoirs and interconnect. The size of the established system is directly proportional to the time allowed for accumulation; larger systems have accreted more material over a longer period of time (de Saint Blanquat et al., 2011; Menand et al., 2011; Cashman and Giordano, 2014).

The main source of silicic magma in the upper crust is stored within magma mush bodies, with volumes of >500 km^3 (Bachmann and Huber, 2019). The upper crustal system is a product of melt movement and ascent from below, as discussed. Hence, the temperature that sustains the magma system is maintained above solidus via injection of melt from below. There must be a high enough rate and volume of input to allow this, but once a mush zone is formed, it is long-lived (Cashman et al., 2017). Due to the highly complex nature of the processes that occur within magma chambers as described, ideas about mush storage and the relinquishing of melt can be drawn from erupted products found in the field. These studies have led to two main types of eruptive product from the mush system: crystal-poor rhyolites, commonly seen as low-crystallinity ignimbrites in the field, and monotonous intermediates, which are thought to contain the mush itself (as outlined by

Bachmann and Bergantz (2008)). These two types and their generalised storage/eruptive environment are shown in Figure 2.3.

Crystal-poor rhyolites are the focus of this study, as their formation and accumulation relate to Stokes' settling processes and extraction via expulsion from a crystal mush pack. Simplified, crystal-poor rhyolites form from this melt segregation via crystal processes such as settling of crystals and plumes of crystals due to contrasts in their density with the surrounding melt under the force of gravity, and micro-rearrangement of the crystal network (Bachmann and Huber, 2019; Cashman and Giordano, 2014), which in turn pushes melt upwards due to compaction at the base of the body to form a 'cap' of molten rhyolitic material at the top of a mush column (Daines and Pec, 2015). This process occurs when convection within the body is halted, i.e. the crystallinity of the body exceeds ~45%, with ~45-65% average crystallinity the reported window of increased efficiency of the resulting gravity-induced compaction (Bachmann and Bergantz, 2004; 2009; Miller et al., 2017). It is noted that this extraction model requires large volumes of mush in order to produce the large quantities of low-crystallinity, high-silica rhyolitic melt that is ultimately ejected from the magma chamber (Streck, 2014).

Monotonous intermediates, defined by Streck (2014) as 'crystal-rich, compositionally intermediate ignimbrites', give other ideas about mush, namely that remobilisation of the mush storage can produce highly crystalline but compositionally homogenous products upon eruption (Charlier et al., 2007). Because mush has a high viscosity and a crystal-lattice yield strength, with critical crystallinity occurring at ~50% (Marsh, 2015), convection is unable to start, or is very slow. However, processes such as underplating and the injection of hot molten magma at the base of the body introduces both increased thermal energy and buoyant exsolved gases into the mush. Partial melting may occur, which allows the unlocking of the crystal network, or the crystals are pushed apart by increased gas content (Huber et al., 2012; Bachmann and Bergantz, 2008). Remobilisation then occurs via convection, and any segregated melt (i.e. a rhyolitic cap) is mixed back into the mush body. Because of this, Huber et al. (2012) has defined the key identifiable difference between the two types (besides their different crystallinities and compositions) as the 'presence or absence of a mush reactivation stage'. Reactivation leads to the production of compositionally homogenous intermediates, while there is no remobilisation involved in the production of crystal-poor rhyolites.

The western United States provides excellent examples of both. Crystal-poor rhyolites include the Bandelier Tuff of Los Alamos Canyon, New Mexico (Broxton et al., 1995; Sommer, 1977; Wolff and Ramos, 2014) and the Bishop Tuff of Long Valley Caldera, California (Hildreth, 1979; Hildreth and Wilson, 2007; Roberge et al., 2013). Both exhibit a high percentage of ash in the matrix alongside pumice clasts and low phenocryst percentages of 7-10 wt.% and are highly silicic. It is also noted that both show an increase in phenocrysts closer to the top of their deposits, as the eruption tapped more crystal-rich compositions in the later stages (as described by Bachmann and Bergantz (2008)).

Meanwhile, monotonous intermediates can be seen in the Fish Canyon Tuff of the San Juan Volcanic Field, Colorado (Bachmann et al., 2002; Lipman et al., 1997) and the Lund Tuff of Great Basin, Nevada (Maughan et al., 2002; Christiansen, 2005). As described, these tuffs are monotonous in their composition and have a

higher phenocryst percentage, from 40-45 wt.% and 47 wt.%, respectively. As they are dacitic, their SiO_2 content is lower than crystal-poor rhyolites, averaging from 60 to 70 wt.%, with phenocryst volume reaching 50 wt.%. Monotonous intermediates such as these have massive eruptive volumes, such as an estimated 5000 km^3 for the Fish Canyon Tuff. The ability to expel such high quantities of intermediate magma has been debated, but it is thought that magma chamber geometry plays a part: the highly zoned crystal-poor rhyolites are sourced from vertically expansive chambers, where sidewall crystallisation and the rise of buoyant interstitial melt is encouraged by the chamber geometry, while monotonous intermediates are derived from laterally expansive, sill-like chambers, where convection can occur throughout the chamber and produce monotonous compositions. For example, the Lund Tuff is thought to have erupted wholesale after the failure of the chamber roof rocks, due to the >50 km diameter of the chamber. A diagram summarising these proposed geometries can be found in Figure 18 of Maughan et al. (2002).

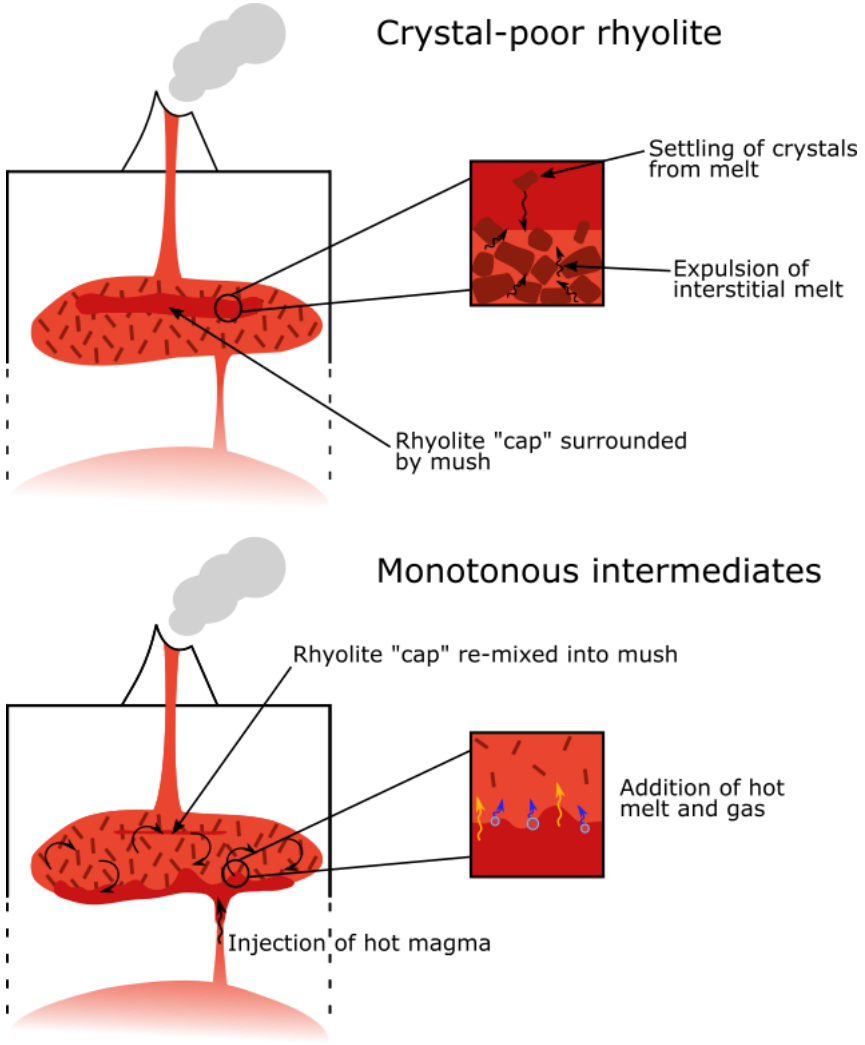

Figure 2.3 – Schematic showing the formation of crystal-poor rhyolites and monotonous intermediates. Crystal-poor rhyolite is a product of gravity settling of crystals out of a body of melt, with extraction occuring from the mush below due to rearrangment of the crystal network and gradual gravity-induced compaction. Monotonous intermediates are the product of remobilisation of the mush body, where convection can occur when the crystal mush is "unlocked" via the addition of heat and gases from an intrusion below.

2.4 Are mushes un-eruptible?

In Section 2.3, two broad types of mush are introduced – evidenced by erupted materials found in volcanic deposits – which appear to relate to two 'families' of processes by which they have been erupted. The mechanisms for the eruption of monotonous intermediates centre around the mush network being "unlocked", via bubbles pushing crystals apart or an increase in temperature being introduced due to underplated magma, leading to the partial melting of crystals in the mush chain, alongside the convective motion of localised crystal plumes (Huber et al., 2010; Bachmann and Bergantz, 2008; Huber et al., 2012). Underplating of hot, mafic magma has been suggested for the homogenisation of the Fish Canyon magma body, for example, where hot magma below moved upwards into the cooler, silicic mush body and introduced heat and volatiles, which may have released a buoyant fluid phase, acting as another source of instability in the chamber (Huber et al., 2009; Parat et al., 2008).

Meanwhile, the mechanisms of the eruption of crystal-poor rhyolites from segregated 'caps' of melt remain contentious, due to the ongoing debate surrounding the physical process of separating crystals from the melt in the first place. Holness (2018) scrutinises the proposed mechanisms of crystal-liquid segregation further, namely compaction, and states that there is not enough microstructural evidence in specimens to support compaction, nor can settling be used without limitation, as the calculations operate on the basis of theoretical models and assumptions.

As stated by Cashman et al. (2017), 'the dynamics of [mush] systems are characterised by compaction-driven segregation of melts and fluids from the crystalline matrix'. Compaction allows the movement of magma upwards through the system, while the mush itself reduces porosity via reorganisation of particles under its own gravity, without distortion occurring (Daines and Pec, 2015). This reorganisation leads to a densified pack of crystals, while interstitial melt and fluids are pushed out (Marsh, 2015). This can be summarised briefly by Darcy's Law, where melt is the migrating fluid, and a partially crystalline zone in a magma chamber, i.e. a mush, is the porous medium

$$q = -\frac{K}{\mu}\frac{dP}{dx} \qquad \text{[Eq. 2.3]}$$

where q is the melt flux, K is permeability, μ is the viscosity of the fluid, and dP/dx is the pressure gradient in the melt. As grain size and melt fraction increases, permeability also increases. Due to compaction, melt moves upwards working in tandem with porous flow, as the compacting matrix fills the space the migrated melt has left behind, reducing the porosity in the area. The melt accumulates at the top of this zone (Daines and Pec, 2015; Scott and Stevenson, 1986), leading to the formation of a crystal-poor 'cap'.

The central issue regarding compaction revolves around the timescales associated with crystal-melt segregation. This segregation is stated to be very slow by Bachmann and Bergantz (2008) when forming a rhyolitic 'cap' above a mush body, citing previous calculations of $10^4 - 10^5$ years for compaction-driven segregation (Bachmann and Bergantz, 2004). However, Allan et al. (2013) provides an example where, geochemically, the separation appears rapid. In their work on the Oruanui magma body of the Taupo Volcanic

Zone, U-Th analyses found melt extraction and accumulation was much faster, on a scale of approximately 3000 years, in contrast to the tens of thousands of years required for the source mush to form. However, this example highlights the complex nature of magma reservoirs, as Allan et al. (2013) states rapid accumulation must have been driven by another mechanism that is more efficient than settling and compaction alone. They propose tectonic events, such as the extension of crust where mush is stored, which would allow melt channels to open and melt to ascend rapidly.

Geochemically, the segregation process appear rapid, however previous numerical analyses have determined compaction to be slow. However, this leads us to the question explored briefly by Allan et al. (2013): what other mechanisms would encourage rapid accumulation and segregation of melt from mush, to form an eruptible melt 'cap'? In this thesis, the role of seismicity in triggering eruptive activity will be explored, as a proposed mechanism of increased melt segregation.

2.5 The role of seismicity in triggering eruptions by extracting melt from mushes

Previous literature, regarding the role of seismic waves in triggering eruptive activity, has focussed on the effects of dynamical stress (i.e. seismic waves, discussed in Section 2.5.1) on the pressure of the system, more notably the pressure changes and dislodgment of gas bubbles within magma. Manga and Brodsky (2006) discuss this overpressure, the increase of which leads to failure and subsequent eruption. Bubbles are cited as the driving force, alongside chamber convection and injection of new molten material. However, the authors note that seismic waves are 'transitory phenomena' and sustaining a critical magmatic overpressure where an eruption can occur requires the involvement of several magmatic processes – it is not likely to occur due to shaking alone.

Rectified diffusion, where the contraction and expansion of bubbles based on surrounding pressures allows for differing saturations of volatiles in the melt, is often highlighted. There are many variables associated with rectified diffusion, such as the saturation in the surrounding magma, compressibility, volatile species, and the initial overpressure of the system. Previous models for rectified diffusion and numerical analyses have found that the pressure changes induced are very small and therefore unlikely to be significant unless the system is already at "critical instability", and that the complexity of the system makes the numerical analyses too simple, such as assuming a bubble is surrounded by incompressible magma in a non-deformable host chamber (Ichihara and Brodsky, 2006; Brodsky et al., 1998). It is still under scrutiny. "Critical instability" is defined here as a body/system that is already at an increased level of overpressure, with a certain volatile content, and at a prone depth within the upper crustal reservoir (Walter and Amelung, 2007; Watt et al., 2009). Magmatic processes induced by shaking at this point may therefore be more likely to trigger volcanic activity.

Another mechanism is advective overpressure, where chamber pressure increases due to the rise of bubbles. A simple model was proposed by Sahagian and Proussevitch (1992) where bubbles from a deeper part of the chamber transport higher internal bubble pressures to the top of the chamber, if the bubble is surrounded by incompressible liquid within a system of fixed volume that prevents the internal pressure of the bubble from

changing. In lab experiments and numerical tests, it was found that a vertical increase in bubble height of 1km carried pressure changes of ~30MPa (Linde et al., 1994), similar to the required overpressure for silicic systems. It was also proposed by Linde et al. (1994) that initiation of this process may be due to seismic waves physically shaking bubbles free. However, this mechanism is not without fault, as the proposed model by Sahagian and Proussevitch (1992) is simplified, and the gas diffusion in both rectified diffusion and advective overpressure can take several seconds or several hours, with a variety of other magmatic processes occurring at any one time. Hill et al. (2002) indicates that processes like rectified diffusion and advective overpressure likely work in tandem to influence bubble changes. The consensus is that bubbles leading to eruptions via seismicity is dependent on the complexity of the chamber system, and also the initial overpressure of the chamber, which must already be at a critical state of instability prior to an earthquake.

2.5.1 Rapid vs slow stressing

When considering stress applied to magma mush systems, it is noted that the proposed compaction model that forms crystal-poor rhyolites is a slow-stress mechanism, where gravity acts over a long timescale to squeeze out the interstitial melt (Bachmann and Bergantz, 2004). The application of seismic stress to this model allows us to consider two broad categories of stress: transient and steady-state (also referred to in the literature as dynamic and static, respectively). The motivation of this thesis is to test the effect of transient stress dynamics on the evolution of crystal-bearing magmas, such as the slow compaction mechanism introduced. Transient stresses are imparted by seismic oscillations in stress, that is, stress that varies dramatically over a period of time. Transient stress associated with seismic waves is at the fore of this project, but it also applies to magma movement as well, such as injection and percolation through mush. While there is controversy over which stress category has a greater influence (Walter et al., 2007), both types of stress are associated with volcanic triggering, though it is noted that steady-state stress occurs largely within a few fault lengths of a quake event and dissipates quickly, compared to transient or dynamic stress that has been studied as part of far-field volcanic triggering, i.e. up to 1000 km away from an earthquake epicentre (Manga and Brodsky, 2006; Linde and Sacks, 1998; Hill et al., 2002).

An excellent example is the 1960 rhyodacitic fissure eruption within the Cordon Caulle Volcanic Complex in the Southern Andes. Approximately 38 hours after a M_w 9.5 subduction zone earthquake, the fissure began to erupt, situated ~240 km from the epicentre. It is considered that, due to the east-west extension caused by the thrusting of the nearby Nazca and South American plates, the magmatic plumbing system below the Complex was deformed horizontally, allowing shallow magmatic structures to activate via seismic pumping (Lara et al., 2004; Barrientos, 1994). In relation to transient versus static stress, Walter and Amelung (2007) refer to other examples, explored statistically, that show volcanoes ~750 km or more from earthquake epicentres have a significant response to those earthquakes, drawing on the landmark analysis carried out by Linde and Sacks (1998). They also note that static stress - stress that is permanent, occurs within a short distance of the epicentre and gradually falls off with that distance, discussed above - would likely only affect eruptive phases if they were very close to the epicentre, i.e. within the few fault lengths that static stress is effective.

While transient stress varies with time, steady-state stress does not. Steady-state stress can also refer to very slow processes, where changes in stress are small over the given length of time. For example, the regional movement induced by tectonic systems will influence magma chambers and their processes, but the stress change and movement of these systems is very gradual. In this project, steady-state stress is observed at the "end" of the shaking event, such as in Figure 2 of de Richter et al. (2015), where the packs being shaken undergo transient stress over time, but end with very minute changes in the packing fraction in the second stage of compaction. This tapering trend is an example of a very slow steady-state process, as the packing fraction will continue to increase, but the change over a long period of time is not significant.

2.5.2 Seismic waves

Seismic waves are the resulting vibrations from often large structural and tectonic movements, referred to as earthquakes. Prominently, rock slip along faults, whether within the crust or as part of plate tectonics (e.g. slip along a subduction zone), causes vibrational waves that radiate outwards from the point of failure. The strength of these waves varies and depends on location and the surrounding geology.

P waves (primary) and S waves (secondary) are two wave types produced during earthquakes. P waves function via compression of the medium they pass through, followed by rapid expansion, transferring energy through both solid and liquid mediums. Meanwhile, S waves shear the medium perpendicular to the direction of energy travel. Because of this, they are only able to pass through solid states (Doyle, 1995). A visualisation of both waves is shown in Figure 2.4.

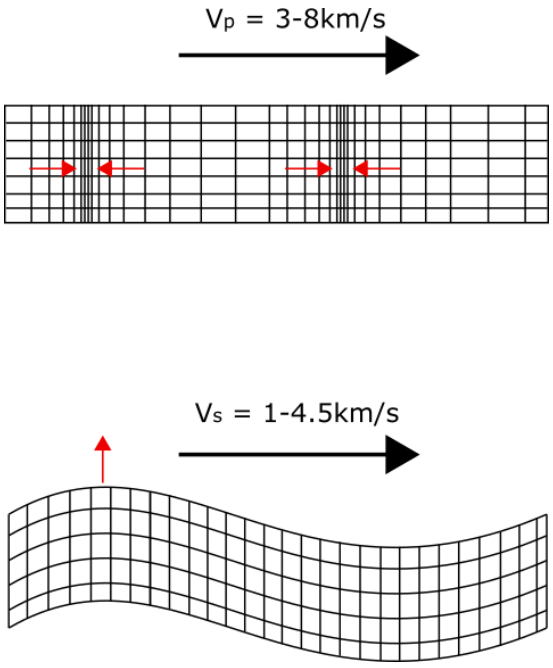

Figure 2.4 - Top diagram shows P wave compressional transport, with localised zones of the medium being compressed before expanding again to transfer energy (red arrows).

Bottom diagram shows S waves and their pattern of shear. Motion of the wave is perpendicular to the direction of transport (red arrow).

Direction of transport shown by large black arrow. Figures adapted from Doyle (1995). Velocity value ranges from multiple sources, stated in the text.

As an indication of wave velocity, amplitude and frequency, several examples can be outlined. It should be noted that seismic studies, utilising both real-time events and synthetic earthquakes, are useful for determining physical properties of the Earth's crust, as well as the structure below major features such as volcanoes. Both methods can give a range of velocities for different rock types and tectonic settings.

While these studies do not always feature specific earthquake events, the cataloguing and processing of large quantities of real-time data over a period of several years can give a general range of velocities for both P and S waves. An example would be a seismic study conducted in southwest Iceland using earthquake data between 1973 and 1999, presented by Tryggvason et al. (2002), where average velocities were 3.4-7.4 km/s and 1.9-4.25 km/s for P and S waves respectively, with variance across the study area occurring due to regional structures, rock types and zones of potential partially molten material (variability shown in Figure 7 and 8 of Tryggvason et al. (2002)). Modelling of the Irpinia earthquake in Italy 2004, for example, produced velocities of 3-8 km/s and 1-4.5 km/s for P and S waves, respectively (Vaccari et al., 1990). A general rule of thumb is that velocity of both P and S waves will increase with depth through the crust, though increased temperature will cause them to decrease (Christensen and Mooney, 1995). Hence, low-velocity bodies are often located under active volcanoes, calderas, and tectonic boundaries like mid-ocean ridges and subduction zones (Lees, 2007).

Amplitude varies greatly on seismograms depending on location of the reading, however it gives indication of displacement due to seismic waves. There are multiple ways of conveying amplitude, including physical displacement (such as in mm or cm) and accelerations of the ground motion. Physical displacement in length units is not often recorded and requires integration to obtain the values. However, it can be noted by eye from seismograms, such as those found in ground motion studies. For example, the Sumatra-Andaman earthquake in 2004 produced massive surface (Rayleigh) waves with vertical displacement of 6-10 mm. P and S waves were smaller, with ranges of 0.5-1 mm and 1-2.5 mm for P and S wave vertical displacement, respectively (Lay et al., 2005; Ishii et al., 2005; Lockwood and Kanamori, 2006).

Amplitude can also be measured via peak ground acceleration (PGA), for both vertical and horizontal movement. Once again, this varies depending on the location of the recording and the regional geology, but it is noted that the amplitude (both physical displacement and the acceleration) decays via an inverse square law ($1/R^b$) (Lay and Wallace, 1995a) over distance, as well as varies with earthquake magnitude (such as Edwards et al. (2011); Frankel (2015); Crowell et al. (2013); Campbell and Bozorgnia (2003), and figures therein). PGA can be measured in either cm/s^2 or g (where 1g = ~980 cm/s^2). Examples include the Yogyakarta earthquake of 2006, where PGA of 0.183-0.303g were recorded for vertical acceleration, and 0.197-0.336g for horizontal, at the YOGI recording station approximately 10 km from the epicentre. Interestingly, at the BJI station 90 km away, these values reduced to 0.015-0.025g and 0.021-0.035g for vertical and horizontal acceleration, respectively (Elnashai et al., 2007). Other examples feature values averaged from a wide range of regional data, such as in Murphy and O'Brien (1977), who note that PGA typically ranges between 1-1100 cm/s^2, or 0.001-1.123g. Very large accelerations have been recorded however, such as during the Iwate-Miyagi Nairiku earthquake of 2008 in Japan, where PGA reached 4.362g, recorded at 3 km from the epicentre (Yamada et al., 2009).

Frequency of shaking can also be recorded, and varies over a wide range, with high-frequency waves having a shorter wavelength, and therefore a smaller period of significance, than low-frequency waves, which oscillate over much longer distances. Frequency values are sometimes available within studies on major earthquakes

and/or ground motion, such as frequencies of 2.5-3 Hz for the Irpinia earthquake (Nunziata, 2004), and a dominant frequency of 0.2 Hz recorded in the Kathmandu Valley during the Gorkha earthquake in 2015 (Wei et al., 2018). Frequencies appear to be dominant between 1 and 5 Hz, however larger has been recorded up to >10 Hz, such as the 0.5-11 Hz site response during the Denali earthquake of 2002 (Boore, 2004), and up to 100 Hz, such as a M_w 4.7 earthquake in Hawaii, 2017 (Butler, 2018).

In this project, we will focus on S waves, for their shearing ability. P waves are not used as their high wavelength would result in an entire magma chamber system being compressed at once, without local effect on crystal mush being significant enough to be studied at this scale. S waves however will shear the medium.

2.5.3 Shaking a mush as a mechanism for melt extraction?

While the compaction and movement of granular packs (both wet and dry) has been studied extensively with relation to manufacturing and transportation of granular or powdered mediums after McGeary (1961), it has recently been brought into experimental magmatic context within the last twenty years. When considering partially molten chambers, seismic waves from magmatic movement or structural failure of local faults, as well as major tectonic movement such as at subduction zones, is likely to travel through these bodies. We can classify partially molten crystal mush as saturated granular packs: crystal aggregates with interstitial melt and fluids able to move within (Figure 2.1, Box A). Many studies have used granular packs, both saturated and dry, to explore grain movement under repeated vibration, and it has been found in saturated packs that oscillation of the solid-liquid mixture encourages the liquid phase to migrate upwards and be expelled as the solid phase reorganises to a more dense packing, pushing this fluid up and out. These studies and their findings support the hypotheses adopted in this project and have aided in forming the numerical-based methodology shown in Chapter 3 and 4.

In a granular pack, densification – defined here as the closure of pore space and reorganisation of grains towards a higher packing fraction – occurs when the pack is subjected to vibration. A study by Lesaffre et al. (2000) shows that the active time and frequency of the vibration are important in determining the behaviour of grains in a shaken pack. They state that the 'applied acceleration [should] be well chosen' – a force strong enough to displace grains due to reduced cohesion (Hanotin et al., 2012), but not so violent as to fluidise the whole pack via convective motion, as others found too high intensity vibrations led to excessive dilation of particles and a decrease in the packing fraction (Scott, 1960; Nowak et al., 1997). This attention to vibrational intensity is mirrored by several other papers, defined by parameter Γ, which is the ratio of peak acceleration to gravitational acceleration (Soria-Hoyo et al., 2008; Knight et al., 1995) and written as follows:

$$\Gamma = \frac{\mathrm{A}\omega^2}{g} \qquad \text{[Eq. 2.4]}$$

where A is the amplitude of the motion, ω is the angular frequency and g is the gravitational acceleration at 9.81 m/s. In varying Γ by changing the amplitude and frequency of the test, as well as altering the physical properties of the pack such as particle density, fluid viscosity and particle geometry, a wide range of scenarios

can be tested by giving these variables real-world values (discussed in Chapter 4). Another highlighted parameter in previous works is the settling velocity, defined by Stokes' Law in Eq. 2.1 (see Section 2.2). While Figure 2.2 shows crystal settling (v_s) is not dominant in high-viscosity, silicic systems, de Richter et al. (2015) focusses on this parameter, as the settling velocity of particles when shaken determines the particle pack response – fast settling, as a product of lowered viscosity and/or increased particle size as well as greater vibrational intensity (Γ), allows for a faster compaction stage with a maximum packing fraction (ϕ_f) attainable on a shorter timescale (de Richter et al., 2018).

These tests have also revealed that compaction occurs in two stages. It was found that vibrated granular packs comprised of spherical particles will evolve from their initial random loose packing fraction (RCL) in the range of ~0.55 to ~0.60, to a closer random packing fraction (RCP) of up to ~0.64, where the granular pack is disorganised and uninfluenced by extra external pressures that would allow even further densification (Lesaffre et al., 2000; Soria-Hoyo et al., 2008; Lochmann et al., 2006; Nowak et al., 1997; Jaeger et al., 1994; Jaeger and Nagel, 1992; Onoda and Liniger, 1990). The two-stage trend has been displayed in previous studies, as in Figure 2 of de Richter et al. (2015) amongst other similar tests (Knight et al., 1995; Lesaffre et al., 2000), where a linear relationship between packing fraction (ϕ) and time (t, seconds) is shown.

A strong increase in ϕ is followed by the tapering from the trend at longer time periods, which emphasizes a two-stage compaction process. The initial stage is termed the 'fast' stage, where voids within the pack fill quickly, followed by the latter 'slow' stage. It is considered that this 'slow' stage never reaches steady-state, possibly due to smaller increments of particle settling occurring as the larger voids have already been filled during the 'fast' stage, further slowed by the particles becoming 'caged' by the neighbouring grains they are in contact with (Lesaffre et al., 2000; Pica Ciamarra et al., 2007). In these studies, it was also found that high-viscosity, fluid-saturated packs took longer to reach the threshold of this 'fast' packing stage - though lubrication given by an interstitial fluid allowed for higher packing fractions to be reached. The increased time taken to densify for high-viscosity examples fits with the crystal settling calculations of this project (Chapter 4), where high viscosity magmas had lower settling velocities, leading to the assumption that compaction and melt expulsion would take longer for these magmas. Despite the variability in timescale, the outcomes for these tests were the same: the particles densified, and the interstitial fluids were expelled.

While studies that link this densification and expulsion process directly to mush are few, it is important when considering the formation of crystal-poor rhyolites. As discussed, they are the product of melt ascent through a mush to the top of a magma chamber, via gravity-induced compaction of the crystal framework and settling. The outcome for both the granular pack tests and the formation of crystal-poor rhyolite is the same, where melt is expelled and allowed to accumulate above the mushy source. This leads us to the question: how would seismic waves effect this compaction, densification, and expulsion process? And will it lead to increased eruption potential due to a higher melt accumulation in real-world scenarios?

Chapter 3. Methodology

This thesis takes a methodical approach of re-analysing previously published data and applying it to new regimes – in this case, magmatic systems. For this reason, there are two principal methodologies worth describing: (1) the methods involved in the production of the dataset that is to be analysed (Section 3.2), and (2) the methods involved in the collection of that data (Section 3.3.). While the methods in (1) are not unique to this thesis, it is worth repeating them for completeness and comprehension of the reader.

3.1 Dimensional analysis and philosophical approach

We use a primary data source from de Richter et al. (2015). In their published work, they present the results of a suite of experiments in which spherical particles of known density are subjected to vertical displacement oscillations at controlled frequency and amplitude. The particles are submerged in a liquid of known viscosity. The particle sizes, shapes, particle properties or liquid properties are all quite different from those of interest in the context of a magmatic system, as real magma reservoirs will be considerably more complex both in composition and in other processes occurring alongside the compaction mechanism being tested, as well as in the diversity of crystal sizes and shapes present. A major difference in viscosity, which in real reservoirs is very high, and difficult to truly synthesise in a laboratory setting. However, we can explore the extent to which the experiments are dynamically similar – and therefore well-scaled – to the magmatic system. Control over the variables, such as the viscosity and particle size, allow mirroring of the complexity of real systems by testing a wide range of potential compositions, as the authors of this primary data source have done. While these may not match exactly, these compositions can then be scaled up and applied to real reservoirs, allowing the development of new lines of enquiry for future study.

3.2 Shaking a pack of solid particles with interstitial viscous fluid

In selecting the source of the data to be used in this project, it was essential that the source related closely to the aims of the project, but also that it provided ample room for expansion of original ideas, allowing the exploration of the subject in greater detail. As shown in de Richter et al. (2015), such a paper should be general enough to allow for this expansion on ideas, and therefore multi-use. The experiments carried out in this source paper and the findings provide a basis for new applications and ideas to be developed. For example, this paper is not centred around the movement of particles in magmatic environments, but the setup and findings are applicable to synthesised magmatic systems, and relate to Stokes' Law as used in this project to understand how particles (i.e. crystals) will move, and then how shaking may alter or increase that movement. It also introduces the concept of "two-stage compaction", where there are two distinct stages of particle reorganisation that may be influenced by different parameters in the test. This does not appear to have been explored in great detail previously, but it should be noted that as a previously unexplored concept it may become a source of uncertainty. The results of the method used in this thesis may therefore aid in its' development. With these qualities in mind, the paper by de Richter et al. (2015) was the selected source of data for this thesis.

The experimental setup is outlined in Figure 3.1, adapted from Figure 1 in the source paper (de Richter et al., 2015). The main components include a tube in which the particle pack is held, and a shaker. The tests were completed using spherical glass beads with ρ = 2200 kg m^{-3}, of which had two diameters: 335 μm and 530 μm. The fluid used to saturate the glass bead pack is a water-emkarox mixture, with an estimated density of 1000 kg m^{-3}. The viscosity of this was variable for each test. The glass tube used to house the pack was 20 mm in diameter, and 10 cm in height, and was affixed to the shaker. Vertical amplitude raged 20-200 μm, and frequencies tested were 30-50 Hz. Once the glass beads were poured into the mixture, they were allowed to settle and the estimated initial porosity (ϕ_0) was 0.58 ± 0.01.

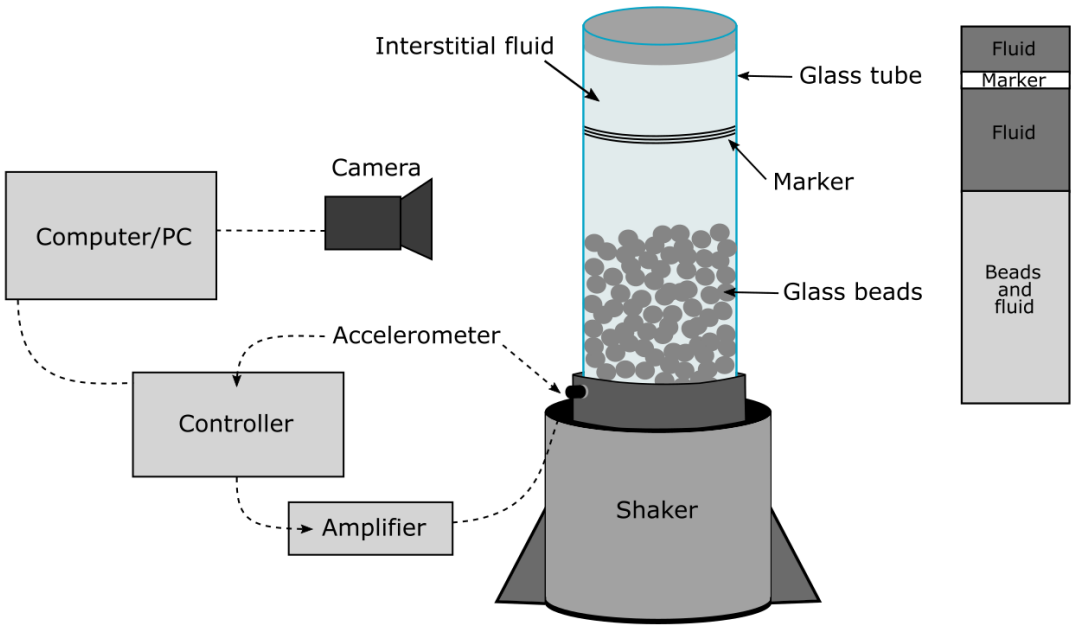

Figure 3.1 – Experimental setup as adapted from de Richter et al. (2015). Schematic shows glass tube on top of a shaker, in which the saturated particle pack is shaken at varying frequencies. Range of particle movement during shaking is captured via accelerometer and video analysis.

3.3 Data acquisition and analysis steps

The WebPlotDigitizer online tool was used to extract data from the source paper. The method is outlined below and in the following figures. First, the desired graph from de Richter et al. (2015) was captured and uploaded into the WebPlotDigitizer online tool, as shown by Figure 3.2. Once uploaded, the plot type was selected as X-Y to produce a graph of linear data, with the axes calibrated manually by plotting points of known value along them (X1, 2 and Y1, 2 in Figure 3.2). The Automatic Extraction tools were then used to highlight the data points of each dataset individually. Each data trend was highlighted using the 'Pen' tool as seen in Figure 3.3 (highlighted yellow in Figure 3.3). When selecting the 'Run' function, each datapoint which had been highlighted was replotted. As the datasets each had densely clustered points towards the top of the trend, the Automatic Extraction tools here were useful in highlighting the overall trend, where individual points could not be plotted exactly.

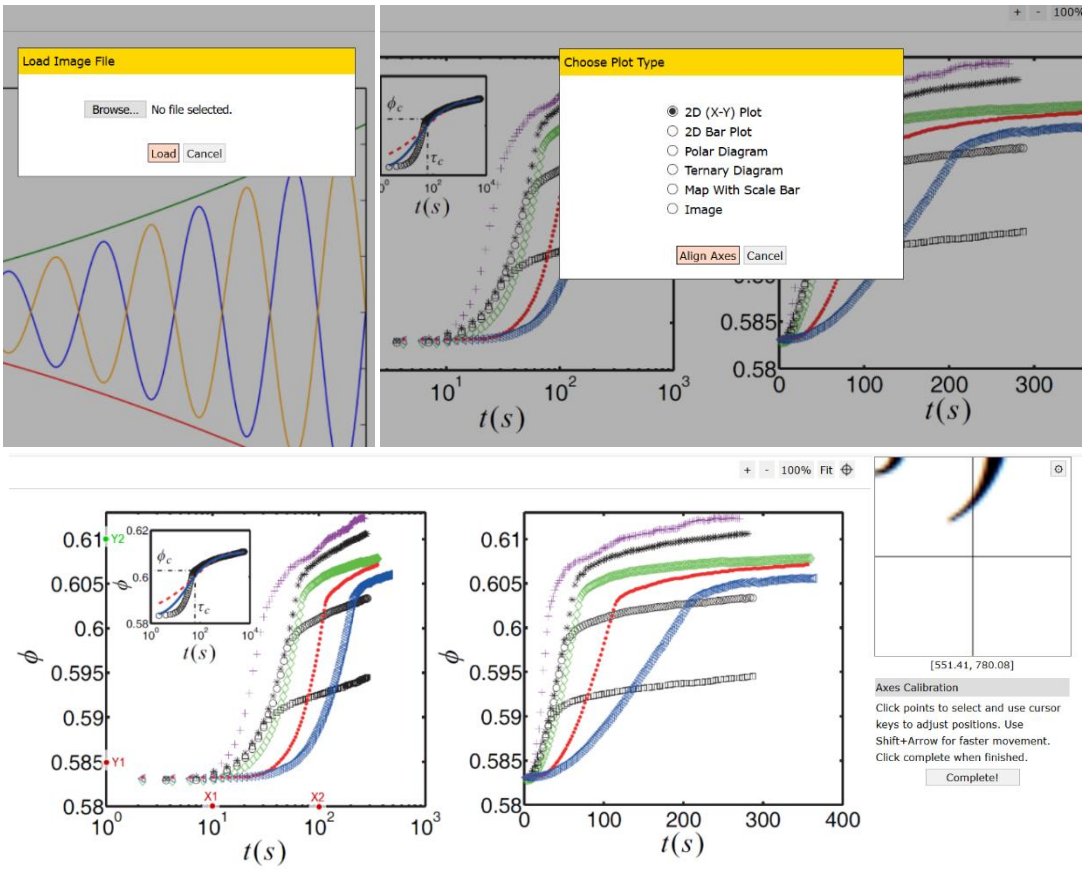

Figure 3.2 – Desired graph uploaded into WebPlotDigitizer. Plot type set to X-Y and calibrated manually.

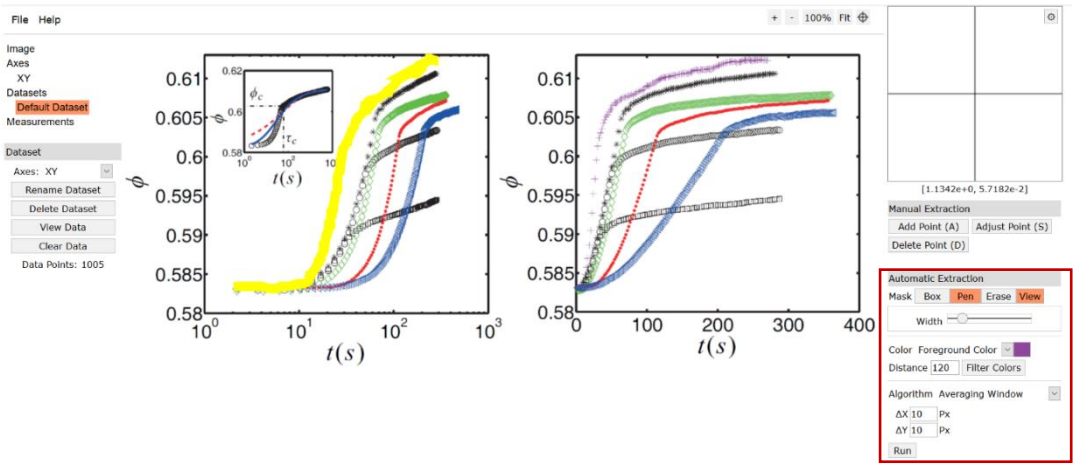

Figure 3.3 – Automatic Extraction tool 'Pen' used to highlight and pinpoint one dataset at a time.

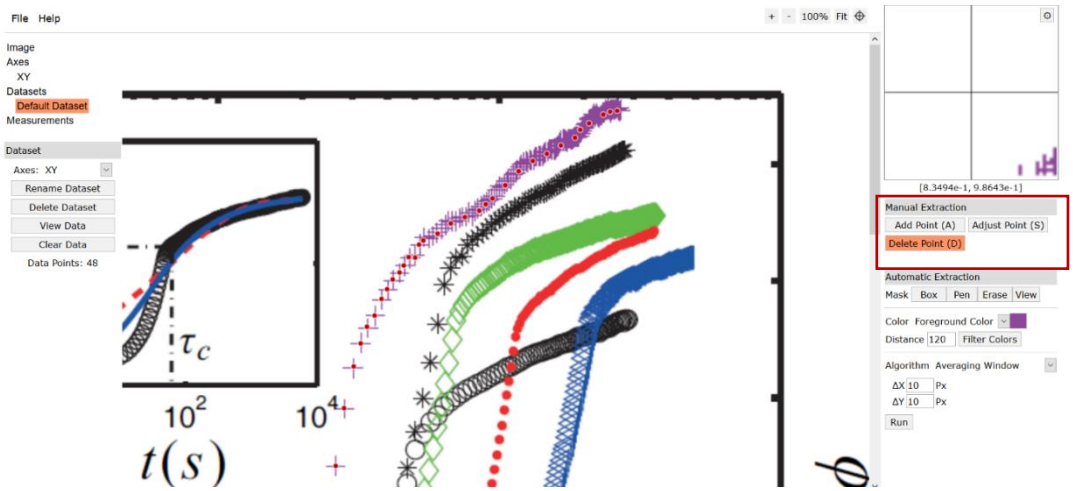

Figure 3.4 – Pinpointed dataset edited using Manual Extraction tools to ensure points aligned correctly.

Figure 3.4 shows the next step, where these highlighted points were manually corrected using the Manual Extraction tools, so that the centre of each individual point was aligned, giving the most accurate data possible.

After each of the datasets had been selected, they were converted into a separate graphical plotting online tool called Plotly, which allowed the trend to be scrutinised for accuracy. From here, the data could then be transferred directly into Microsoft Excel, without downloading separate .CSV files for each dataset (Figure 3.5).

Once all the data was compiled, it was plotted in Microsoft Excel, where final adjustments could be made for presentation, quality and accuracy, shown in Figure 3.5. The end result is shown in Figure 4.1 (a) of Chapter 4.

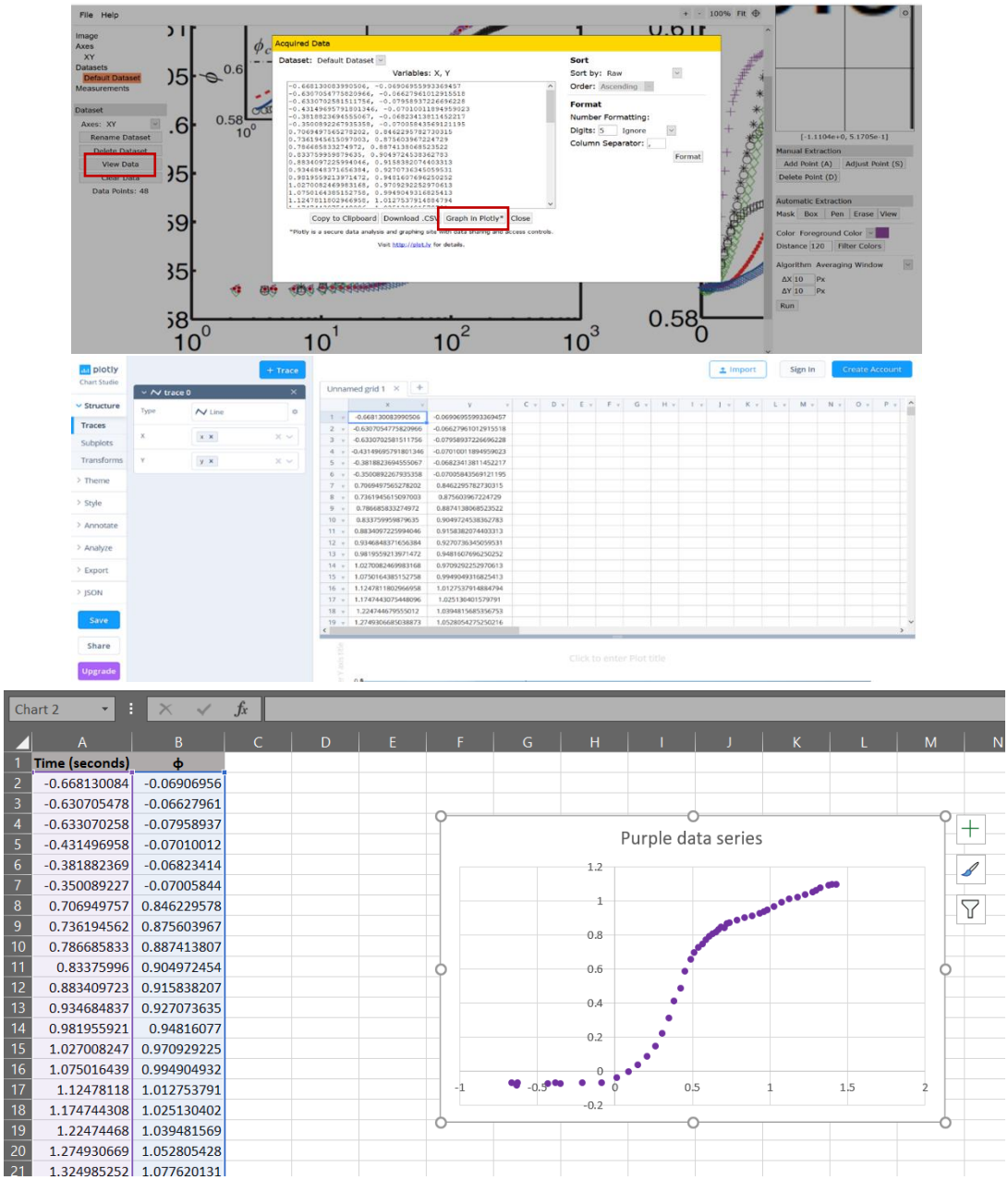

Figure 3.5 – Dataset transferred to Plotly to assess acquisition. Data was then copied to Microsoft Excel.

3.4 Sources of uncertainty

There were some uncertainties encountered when using the WebPlotDigitizer method and with the source paper itself. When acquiring data, there were physical errors such as when aligning the axes of the figure and with plotting every individual point, due to human error and some loss of quality or resolution when copying over the figure into the program. In particular, it was difficult to plot every individual point for each data trend, as the points were densely clustered towards the top of the trend. While this method can provide a close match to the data and the trend of that data cluster, it was impossible to plot every point individually within the clusters. There was also human error when trying to plot the very centre of each data point, to get an accurate reading as possible.

Within the source paper itself, it is noted that the data found is the first to show a "two-stage" compaction, where a period of fast compaction is followed by a slower stage, as previously mentioned. While this has been noted before (such as in Lesaffre et al. (2000)), the two-stage compaction has only been touched upon both theoretically and experimentally, with little detail into the particle movements at the micro-scale. Many previous experiments that focus on particle interaction in compacting granular packs have shown a homogenous compaction, and have predominantly featured "dry" packs, without interstitial fluid (for example, Soria-Hoyo et al. (2008)). While this paper encourages the development of new ideas and the study of particle dynamics in more detail, it is based on only a handful of previous work on saturated media, which may in turn produce error as the topic has yet to be studied extensively.

There are deviations in the experimental setup that should also be addressed. It has been noted that the setup was not constructed with magmatic systems in mind, and hence the materials used do not exactly reflect the composition of a crystal mush. The largest deviation is the viscosity of the confining fluids used for each. In the tests, the fluid viscosity is from 19-60 mPa s, or 0.019-0.060 Pa s. General viscosities for magma range between 1-100 Pa s for basalt and 10^7-10^{10} Pa s for rhyolite (Lesher and Spera, 2015). Hence, the experimental viscosity is exceedingly small, though it is noted that synthesising real magmatic viscosity would be difficult. Because of this, it must be considered that the particles (i.e. crystals) within magma chambers may further be inhibited by these higher viscosities, as well as other factors such as chamber pressure. For the scope of this thesis, the viscosities remain suitable, but future work could place an emphasis on the deeper effects of chamber environment. From this uncertainty however, the question can be asked about how "strong" shaking must be to overcome high viscosity limitation, when considering the seismic waves which will act upon the chambers considered in this study. The strength and fluctuation of seismic waves is elaborated on in Chapter 5.

The particle sizes used in the experiments fit expected crystal sizes found in real magmas, though are on the small end of the spectrum, as crystals, especially phenocrysts as depicted in Stokes' Law settling, can be up to 5mm or more. Crystals will also have variable shapes, which is not taken into account by the particles used in the experiments, which follow Stokes' Law of settling spheres. Arbitrary shapes found in real crystals may affect the level of compaction achieved, so that it is not as neat as in the experimental findings.

Chapter 4. Results: seismic shaking of crystal mush

This chapter deals with the findings of this thesis and the applications to natural systems. This takes several steps. First, the analysis of the data as from de Richter et al. (2015) will be laid out, and conclusions drawn as to the relationship between granular pack oscillation and the level of compaction achieved, as well as the role of Stokes' Law in the compaction process. Second, Stokes' Law and the movement of particles within real magma chambers is explored. As a simplified rule-of-thumb, when a saturated particle pack is shaken, the particles within should reorganise to a compacted, more efficient structure. However, this reorganisation is subject to the Stokes' settling time of those particles as they work against their confining fluid (introduced in Chapter 2) and also the acceleration induced by the shaking itself, which can be defined by using the equation calculating the ratio of peak to gravitational acceleration, shown by Eq. 2.4 (Section 2.5.3). Conclusions from these experiments can then be applied to real magmatic systems.

4.1 Raw data from de Richter et al. (2015)

As outlined in Chapter 3, de Richter et al. (2015) sets out an experiment where a saturated granular pack is shaken, with the internal dimensions of the pack varying (viscosity, particle size), as well as the intensity of the shaking (represented by Γ). In Figure 4.1 (a), the raw data taken from this study is presented, alongside Figure 4.1 (b), where the same data has been scaled by the Stokes' timescale of the experiment, collapsing the data to a single curve that aids in our observations.

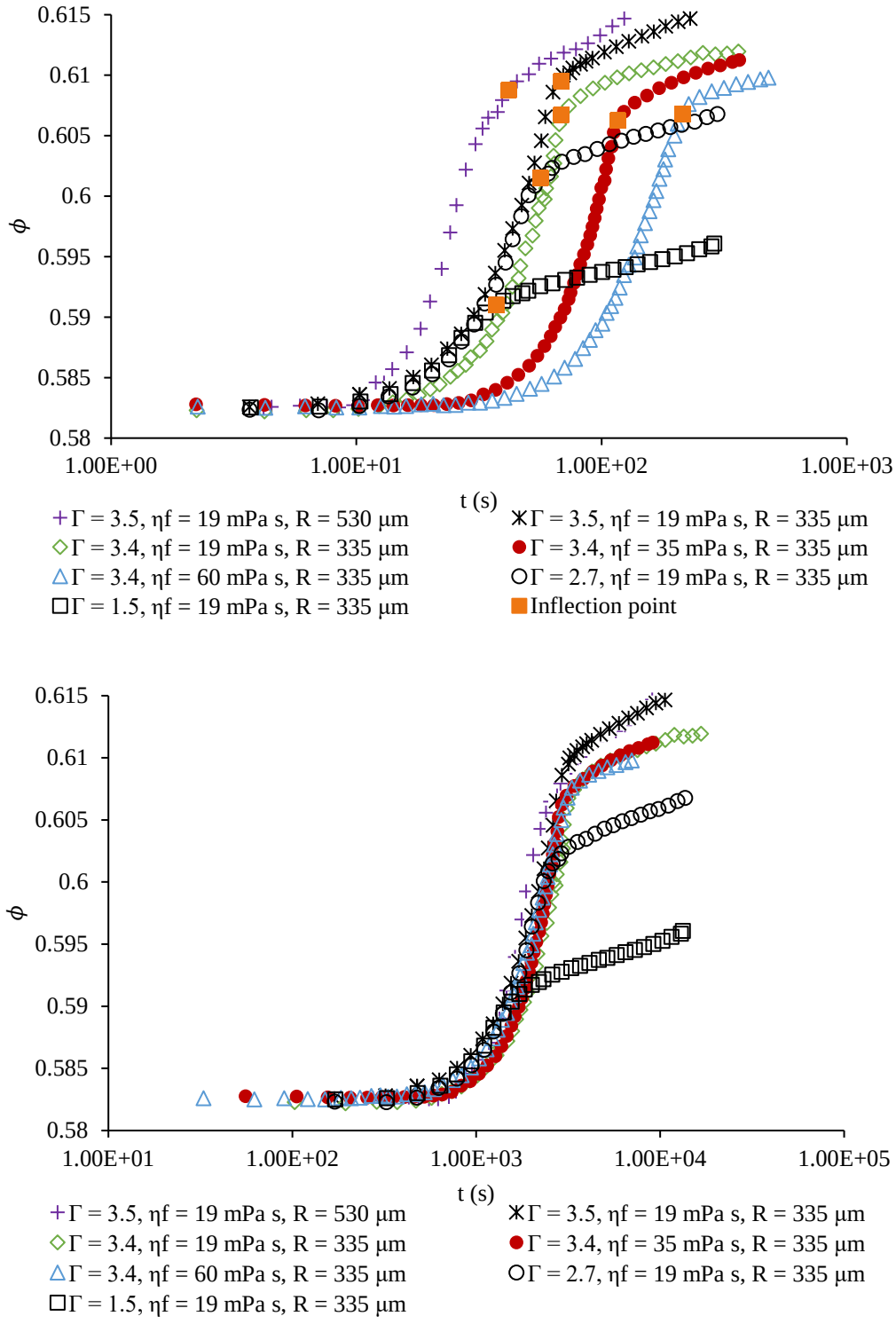

Figure 4.1 – (a) shows the raw data as taken from de Richter et al. (2015) and produced via the methods set out in this thesis (Chapter 3). Datasets with varying pack setup (fluid viscosity and particle size) and shaking parameters (indicated by Γ) are shown to increase to a higher-level compaction as they are shaken. Orange squares indicate the inflection point, where compaction changes from the first phase to the second. (b) shows the same data, collapsed to a uniform trend.

As shown in Figure 4.1, the shaking conditions of each experiment always feature Γ > 1. Using the arguments provided in Section 2.5.3, it can be assumed that when Γ < 1, there is not sufficient vibrational energy to allow for particle remobilisation when a pack is shaken. When Γ > 1, such as presented here, particles are remobilised, allowing for compaction of the grains within the pack.

Using Figure 4.1 (a), two conclusions can be drawn. First, the viscosity of the saturating fluid (η_f, presented hereafter as μ according to Stokes' Law) plays a controlling role in the first phase of each dataset, on the slope prior to the inflection point. Evidence for this is observed particularly well in the green, red, and blue datasets, where Γ (and therefore A and ω, the shaking conditions) is the same for each, with a value of Γ = 3.4. Particle radius was also constant, where R = 335 μm (0.335 mm). The variable parameter for these datasets was the viscosity, with values of μ = 19 mPa s (0.019 Pa s), 35 mPa s (0.035 Pa s) and 60 mPa s (0.060 Pa s). This viscosity determines the dataset trend position along the x-axis, shown in Figure 4.1 (a). The blue dataset, with the largest viscosity of 60 mPa s, requires more time for compaction (represented by packing fraction ϕ) to initiate. Tests with low viscosity will initiate compaction trends at a shorter timescale, such as the green dataset with a viscosity of 19 mPa s. However, the variation in the viscosity does not affect the ϕ reached, with each of these datasets producing an inflection point at ϕ = ~0.606. The level of compaction is not affected, but the timescale over which it is active is.

Second, the three black datasets show the effect of change in Γ value, while the pack composition is fixed at μ = 19 mPa s and R = 335 μm. As these values are equal across all three datasets, the position of the inflection point is therefore controlled by Γ. With the first phase controlled by viscosity, the second phase is determined by the shaking conditions.

Interestingly, the effects of Γ can be explored further between all the datasets. With low Γ, such as the black square dataset where Γ = 1.5, the first phase of compaction is reduced in comparison to datasets with higher Γ. Therefore, Γ must be significant to produce a higher level of compaction. However, while it is noted that Γ controls the inflection point ϕ value, it does not appear to control the maximum packing fraction (ϕ_f) that can be achieved by any given dataset. For example, the purple and green datasets both have similar Γ values, of 3.5 and 3.4 respectively. However, the ϕ_f reached during the second stage is different, despite the similarity in Γ. The purple dataset goes on to reach ϕ_f = ~0.615, while the green dataset tapers to ϕ_f = ~0.612. Maximum ϕ achievable is therefore likely controlled by a collection of parameters, rather than Γ alone. The purple dataset differs from others via the particle size, where R = 530 μm (0.530 mm).

In Figure 4.1 (b) we show the data from Figure 4.1 (a), but where we have performed a linear transformation of the x-axis values. That is, we have re-scaled the time values. The approach given here and shown in Figure 4.1 (b) is driven by an intuition that a pack of particles that is shaken in a viscous fluid should initially respond over times proportional to a Stokes' timescale on the particle scale. That is an intuition that can be tested empirically using the data in Figure 4.1 (a). It is also an intuition that is borne out by the above phenomenological analysis of the data – that the controlling effect on the viscosity is to retard the time over which the pack responds to shaking. To test this, we introduce a Stokes' time:

$$\lambda_s = \frac{R}{v_s} = \frac{9\mu}{2\Delta\rho g R} \qquad \text{[Eq. 4.1]}$$

In general, we can further state that the timescale of active compaction, where particles are reorganising, is proportional to the Stokes' parameters, due to the interaction and resistance between the fluid viscosity and particles as explained. This is captured by Eq. 4.2:

$$\lambda \propto \mu \text{ or } t \propto \frac{1}{R} \qquad \text{[Eq. 4.2]}$$

where λ is the time required for reorganisation, μ is the viscosity, and R is the particle radius. As the viscosity increases, time required for reorganisation (i.e. R/v_s) also increases, meaning high viscosity fluids will inhibit particles and they will take longer to settle. Furthermore, as particle size (R) increases, time for reorganisation (v_s) decreases, as large particles will settle quickly, though this is more effective in low viscosity magmas, where there is less resistance to particle movement. This can further be written as

$$\bar{t} = \frac{t}{\lambda} = \frac{2\Delta\rho g R}{9\mu} t \qquad \text{[Eq. 4.3]}$$

where $\bar{t}$ is the dimensionless time, as calculated via the parameters that feature in Stokes' Law (Eq. 4.1; Eq. 2.1). In Figure 4.1 (b) we show the results from Figure 4.1 (a) but where we re-cast the time axis as $\bar{t}$ in place of t. We find that the first part of the experimental results all collapse to a universal description, centred around $\bar{t} \approx 10^3$. The collapse of the data suggest that Eq. 4.3 captures the dominant physics occurring in the first part of compaction. The remaining variability after the inflection point appears to be controlled by Γ - the shaking characteristics.

These findings, and the Stokes' settling times for real-world magmas are calculated in Section 4.2. In Chapter 5 we then explore the Γ parameter, as first introduced in Section 2.5.3, and then apply it to the selected case studies of this thesis.

4.2 Stokes' Law in magmas

As introduced in Chapter 2 and recapped here for clarity, Stokes' Law is defined as:

$$v_s = \frac{2\Delta\rho g R^2}{9\mu} \qquad \text{[Eq. 4.4]}$$

where $\Delta\rho$ is the density difference, g is the acceleration (9.81 m/s), R is the radius of the crystal and μ is the viscosity of the melt. Using parameters on the right-hand-side of Eq. 4.4 ($\Delta\rho$, g, R and μ) we can produce estimates for v_s for magmas on Earth, utilising compositional data from melt inclusions, sourced from various

well-known locations and of basaltic to rhyolitic composition. $g = 9.81\ \mathrm{m.s^{-1}}$ is taken to be constant for magmas near the Earth's surface, while the other parameters are compiled from the chemical composition data. It is noted that *R* does not vary systematically as a result of composition; it is more associated with the time available for crystal growth, which varies for each volcano or scenario due to magma chamber geometries and conditions, as well as other factors. However, all parameters vary depending on the bulk composition of the magma in question, including the key crystallising phases, their densities and the bulk viscosity of the magma. For example, basaltic magmas may crystallise olivine predominantly (ρ_c= 3320 kg/m^3), while a rhyolitic magma's key phase could be quartz or feldspar (e.g. for quartz, ρ_c = 2650 kg/m^3). The density difference also applies to each melt type, with ρ_m= 2670 kg/m^3 for dry basaltic magma and ρ_m = 2360 kg/m^3 for dry rhyolite (Lesher and Spera, 2015). This then manifests as $\Delta\rho$ = 650 kg/m^3 and $\Delta\rho$ = 290 kg/m^3 for each, respectively.

These differences are important overall, but variations in viscosity (μ) appear to be more significant for determining the settling velocity. For example, viscosity for a dry basaltic melt may be 100 Pa s, but for a dry rhyolitic melt can be 10^{10} Pa s (Lesher and Spera, 2015). An increased viscosity could limit particle movement in a melt, hence the need to test a range of viscosities across the magma types.

This method using Stokes' Law can be applied globally, for a more detailed analysis and to compile data for v_s on Earth. Explored with the reasoning above, there is an apparent consistency for *R* and $\Delta\rho$ across the compositional spectrum. Hence, we can potentially identify that v_s may be a universal law across magmas on Earth, as proposed in a simplified version of Eq. 4.4:

$$v_s = \frac{A}{\mu} \qquad \text{[Eq. 4.5]}$$

where $A = 2\Delta\rho g R^2/9$ and is proposed to be constant. This law is important because crystal composition, size and melt properties are no longer required to constrain v_s, simplifying any further tests required. It is also useful for present and future projects that study and compare settling within magmas on other planets.

In order to test the possibility that there exists a universal form of Eq. 4.4 for magmas on Earth (e.g. Eq. 4.5), we applied the law to compositional data from the following eruptions/eruptive phases: Belknap (2635-1400 BP), Mount Washington (~300 ka) and North Sister (70 – 55 ka) volcanoes of the Cascade Range (Mordensky and Wallace, 2018; Hughes, 1982); the 1991 eruption of Mount Pinatubo (Borisova et al., 2005; Rutherford and Devine, 1999); Santorini (deposit age range of 184 ka to present, last eruption 1950) (Druitt et al., 2016; Cadoux et al., 2014; Barton and Huijsmans, 1986); the 1980 eruption of Mount St Helens (Rutherford et al., 1985; Blundy and Cashman, 2005; Melson, 1983); the 1996 eruption of the Soufriere Hills volcano (Devine et al., 1998; Barclay et al., 1998; Horwell et al., 2013; Shibano et al., 2012); Sakurajima (deposit age range 1471 – 1955) (Araya et al., 2019; Nakamura, 2006; Yanagi et al., 1991); Popocatepetl (deposit age range 1994 – 1998) (Atlas et al., 2006; Straub and Martin-Del Pozzo, 2001; Witter et al., 2005); and the Taupo Volcanic Zone (deposit age range ~340-0.7 ka; (Begue et al., 2014; Allen and McPhie, 2003; Cole et al., 2014; Gelman et al., 2013; Smith et al., 2005). A summary is available in Appendix A.

For each site listed above, we compiled information from which the parameter A can be found (Eq. 4.4). Information included:

- The magma storage temperature mostly calculated via mineral-melt thermometers (e.g. in the case of the Sakurajima eruption series, this was 950-970°C; (Araya et al., 2019)). Fe-Ti oxides were also calculated, alongside mineral-melt analyses (e.g. in the case of the 1980 Mt St Helens eruption, where temperature was 930°C; (Rutherford et al., 1985)). Temperature was used in the calculation of μ using Giordano et al. (2008) and ρ_m using Best (2003).
- The major element melt chemistry was estimated from glass compositions typically analysed using electron microprobe spot analyses. The major element chemistry is a direct input to the μ calculation using Giordano et al. (2008) and the melt density ρ_m using Best (2003).
- The dissolved water concentration in the melt was estimated from electron-microprobe analysis (EMPA), as well as Fourier transform infrared spectroscopy (FTIR) (e.g. for the Taupo Volcanic Zone analysis, H_2O was 4.4-4.8 wt.%; (Begue et al., 2014)).
- The dominant phenocryst phase mineralogy (e.g. in the case of the 1991 eruption of Mt Pinatubo, this was quartz; Borisova et al. (2005)). The phenocryst phase mineralogy was converted to a density ρ_c using standard densities (e.g. from Deer et al. (2013)).
- The crystal size R was estimated from photomicrographs of the phenocryst phases, or was reported directly (e.g. in the case of the Santorini eruption series, this was 0.5-2 mm; (Barton and Huijsmans, 1986; Druitt et al., 2016)).

4.2.1 Universality and the value of A

Figure 4.2 shows our results using the volcanic data compiled to investigate Stokes' Law. From this, we concluded that the crystal size (R) and the viscosity (μ) had the greatest effect on settling velocity. A higher μ meant there was less ability for the fluid (i.e. the magma) to flow, and in turn any particles settling through it would not be able to settle at great speed. It was also found that larger crystal sizes did increase the settling speed for all viscosities, but was particularly effective for low viscosity magmas. Reynolds numbers (Re) calculated for each dataset were < 1, implying the flow within these hypothesised conditions was laminar, and therefore turbulence could be disregarded. Large particles sizes did increase the Re number, but only by a small margin.

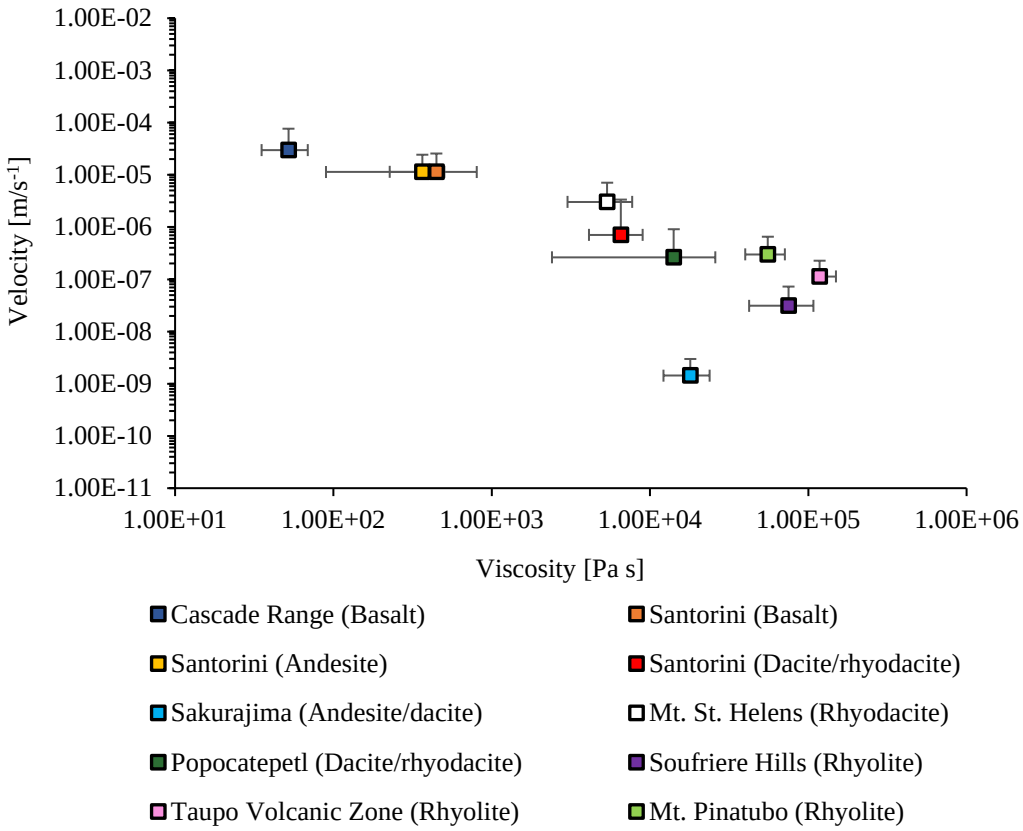

Figure 4.2 – Graph showing the relationship between viscosity of a magma in Pa s, versus the velocity of crystals settling within, using the averaged values of each dataset and determined by their melt inclusion (MI) compositions. A negative trend is shown, with basaltic MI compositions such as the Cascades basalt producing higher velocities in accordance with lower viscosity magma. The opposite can be said for rhyolitic MI examples like the Taupo Volcanic Zone, where a lower settling velocity is found for crystals in a higher viscosity magma.

4.3 Application to magmatic systems

By combining Stokes' Law and Γ, which summarises the shaking parameters, the total percentage of compaction can be calculated, i.e. the initial packing fraction can be taken from the final packing fraction, to produce a percentage of reorganisation that directly translates to the percentage of melt removed from the interstitial space of the pack. This then can be applied to mush bodies, where a certain percentage of melt can be removed under seismic shaking. This simple calculation is constructed as $\phi_i - \phi_f = melt\ expelled \times 100$, which results in a percentage of expulsion. Given by Figure 4.1, initial packing fraction (ϕ_i) was 0.585, with final packing fraction (ϕ_f) reaching a maximum of 0.615. Hence, the melt expulsion achieved in the conditions of the experiments by de Richter et al. (2015) is ~3%. Theoretically, this can be applied to mush bodies and the volumes of mush contained, to determine an approximate volume of melt expulsion under shaking from those bodies. However, as noted in Section 1.1, exact volumes of mush reservoirs are difficult to determine, due to issues with the resolution of methods such as seismic tomography (Lees, 2007), though methods such as InSAR and gravity surveys may provide clarity. Some volumes have been constrained, such as for Laguna del Maule, which has an approximate mush volume of 115 km^3, with a 30 km^3 melt-dominated

zone within (Wespestad et al., 2019; Singer et al., 2018). If the ~3% extraction is applied, around 3.45 km^3 of interstitial melt may be removed via seismic shaking. However, this is likely inaccurate due to the variation of packing fraction and interstitial melt content in different parts of the reservoir so that extraction is not consistent, the melt-dominated zone already present which indicates a region of efficient melt segregation without seismic forcing (Miller et al., 2017), and the influence of other processes already occurring, which are not accounted for. This extraction value can only be used as a general estimate, but opens up future exploration should more accurate reservoir volumes become available.

When investigating whether a mush body will compact under the dynamic stress of passing seismic waves, acceleration data can be used to calculate the Γ at distances between the source of the earthquake, and the volcano associated with that event. In plotting the variation of Γ across distance, it can be determined at what distance the acceleration of ground motion is significant enough for particles to remobilise and for increased melt extraction to occur within chambers under the volcanoes featured in the case studies of this thesis. If these volcanoes lie within this distance boundary of significant acceleration, the role of seismic forcing may then become relevant in the eruptions associated with the earthquake events to be studied. If they do not, then the role of seismicity in volcanic triggering may therefore be extremely minor, or largely insignificant.

Chapter 5. Discussion

As determined by the methodology and results set out in Chapters 3 and 4, the results can now be placed within the context of natural volcanic scenarios. In this chapter, the discussion focusses on whether the findings – where $\Gamma > 1$ is indicative of particle reorganisation and successive melt extraction through compaction – are applicable to natural systems and how they fare alongside other proposed mechanisms that may trigger volcanic activity during or as a result of earthquake shaking. They have been applied to case studies where volcanism was supposedly the result of high-magnitude earthquake events, and the relevance of the melt extraction mechanism using Γ is critically analysed.

5.1 The dimensionless acceleration Γ

The radiation of seismic waves through the heterogeneous crust is complex. Interactions between seismic waves and layered stratigraphy of variable lithologies or porosity and partially molten bodies such as found in the interior of active volcanoes, can result in non-uniform wave behaviour that is difficult to predict (Aki, 1980; Carcione et al., 2020; Lay and Wallace, 1995a). Central to this thesis is the question: can a seismic wave be sufficiently strong to induce crystal movements in a magma mush body? The consequence of crystal re-organisation is melt liberation. But in order to answer this question, we must define what we mean by "strong" in the context of shaking. This was introduced in Section 2.5.3, where the shaking of mush was proposed as a mechanism for melt extraction from the crystal framework, to produce volatile and eruptible rhyolitic 'caps' at the top of a mushy storage region. Eq. 2.4 in that section defines the dimensionless ratio of peak acceleration to gravitational acceleration as Γ (repeated here for clarity):

$$\Gamma = \frac{A\omega^2}{g} \qquad \text{[Eq. 5.1]}$$

where A is the wave amplitude (with dimensions of length), ω is the angular frequency (with dimensions of inverse time) and g is the gravitational acceleration, where we take $g = 9.81\ \mathrm{m/s^2}$ for the upper crust of the Earth. As previously noted in Section 2.5.2, the amplitude and frequency of seismic waves can vary greatly, and also decay over time and distance travelled (Lay and Wallace, 1995a; Campbell and Bozorgnia, 2003; Midorikawa, 1993; Edwards et al., 2011; Crowell et al., 2013; Frankel, 2015). It is clear from the experimental analysis that the dynamics of particle movements in viscous fluids can be extremely sensitive to Γ – controlling both the total amount of particle pack reorganisation (i.e. controlling the final particle volume fraction that is reached, ϕ_f) and the transitions in the dynamic regimes. Even more fundamentally, Γ controls whether or not crystals may move at all. If $\Gamma \ll 1$, then the accelerations induced by seismicity are less than those imparted by gravitation, and therefore crystals will not move in response to seismic shaking. However, if $\Gamma \gg 1$, then we assume that the seismic accelerations overcome gravitational acceleration and may induce crystal migration, movement, and reorganisation. While de Richter et al. (2015) did not cross the boundary $\Gamma = 1$ in their experimental work (their experiments are exclusively at $\Gamma > 1$), they did perform experiments as low as $\Gamma =$

1.5, which is within an order of magnitude of $\Gamma = 1$ and particles still moved. Therefore, we might reasonably take $\Gamma = 1$ to be a critical value controlling the dynamic switch between crystal reorganisation ($\Gamma > 1$) and no crystal reorganisation ($\Gamma < 1$). However, when plotting the particle fractions achieved (ϕ_f), the data show a trend that could possibly be extrapolated down, so that ϕ_f may in fact change even when $\Gamma \gtrsim 0.2$ (Figure 5.1), as above this point, the packing fraction may increase above the initial (red line on graph). Therefore, $\Gamma > 0.2$ may be significant, but the reorganisation will be limited and therefore have less impact on compaction and subsequent expulsion of liquid from the pack. The fact that a regime transition does not sit exactly at a dimensionless variable of unity is reminiscent of other dimensionless variables such as the capillary number where the regime boundary occurs between 0.1 and 10 of that dimensionless group (Llewellin et al., 2002). The task here then is to place constraint on Γ for some large earthquake events on Earth, and determine at what distances from source the shaking is significant.

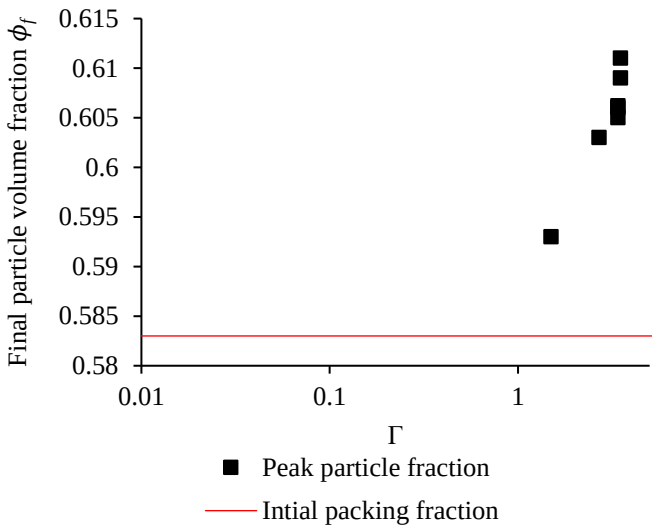

Figure 5.1 - The final packing fractions (ϕ_f) of the experiments by de Richter et al. (2015). The data appears to show a trend, which may imply that (ϕ_f) approaches the initial ϕ as Γ is reduced from $\Gamma > 1$ to around $\Gamma = 0.2$. This may lead to $\Gamma > 0.1$ being indicative of particle remobilisation, where a final particle packing fraction above the initial (red line) can be reached, but confirmation of this in the region $0.2 > \Gamma > 1$ would require further experimentation.

5.2 Basic properties of large seismic waves

The properties and behaviour of seismic waves is complex and highly dependent on parameters such as earthquake magnitude, regional geology through which the wave propagates, including partially molten bodies, and the heterogeneities the wave will encounter, where wave energy attenuates due to geometrical spreading, scattering, and reflection off of boundaries (Lay and Wallace, 1995b). The variability in seismic motion also depends on fault properties, such as directivity and rupture velocity and length, further complicating the movement and acceleration of seismic waves through the crust (Graizer and Kalkan, 2007; Udías, 2000a). Usefully, much of the variability in the source is captured by the seismic magnitude M_w, such that roughly speaking, the packet of frequencies and amplitudes of the full wave train will scale with M_w, and M_w can be estimated readily from seismology measurements. As outlined in Section 2.5.2, body waves (P and S) are the waves on which this project focusses. When determining how shaking via seismic waves affects partially molten bodies within the Earth's crust, the variability of these waves must be accounted for, as no two earthquake events are the same.

In order to estimate Γ, one could find estimates of ω and A independently and use those to compute Γ. In practice, the linear frequency of a wave is usually given as f, which is related to ω via $\omega = 2\pi f$. An alternative approach would be to find the accelerations induced by seismic waves α, which can be measured by seismologists, and to assume that an equivalent definition of Γ is $\Gamma = \alpha/g$. Here both options will be explored, however, we can immediately note that while f is often reported, A is only poorly constrained, which may render constraint of α more tractable for any pursuit of Γ. A full 'packet' of a seismic wave is called a 'wave train' and is composed of a continuum of frequencies. Fourier analysis of a full wave train can be used to pick out dominant frequencies (Lay and Wallace, 1995d). Similarly, a wave train is composed of a range of amplitudes of motion. As waves radiate from a source in three dimensions, the amplitudes of the wave decays, as well as the frequencies (discussed below). Therefore, it is immediately clear that if a given earthquake can indeed induce shaking at $\Gamma > 1$, as the seismic wave train radiates, Γ will fall below $\Gamma = 1$ at some distance from source. This may mean that a magma body's distance from a large seismic event is a first order control on the propensity for magma shaking to induce crystal movements. A first point of interest is the radiation and decay rule for seismic wave trains.

With distance from source, amplitude decays. The simplest decay law is known as the 'inverse square law' where $A(R) \propto 1/R^2$ (Voudoukis, 2017; Bullen and Bolt, 1985b). This decay law is general, and governs the decay of a wide range of waves that radiate into 3-dimensional space. Most famously, this decay law governs how light spreads out from a source, and can explain how lights appear dimmer the farther away from them an observe stands (Uthe, 2004). In the context of seismic waves, while the amplitude decay appears to follow a law that does have the general form $A(R) \propto 1/R^b$, measurements do not necessarily yield $b = 2$ as the exponent (Lay and Wallace, 1995a). Manga and Brodsky (2006) propose that $b = 1.66$, whereas Edwards et al. (2011) showed that $b = 1.1$ in the first 70 km from source, $b = 0.4$ for the 70-120 km interval, and $b = 1.4$ in the far field at >120 km. That analysis makes it clear just how variable crustal heterogeneity might be, and how it governs the attenuation factor. In Figure 5.2, the law with $b = 1.66$ is given. Specifically plotted is the function $A/A_0 = k/R^b$, where A_0 is the peak amplitude at the source itself, and k is a dimensional constant that appears simply to render the equation dimensionally consistent. We take $b = 1.66$ (Manga & Brodsky, 2006) and $k = 1$. We note that A_0 is largely unknown but would be the parameter that varies with M_w.

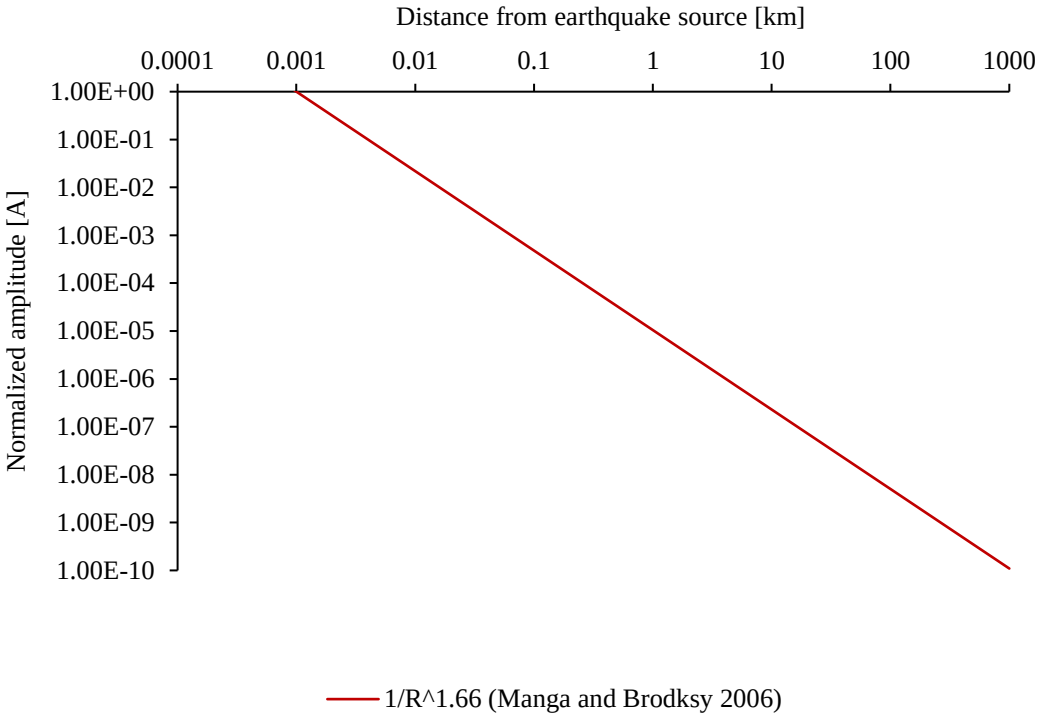

Figure 5.2 – Graph showing a simple normalised decay relationship as highlighted by (Manga and Brodsky, 2006), where amplitude (A) decays over distance.

In understanding how the amplitude varies with distance and magnitude, the effect of high-amplitude shaking can be discussed when a crystal mush body is placed within the vicinity of an earthquake capable of reorganising the crystal framework within that mush, leading to compaction, melt expulsion, and possible eruption. Figure 5.2 emphasises the importance of understanding how far from a seismic source a volcanic system is. A clear conclusion here is that seismic amplitude is difficult to constrain, and that even if the decay pattern is well understood (Figure 5.2), the missing value is A_0 – which is crucial to understanding if Γ is greater than unity, or not.

Similar to the seismic amplitude, seismic waves function over a wide range of frequencies. They can be as low as 3 x 10^{-4} Hz (Lay and Wallace, 1995c), up to >100 Hz, such as on March 9, 2017, where a M_w 4.7 earthquake occurred north of Moloka'I, Hawaii, with frequencies up to 165 Hz (Butler, 2018). Very low frequency earthquakes (VLFEs) have been explored, with typical frequencies 0.01-0.1 Hz (Masuda et al., 2020), such as at Nankai Trough, Japan (Ito and Obara, 2006) and Cascadia in north Washington, United States (Ghosh et al., 2015). The frequencies of waves that will result from tectonic or volcanic earthquakes are within the region of 5-15 Hz for high frequency (HF) events, and 1-5 Hz for low frequency (LF) events (McNutt and Roman, 2015). An example would be the Maule earthquake in Chile in 2010, which had frequencies ranging between 1 and 6 Hz (Boroschek et al., 2012; Boroschek and Contreras, 2012). These waves will propagate through a wide range of lithologies, rheologies, and will encounter geological interfaces such as fractures, faults and fluids. Hence, the waves will attenuate and the frequency content may change during propagation (Shearer, 2009; Kennett, 2001). Low-frequency waves have longer wavelengths and attenuate less over longer distances, whereas high-

frequency waves generally attenuate more rapidly over short distances (Dalton and Ekström, 2006). The relation between wave parameters such as velocity, frequency and wavelength is simple, where $velocity = frequency \times wavelength$. An example is given by Lay and Wallace (1995c) shows that, at a velocity of 5 km/s, a wave with a frequency as low as 0.0003 Hz will have wavelength of 15,000 km. Using this example, where velocity is 5 km/s and frequency is 0.1 Hz, wavelength is 50 km, indicating that for a fixed wave velocity, as the frequency increases, the wavelength will decrease and undergo greater attenuation. When considering the effect of seismic waves on volcanic plumbing systems, previous work in this field indicates that triggering of magma movement/eruptive activity can occur over great distances (Linde and Sacks, 1998; Manga and Brodsky, 2006). Hence, low frequency waves are more suitable for this study, as they will propagate further, though it is noted that the dominant frequency content is not known exactly due to the highly variable nature of these waves and the scope over which they work.

When solving Eq. 5.1, we can apply example displacement amplitudes (A), such as P_d, which is the initial peak displacement amplitude, and the frequency ranges outlined above. P_d varies widely and is used within Earthquake Early Warning (EEW) systems in various locations, such as Taiwan, Japan, Mexico and Southern California (Allen et al., 2009; Wu and Kanamori, 2005), to determine the magnitude of a rupture to warn nearby populations. As shown in Figure 3 of Wu et al. (2007), where P_d was ~0.001-0.1 cm for earthquakes in southern California, and ~0.01-10 cm in Taiwan, highlighting the variance. Crowell et al. (2013) uses four case studies in Figure 1 of their paper, which shows the displacement associated with P_d in displacement (cm) versus seismogeodetic data and strong motion data. For the M_w 5.4 Brawley earthquake, displacement is within 1-5 cm at 11 km from the source. The largest earthquake, the M_w 9.0 Tohoku-oki earthquake, showed displacement of around 2.5 cm, at a distance of 233 km from the source. While this value appears low for such as high magnitude earthquake, the distance should be noted – even after travelling more than 200 km, the P_d detected at this point was still high. If it had been detected closer to the source, it is likely the displacement would be even higher. Furthermore, Figure 2 of Crowell et al. (2013) shows that P_d decreases with distance for all earthquake magnitudes, though it saturates and overlaps at high magnitude, so that high-magnitude values may be underestimated.

When calculating Γ using Eq. 5.1 and the P_d values for the events given by Crowell et al. (2013), $\Gamma = 0.0004$ at a low frequency of 0.1 Hz, up $\Gamma = 5$ at 5 Hz for the Brawley event, and $\Gamma = 0.001$ up to 2.5 for 0.1 to 5 Hz respectively, for Tohoku-oki. As noted, the displacements here are variable with distance, and only wide ranges can be calculated due to the variance of parameters such as frequency.

With these factors in mind, it can be concluded that the parameters A and f are highly variable and therefore it becomes difficult to use them as part of the scaling analysis here, though not impossible, particularly when considering low frequency events where wavelength is sufficiently low to act over the distances between earthquake sources and volcanic features. The analysis can be simplified by utilising the acceleration α, as outlined next.

5.3 Peak ground acceleration as a proxy for peak accelerations?

As highlighted in Section 5.2, Γ can be explored via two methods. As set out in Eq. 5.1, the amplitude (maximum displacement) and frequency calculate the acceleration of the wave ($A\omega^2$). However, there are issues in the acquiring of these values, and how they decay with distance (Section 5.2). Displacement is rarely recorded, and it can be presumed difficult to compute or take from seismometer/accelerometer readings as they require computation (Bullen and Bolt, 1985b). Furthermore, frequency is measured in the range of 0.1 Hz up to around 5 Hz or more (VLFEs and LF events as noted in Section 5.2; Masuda et al. (2020); McNutt and Roman (2015)), and is variable within individual events, such as the 2010 Maule earthquake (Boroschek et al., 2012; Boroschek and Contreras, 2012). Hence, calculating Γ via Eq. 5.1 has drawbacks due to these issues. As proposed in Section 5.2, $A\omega^2$ can be supplemented by a wave acceleration value taken directly from accelerometer readings, which eliminates the need to find uncertain displacement and frequency values when calculating Γ. These wave accelerations (α) can use peak ground acceleration (PGA), thereby redefining Eq. 5.1 as

$$\Gamma = \frac{\alpha}{g} \qquad \text{[Eq. 5.2]}$$

Significant earthquakes with moderate to large magnitudes show that peak ground acceleration (PGA) can reach values that exceed $\Gamma = 1$ within the near-field zone around the rupture (Udías, 2000b). Example localities where earthquakes with $\Gamma > 1$ have been found include the Himalayas, which frequently experience high-magnitude earthquakes where PGA can be expected to exceed values in the range $1 \geq \Gamma \geq 1.5$ close to the rupture zone based on comparisons of previous earthquakes that have occurred there (Parvez et al., 2001), and also the M_w 6.9 Iwate-Miyagi Nairiku 2008 earthquake in Japan, where PGA up to $\Gamma = 4$ was recorded approximately 3 km from the epicentre, the highest PGA recorded to date (Yamada et al., 2009). With increasing magnitude, initial PGA increases; using the collated USGS Atlas Shakemap, two earthquakes studied as part of the case studies within this thesis are the 2006 M_w 6.3 Java earthquake, and the 2004 M_w 9.1 Sumatra-Andaman earthquake. For the Java earthquake, PGA close to the epicentre was $\Gamma = 0.5$, while for the Sumatra-Andaman earthquake, stations close to the epicentre recorded a PGA of $\Gamma = 0.9$ (USGS, 2020a; f), indicating acceleration variance between earthquake magnitudes.

To find a wide range of PGA values, we can explore the USGS Shakemap Atlas online tool, which provides catalogues of PGA and P_d. For several target earthquakes associated with suspected volcanism, horizontal PGA values were extracted from the seismic stations relevant to the target area and their epicentral locations plotted in GoogleEarth™, to determine the distances of those stations from the rupture zone and the involved volcanic centres, showing how the PGA decayed away from the epicentre (USGS, 2020a; b; c; d; e; f; g). The PGA values are typically reported in factors of g, which we note is identical to Γ. Therefore, when quoting dimensional accelerations in m/s^2, we can use PGA $= \Gamma(g)$. These compilations of PGA data are discussed in Section 5.4.

5.4 Case Study earthquakes associated with volcanic activity

The calculation of the Γ parameter was carried out for all case studies, as shown in the subsections below. For each, the accelerations were analysed, especially where $\Gamma > 1$, with particular attention paid to the seismic stations located closest to the volcanic centre being studied. The point at which $\Gamma > 0.2$ was also noted, as a lower bound of interest (see Section 5.1). While this application is broad, the aim of this project is to determine whether shaking can be a mechanism for eruption triggering.

Each case study has been chosen based on its level of knowledge in the scientific community, the amount of data available, the time between the earthquake event and eruptive activity, and the magnitude, as this project is particularly interested in the effects of high-magnitude earthquakes on volcanoes, which according to the literature appear to be more attributed to cases where apparently-triggered volcanism has occurred. The PGA data was obtained using the USGS Shakemap Atlas, where data from multiple sources has been collated into one highly accessible and visual tool. The Shakemaps used are available in Appendix B. Distances between localities have been calculated in GoogleEarth™. In each section, a description of the event is given, as well as the PGA range recorded. Γ values noted in each description are also available together in Figure 5.3 (a-d) below, and summarised in Appendix C. This section is then followed by the application of Γ to melt extraction for each of these locations.

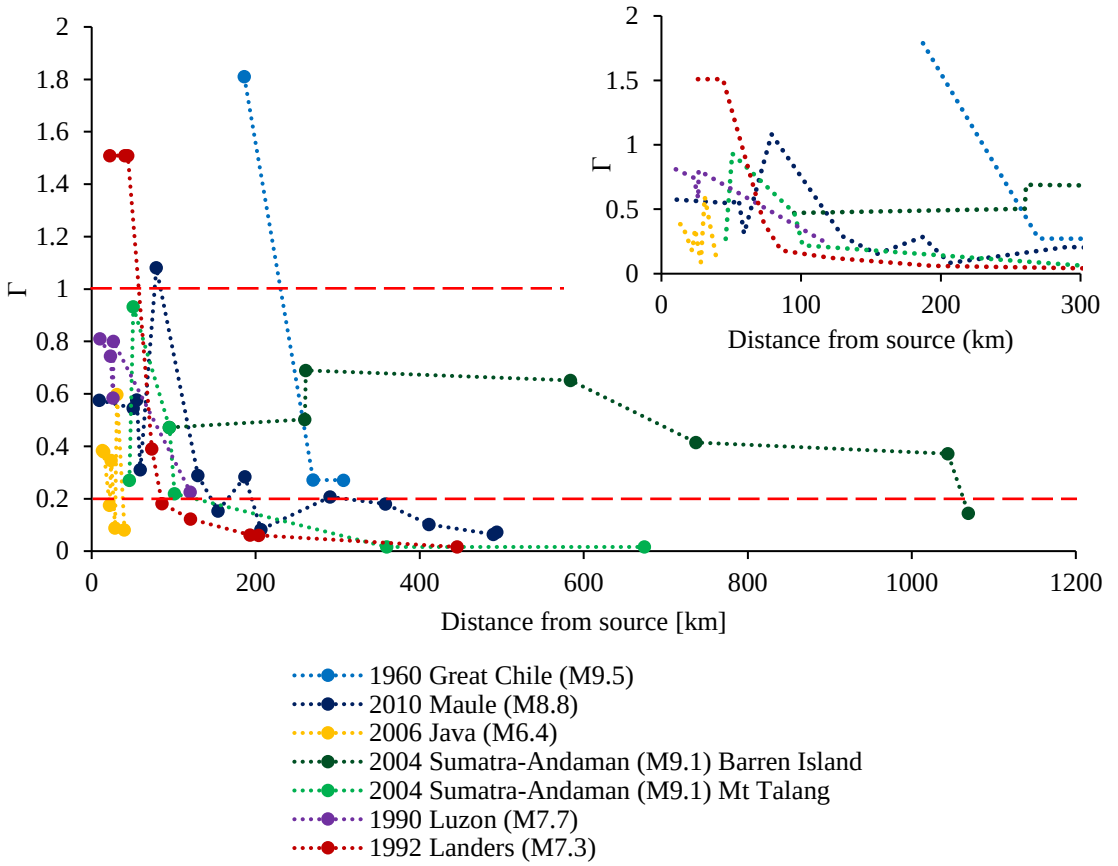
Γ
Distance from source [km]
Distance from source (km)
1960 Great Chile (M9.5)
2010 Maule (M8.8)
2006 Java (M6.4)
2004 Sumatra-Andaman (M9.1) Barren Island
2004 Sumatra-Andaman (M9.1) Mt Talang
1990 Luzon (M7.7)
1992 Landers (M7.3)

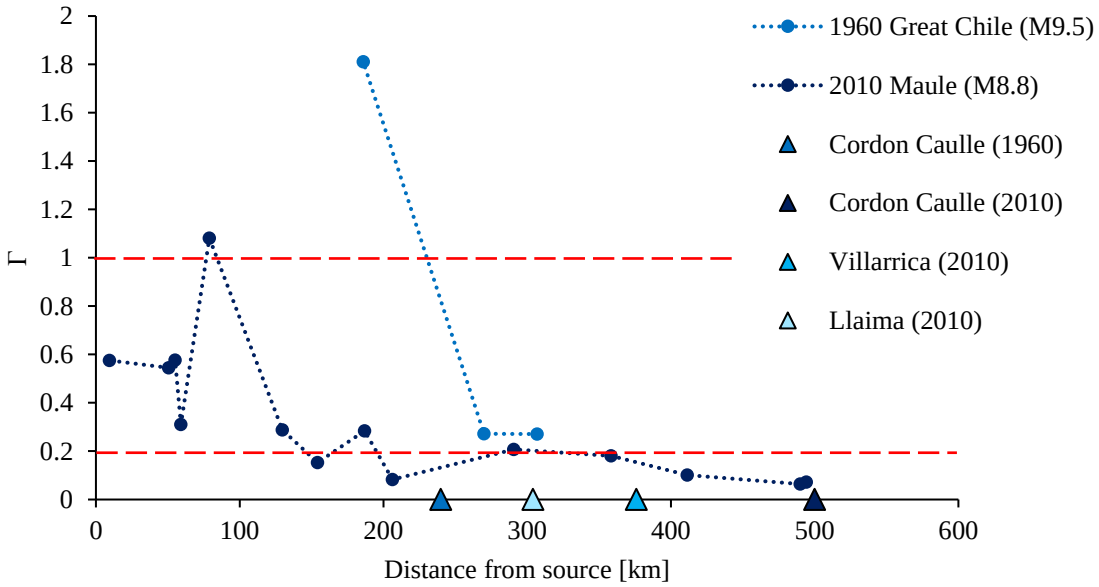
Γ
Distance from source [km]
1960 Great Chile (M9.5)
2010 Maule (M8.8)
Cordon Caulle (1960)
Cordon Caulle (2010)
Villarrica (2010)
Llaima (2010)

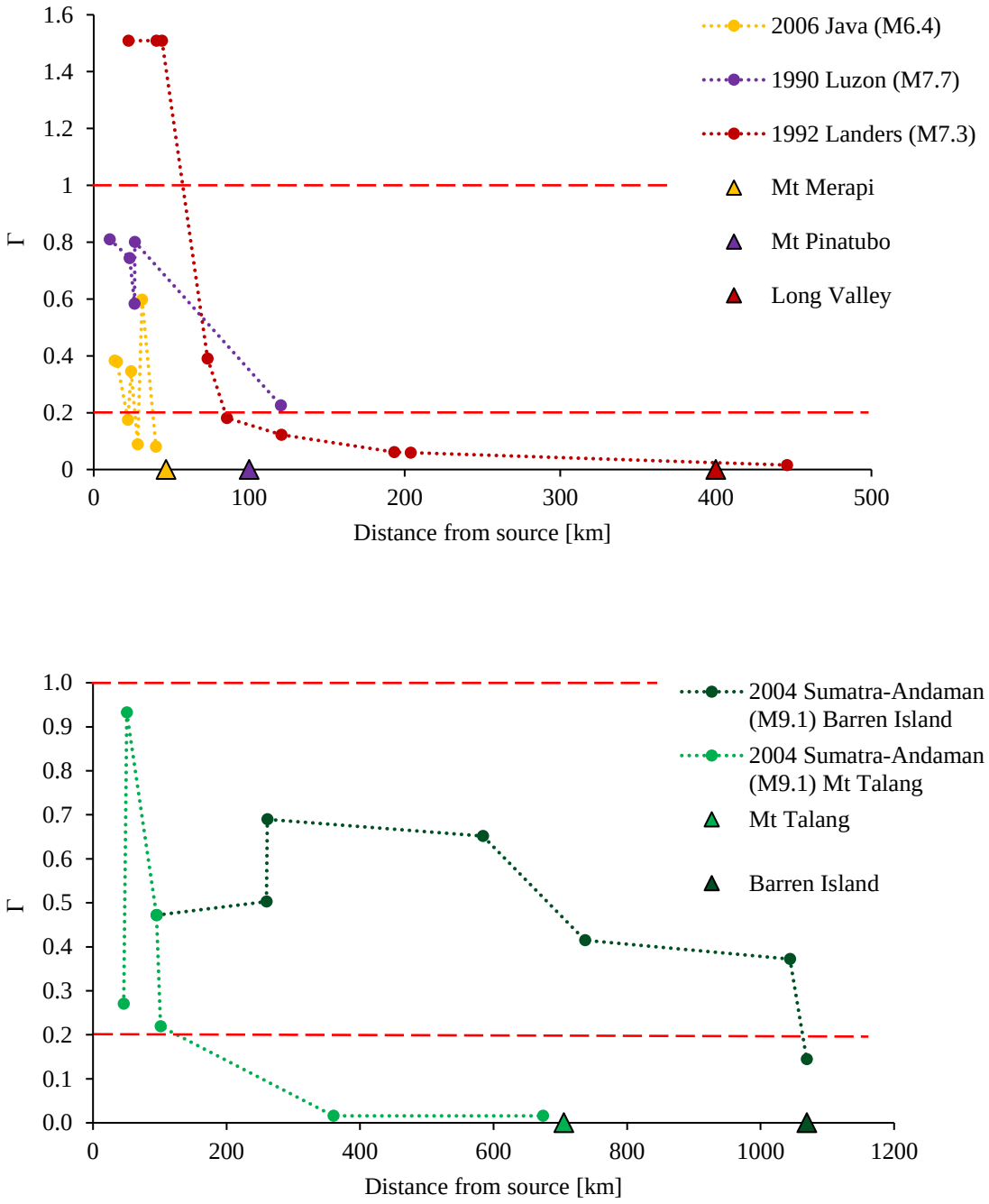

Figure 5.3 – A series of graphs showing the Γ values decreasing with distance. As shown, the decay does not appear to follow a single decay relationship, potentially due to regional geology affecting wave attenuation. Graph (a) compiles all case studies, with inset graph zooming in on a 300km boundary, where much of the attenuation appears to occur. Graph (b) shows the 1960 and 2010 earthquake events in Chile, with coloured triangles showing the location of the respective volcanoes from the source. Graph (c) shows events for the Java, Luzon and Landers earthquakes, with their respective volcanoes, and graph (d) shows the same for the Sumatra-Andaman earthquake, the attenuation of which appears to have occurred over a greater distance. The M_w 8.7 2005 event is not shown on the graphs due to insufficient data. The bracket in which Γ indicates enough energy for particle movement ($2 \geq \Gamma > 1$) is indicated with red dashed lines.

5.4.1 Case Study: The Java earthquake of 2006, and Mount Merapi

Mt. Merapi in Java has often been at the centre of studies surrounding external forcing on volcanic bodies (Walter et al., 2007; Richter et al., 2004), and has a detailed witness history, where earthquakes have been regarded to produce or coincide with increased volcanic activity (Voight et al., 2000). As a highly active volcano prone to long eruptive cycles, it has been considered in this thesis due to its coupling with the major earthquake of 2006, and due to its close distance to the rupture zone of this event.

The earthquake in Java occurred on May 26, 2006, located close to Yogyakarta. There has been debate over which fault line was central to the rupture, but analysis revealed a rupture zone approximately 10km east of the Opak fault (Kawazoe and Koketsu, 2010; Tsuji et al., 2009). The M_w 6.4 event was situated ~50 km from Mt. Merapi, which was showing activity at the time of the earthquake. A 72-hour lag occurred between the events. According to Walter et al. (2007), the earthquake promoted dome-building activity at the time, as well as collapse. They remark a daily dome growth of around >150,000 m^3. Harris and Ripepe (2007) note an increase in the heat and volume flux at the volcano three days after the event, which then lasted a further nine days. Shaking duration was of around 60 seconds, and a fault rupture length of about 20 km has been proposed (Elnashai et al., 2007).

Using the USGS Shakemap tool (USGS, 2020a), a series of stations were selected between the epicentre and Mt. Merapi to calculate Γ. The station closest to the epicentre was approximately 13.5 km north-west, where $\Gamma = 0.383$. Meanwhile, the station most distant from the rupture and closest to Mt. Merapi, at a distance of 7 km to the volcano (or 40 km from source), recorded $\Gamma = 0.081$. As discussed previously, the PGA, and therefore the calculated Γ, decreases with distance from the rupture, with the relatively low values also correlating with the moderate magnitude of this event. Over a distance of around 26.5 km, the acceleration had decreased by ~0.3. Interestingly however, at a midpoint between the two features (18.6 km from the volcano and 31 km from source), the acceleration increased to $\Gamma = 0.598$. The reason is uncertain, but it may refer to the variability indicated by Edwards et al. (2011), due to crustal heterogeneity and variations in regional geology. Besides this, it decreases according to the attenuation discussed previously. First analysis of these accelerations, presented in Figure 5.3 (c), indicates that they are highly variable at this location, even within very short distance of the rupture zone. Regional geology and a lower magnitude may help to explain this. At the volcano, around 50 km from the source, $\Gamma < 0.2$, implying there acceleration is not sufficient for the particle reorganisation mechanism explained, even within this short distance.

5.4.2 Case Study: The Luzon earthquake of 1990, and Mount Pinatubo

This case study was selected due to the high magnitude of the contributing earthquake, and the 9-month time gap between the event and volcanic activity at Mt. Pinatubo in 1991. This time gap is problematic however, as with longer periods of time between events, it becomes harder to truly know if they are related at all. The Luzon earthquake has been included in this study to explore if there could be a plausible connection in the context of near distance, but delayed, triggered volcanism.

The Luzon earthquake struck on July 16, 1990. The M_w 7.7 event's source was ~100 km northeast of Mt. Pinatubo, along the Philippine Fault with a total rupture length of 100-125 km in a predominantly north-west direction, with a speed of 2.7-2.8 km/s. Shaking occurred for 30-35 seconds (Yoshida and Abe, 1992; Velasco et al., 1996; Bautista et al., 1996). While the connections between the event and the eruption of Mt. Pinatubo on April 2 1991 are not strong, Bautista et al. (1996) summarises the likelihood and what mechanism may have been at play. They propose that compression, induced by the seismic shaking or by stressed and activated local faults, may have allowed the movement of molten basalt up into the dacitic chamber, causing unrest. This stress, predominantly static, correlates with the relatively short distance between the localities. Immediate activity is comprised of low-magnitude aftershocks around the volcano, with a M_w 4.8 event occurring mere hours after the Luzon event, originating approximately 10 km away from the dome at the volcano summit. Other small events followed, but they were few. Most aftershocks associated with the earthquake occurred to the north and northwest of the rupture zone (Yoshida and Abe, 1992). However, the study by Bautista et al. (1996) proposes more questions that it can answer, and concludes that a connection between the two events is 'plausible', but in need of a considerable amount of analysis.

Using the USGS Shakemap Atlas, PGA was obtained for several stations concentrated around the rupture zone (USGS, 2020c). Most stations were within 30 km of the fault, where Γ varied between 0.5 and 0.8, as expected based on the observations of wave attenuation over distance. The station closest to the rupture, at a distance of 10 km, gave $\Gamma = 0.810$. There are few points available within short distance of the volcano. The closest station was 80 km away from the volcano, to the northeast. Another nearby station was 89 km away, to the southeast within the city of Manila. At these stations, $\Gamma = 0.584$ and $\Gamma = 0.226$, respectively.

These values are significant despite not surpassing 1. The recorded PGA 80 km from the volcano is approximately 26 km from the source, directly to the southwest, and therefore falls within the 30 km boundary where Γ is sufficient. Between this zone and the most distant station in Manila, 120 km south of the source, the acceleration had decreased by ~0.6. As Mt. Pinatubo is ~100 km from the source, it can be expected that acceleration around the volcano may be around 0.3 (Figure 5.3 (c)), which may support shaking being "strong" enough to induce minor changes within the volcano via particle remobilisation, even if the effect is delayed, as the minimum boundary for sufficient particle remobilisation is $\Gamma = 0.2$.

5.4.3 Case Study: The Sumatra-Andaman earthquake of 2004, and links to Mount Talang and Barren Island

This case study is controversial, with few authors proposing a connection between the rupture of 2004 and the activity at both Mt. Talang and Barren Island in 2005. However, due to the directivity of the rupture zone, the sheer magnitude of the earthquake, and the many PGA values collected over the long distance, it should also be included in this study as an example of distant and delayed potential triggered volcanism. The links between the rupture and activity have been summarised by Walter and Amelung (2007), where southward stress transfer caused successive earthquakes that may have triggered Mt. Talang, particularly after the M_w 8.7 Nias-

Simeulue earthquake in March 2005, with activity at Mt. Talang less than two weeks later. Barren Island also showed activity, and the region had many aftershocks. For Mt. Talang, the PGA values of both the main rupture in 2004 and the 2005 rupture were explored, to understand whether the aftershock, which occurred closer to the volcano, had a greater effect. However, the 2005 event only provided two stations at a great distance (300-400 km) from the volcano, so the values calculated do not convey the trend of decay reliably. For Barren Island, the accelerations for the 2004 event are critiqued only.

The Sumatra-Andaman earthquake occurred on December 26, 2004. It registered as M_w 9.3, and had world-wide implications due to its sheer size, including a tsunami. Park et al. (2005) states that, within 21 minutes of the rupture, all points on the Earth's surface were vibrating. Shaking durations vary from ~500 seconds, up to >1000 seconds. The long period of shaking is derived from the rupture speed fluctuation across segments of the fault, between slow- and fast-rupturing speeds of as low as 1.3 km/s up to >3.0 km/s, (Ishii et al., 2007; Banerjee et al., 2005), such as described by Ammon et al. (2005), where the first 40-60 seconds showed slow rupture, before speeding up. The very large magnitude and long duration of this event is testament to the regional tectonic setting, with convergence along the Sumatra Trench between the Indo-Australian Plate and the Eurasian Plate (Lay et al., 2005; Sørensen et al., 2007). Visual representations of the rupture and the energy produced, as well as the northward directivity, are available in Figure 3 of Ishii et al. (2007). The M_w 8.7 Nias-Simeulue earthquake was directly south of the 2004 event, along a ~400 km rupture of the Sunda megathrust (Briggs et al., 2006). Like the 2004 event, rupture velocity varied with a range of 1.5-2.5 km/s (Konca et al., 2007), but had a much shorter duration on account of its shorter rupture length and slightly lower magnitude, of 80-90 seconds (Ishii et al., 2007).

First, the PGA dataset composed for Barren Island has been analysed. Using the USGS Shakemap Atlas, it is clear from a glance that the accelerations produced by the 2004 event were large, and directed towards the north, made visible in Figure B.3 of Appendix B (USGS, 2020f). As backed up by Ishii et al. (2007), much of the energy produced was concentrated towards the north-northwest of Sumatra, up to around 1300 km away. Barren Island sits approximately 1060 km away. While this distance is greater than the range as proposed in the statistical analysis by Linde and Sacks (1998), the concentration of energy to the north, placing Barren Island in the line of rupture, supports the instance of increased activity at the volcano, based on the position of the aftershocks after the main event (Mishra et al., 2007). Activity at the volcano is largely Strombolian, with lava flows of basaltic to andesitic composition. It has shown intermittent activity in the last twenty years (Sheth, 2014). The increase in eruptive activity since the 2005 eruption has piqued interest in the potential connection between the volcano and the 2004 earthquake, as well as the aftershocks that were concentrated in the area (Mishra et al., 2007; Laluraj et al., 2006). However, not all agree with the causal relationship as given by Walter and Amelung (2007) – it is noted by Sheth (2014) that other significant eruptions at Barren Island have not been triggered by regional tectonic events in the past, such as activity in 1991 and 1994-5.

Despite the uncertain links, the Γ has been calculated from the USGS data using Eq. 5.2. The closest station to the epicentre of the 2004 event was 95 km away to the north, and 759 km from Barren Island. Here, $\Gamma = 0.472$. Interestingly, the acceleration appeared to increase over the distance to the volcano, possibly due to the geology

of the island chain, to a maximum Γ of 0.690. The closest station to the volcano was 103 km to the west (and 1069 km away from the source), where $\Gamma = 0.145$. The variation in Γ can be seen in Figure 5.3 (d), and indicates that Barren Island may not have undergone sufficient acceleration to induce particle remobilisation (lower bound of $\Gamma = 0.2$), though the intense duration of shaking may have had some effect.

When determining Mt. Talang's relation to the two earthquakes, studies agree that Mt. Talang has been involved with various earthquake events around this region, as it is one of the most tectonically active locations in the world (Bebbington and Marzocchi, 2011). Spikes in activity at many Indonesian volcanoes are noted by Bebbington and Marzocchi (2011) after the 2004 earthquake, as well as in relation to the many aftershocks that came after, such as a M_w 6.7 aftershock occurring on April 12, 2005, which was immediately followed by ash ejection at Mt. Talang on the same day (Fiantis et al., 2010; Cassidy, 2015). Authors refer to Mt. Talang's activity after both the 2004 and 2005 events generally (e.g. Kamesh Raju et al. (2012)), but specific connections do not appear to have been explored. It has been analysed, however, by Bebbington and Marzocchi (2011), alongside Indonesia's other numerous volcanoes. After compiling activity following notable earthquakes in the region, this study supports the proposal of delayed triggering, such as described by Walter and Amelung (2007). For Mt. Talang, they base triggering/eruption potential on three factors: it is relatively 'slow' in triggering, meaning it features often delayed activity as based on the analysis of this study; it requires local influence, i.e. earthquakes within the more immediate vicinity; and the minimum magnitude required to produce activity at the volcano should be within the 'moderate' range. These factors, as well as factors of other volcanoes in the area, are available in Table 4 of Bebbington and Marzocchi (2011).

Using the USGS Shakemap Atlas tool (USGS, 2020f), the 2004 event had stations within the area that can be used in the Γ calculations, but for the M_w 8.7 Nias-Simeulue 2005 event, there are only two, with the closest station ~369 km away from the volcano. Instead, for the 2005 event, using the USGS Shakemap display map only (Appendix B, Figure B.4), it is shown that acceleration in the area of the volcano was in the region of $\Gamma = 0.02$ to 0.05 (USGS, 2020d). The 2004 event gave accelerations of $\Gamma = 0.932$ around 50 km south of the rupture, and $\Gamma = 0.016$ at the station closest to the volcano, around 39 km away to the west. As expected, the acceleration produced in this high-magnitude event is very high, but Mt. Talang's distance from the 2004 rupture zone (705 km to the southeast) means this decreased considerably. At 101 km from the source to the southeast, $\Gamma = 0.219$, a very quick reduction of ~0.7 within 50 km. The small accelerations that Mt. Talang experienced, especially after the 2004 event, may have been the result of the northward rupture direction, away from Mt. Talang, as the amplitudes of the waves directed to the north and to the south would be different (Bullen and Bolt, 1985a). The 2005 event, which was closer to the volcano, $\Gamma = 0.911$ at 100 km, and $\Gamma = 0.543$ at 185 km, a decrease of ~0.4 within 80 km, showing that even very large magnitude earthquakes can decay quickly. This, alongside the 2004 event findings, indicates that the boundary of significant acceleration is likely within 100-200 km of the source and will therefore not encompass Mt. Talang.

5.4.4 Case Study: The Landers earthquake of 1992, and seismicity at Long Valley Caldera

The Landers earthquake, and the subsequent increased activity at several sites across the western US (Johnston, 1995; Hill et al., 1995), is unique amongst the selected case studies. As well as being one of the most studied earthquake events originating in the US, it is attributed to triggered seismicity across the west of the country, though did not trigger a volcanic eruption. The Landers earthquake increased local seismicity within Long Valley Caldera in particular. Johnston (1995) stresses that 'triggered seismicity and deformation were recorded simultaneously for the first time' at the caldera, making this an interesting case study even if no volcanic activity was made visible at the surface. This was made accessible to scientists by Long Valley's extensive seismic and deformation monitoring network (Hill et al., 1995).

The Long Valley caldera sits more than 400 km away from the M_w 7.3 Landers earthquake source, which originated in the Mojave Desert on June 28, 1992. As a strike-slip rupture, it propagated to the north-northwest over five overlapping faults (Hauksson et al., 1993), with a total length of between 70 and 85 km. Rupture velocity was in the region of 2.5-2.7 km/s, and duration approximately 25 seconds (Sieh et al., 1993; Velasco et al., 1994; Wald and Heaton, 1994). Johnston (1995) notes that the triggered seismicity at Long Valley occurred within the southwest quadrant, in a 5 km by 15 km area. This quadrant was active from around 1980 up until the time of the earthquake, with resurgence domes under construction. The seismicity occurred almost immediately after the Landers event and was shallow, at 2 – 10 km depth (Hill et al., 1995; Johnston, 1995). The authors also note that the caldera had undergone high-magnitude earthquake events before, including the 1989 M_w 7.2 Loma Prieta earthquake, and the 1992 M_w 7.1 Petrolia earthquake. However, despite the similar magnitudes between the three events, only the Landers event appeared to produce any significant effect on activity and seismicity at the caldera, possibly due to the ongoing deformation with the growth of the resurgence domes.

Using the USGS Shakemap Atlas, the extensive network of monitoring is evident (Appendix B, Figure B.5). For these calculations, stations were chosen on a direct path between the rupture zone and the southwest side of Long Valley caldera (USGS, 2020b). Close to the rupture, within ~45 km, $\Gamma = 1.509$. As seen in other case studies, the acceleration decreases quickly – at around 73 km from the source, $\Gamma = 0.390$, and at 120km, $\Gamma = 0.122$. The station closest to the southwest of the caldera was ~10 km away, with very small accelerations of $\Gamma = 0.016$.

Over a distance of ~400 km, the acceleration decreased by ~1.5, and at the volcano, $\Gamma < 0.1$ (Figure 5.3 (c)). This indicates that shaking at the caldera was not powerful enough to trigger activity, though triggered seismicity occurred immediately after the event within a region of dome building.

5.4.5 Case Study: The Great Chilean earthquake of 1960, and Maule 2010

Chile is frequently shaken by high-magnitude earthquakes due to its location along the Nazca-South American subduction zone (Elnashai et al., 2010). On May 22, 1960, the largest earthquake ever recorded struck off the

west coast of Chile at M_w 9.5, also known as the Valdivia earthquake. The sheer size of this event corresponds to the rupture length of ~1000 km, with a velocity of 3-4 km/s. It is widely attributed to the subsequent fissure eruption of Cordon Caulle two days later (Lara et al., 2004; Barrientos and Ward, 1990; Plafker and Savage, 1970). Unfortunately, "on-the-ground" observations are sparse, but some PGA values can be obtained from the USGS Shakemap Atlas (Appendix B, Figure B.6). From three stations at different distances from the epicentre and volcano, values obtained are $\Gamma = 1.810$ (186 km from epicentre), $\Gamma = 0.272$ (270 km from epicentre), and $\Gamma = 0.271$ (307 km from epicentre), a decrease of ~1.5 over 121 km (USGS, 2020g). As shown, the acceleration is higher when closer to the source, supported by the discussion previously. However, due to the age of the event and the lack of observation at the time, there is little data available on the Shakemap Atlas.

We can draw more observations from a more modern example: the Maule earthquake, occurring on February 27 2010, along the same subduction zone approximately 230 km north of the 1960 event, with a magnitude of M_w 8.8. This event has been attributed to a delayed eruption at Cordon Caulle on June 4 2011 (Mora-Stock et al., 2014). The rupture zone involved was smaller, at ~500 km long, and had a slower rupture velocity of 2-3 km/s (Hicks et al., 2014; Vigny et al., 2011; Saragoni et al., 2010; Elnashai et al., 2010). It had a duration of approximately 150-180 seconds. PGA values are more abundant for this event, and ranged from <0.01 g up to ~0.7 g. Elnashai et al. (2010) highlights two of the highest recordings in the region from stations CCSP and MELP, with values of 0.65 g (109.1 km from epicentre) and 0.78 g (283 km from epicentre), respectively. Other studies show PGA values that are higher still – up to 0.9 g, with a recording of >1 g in the city of Cauquenes, Chile, approximately 55 km from the epicentre (Saragoni et al., 2010).

From the USGS Shakemap Atlas (USGS, 2020e) and using Eq. 5.2, within ~60 km maximum Γ was 0.577, down to 0.310. Interestingly, at Concepcion large accelerations of $\Gamma = 1.081$ were recorded, with an average of the region ~0.7, despite being 79 km from the source. Accelerations continued to decrease, with $\Gamma = 0.101$ at 411.5 km from source, up to 494 km from source (88 km away from Cordon Caulle) where $\Gamma = 0.072$. If Γ is notable when it is >0.2, the radius in which shaking may cause particle mobilisation or have an effect on other process is within ~300 km from the source (Figure 5.3 (b)). The most activity however might be expected within the 60 km boundary, or within 80 km when considering the very high accelerations recorded at Concepcion.

Two other volcanoes were also considered for the 2010 earthquake event: Villarrica, which is 376 km from the epicentre, and Llaima, which is 304 km from the epicentre, in comparison to Cordon Caulle which is approximately 500 km away. A study by Mora-Stock et al. (2014) concludes that, between the 2010 event and Cordon Caulle, there was triggered activity, but for Llaima and Villarrica, there was nothing besides fumarolic degassing and minor seismic tremors in the months after the earthquake, despite the volcanoes being closer to the epicentre and therefore likely to undergo much stronger ground motions. This is supported by Pritchard et al. (2013), who used InSAR to study ground subsidence around the Nevados de Chillán range just southeast of the epicentre, as well as measurements on Llaima and Villarrica. Again, some fumarolic activity was noted, but not enough activity to be classed as an eruption. The USGS data for this event indicates $\Gamma = 0.180$ at 25 km from Villarrica, and $\Gamma = 0.207$ at 74 km from Llaima. All three volcanoes lie outside of the lower bound

for particles remobilisation within mush ($\Gamma = 0.2$), but connections have still been made between the 2010 event and the delayed eruption at Cordon Caulle in June 2011. This is potentially due to other mechanisms, and has been discussed further in Section 5.6.1.

5.5 Shaking duration

In Section 5.3, we have established that $\Gamma > 1$ is possible in the near-field, and has occurred close to volcanic centres for which a link between volcanic eruption and seismicity has been proposed. Similarly, $\Gamma > 0.2$ is common in those scenarios. This leads us to conclude that some crystal pack reorganisation may be possible during seismicity that interacts with magma mush. The next component of our model that needs assessing, is the duration of shaking t_w. In Chapter 4 we show that it is the duration of the shaking that controls the extent of particle reorganisation, and therefore the kinetics of the process are limited by the duration of seismic waves. Formally, we showed that the kinetics are limited by a Stokes' time where the dimensionless time is $\bar{t} = t_w 2\Delta\rho g R/(9\mu)$. This will be discussed here.

When considering the shaking of a saturated granular pack, the length of time it undergoes oscillation is important. In an extremely simplified analogy, if we were to shake a tube of "mush", synthesized from beads and a viscous fluid like in the method outlined in Chapter 3, for a few seconds, it is unlikely there will be any significant particle movement to allow for redistribution. However, if we take the same pack of "mush" and shake it over a longer timescale at a persistent acceleration, then the beads would become more organised over the longer duration, remobilising into a more efficient structure within the fluid. Another example would be that, during large magnitude earthquakes where PGA and shaking intensity can be very high, it is noted that buildings can sustain even these large accelerations without major damage so long as the duration over which those accelerations act is short. The duration of a vibration should be considered alongside other factors such as the amplitude, as it has a critical control on the response to the shaking (Trifunac and Brady, 1975).

As every earthquake event is different, the duration of ground shaking varies greatly, and cannot be quantified perfectly. However, a study by Trifunac and Brady (1975) shows how durations can be calculated for varying earthquake intensities. They give a range of ~10-50 seconds, as calculated from 188 acceleration records, over a range of shaking intensities. Interestingly, as shown in Figure 5a of the study, as intensity increases the duration of shaking appears to decrease. They explain this as a result of the frequency, where higher frequency waves involved in high intensity events – which have shorter wavelengths and a greater attenuation, as previously discussed – react to the heterogeneities of the event locations, and therefore fall off and reduce the duration of effective shaking. Dobry et al. (1978) notes that, based on several previous studies on quantifying earthquake shaking durations, as magnitude increases, the duration increases as well, linked to the increased size of the earthquake rupture zone associated with large magnitude earthquakes. This is displayed in Figure 1 of their paper. They used 84 events of varying magnitudes to calculate the effective durations, resulting in durations of <10 to 40 seconds maximum.

The duration of shaking for each case study in this thesis was variable, and therefore had different effects on the potential for particle remobilisation to occur ($\Gamma = 0.2$). For long shaking duration, the effect may potentially be greater on particle remobilisation, as there is more persistent energy over a longer length of time to allow for particle movement, though the resulting melt expulsion may still be minor and the effect of particle remobilisation therefore minimal. As indicated by Trifunac and Brady (1975), long periods of shaking can cause significant accelerations and damage, even when the magnitude of the earthquake is low. For example, the Java earthquake shook for 60 seconds, and despite the accelerations reaching sufficient levels within 50 km between the source and Mt. Merapi, the prolonged shaking may have exacerbated disturbances within the volcanic plumbing system, though based on the accelerations this may not be to do with mush remobilisation and segregation processes. While the Java earthquake was moderate in magnitude, the effect of prolonged shaking is better captured by the Maule 2010 earthquake, which highlighted an interesting relationship between three volcanoes: Cordon Caulle, which erupted the following year, and Villarrica and Llaima, which despite being closer to the source, did not erupt. However, for all three volcanoes, the accelerations enacting upon them during the event were < 0.2, implying insufficient energy for remobilisation. Similar to the case of Mt. Merapi, which also had insufficient energy for particle movement, the duration of shaking may be the key to volcanic activity at these volcanoes, even if the effect is delayed. The duration of shaking for the Maule earthquake was 150-180 seconds, and is intense for the high magnitude of the event. The Maule 2010 event had both a high magnitude and an extended duration, the effect of which is evidenced by the very high accelerations recorded around the affected region. Therefore, despite the low acceleration acting upon the volcano, it is possible that the intense duration and magnitude influenced other volcanic processes, but not necessarily mush reorganisation.

Rupture directivity is also an important factor and influences the duration of shaking. The Sumatra-Andaman earthquake of 2004 had a very intense period of shaking associated with it. At Barren Island, $\Gamma = 0.145$, falling below the lower bound of sufficient energy for particle remobilisation. However, the variable speed of rupture, which extended the duration of shaking, as well as the rupture directivity towards Barren Island, complicates the picture, as a long period of ground motion may allow for continued particle movement even if the accelerations acting upon the mush body is low and the melt expelled in such a scenario is small in volume. The influence of rupture speed and directivity, and therefore the duration, is also apparent for Mt. Talang, which had very low accelerations acting upon it after the 2004 event. As Mt. Talang is far from the source and in the opposite direction of fault slip, the acceleration was extremely low and likely insignificant, even when shaking occurred over a long period of time.

The Luzon earthquake and the Landers earthquake both had short durations, at 30-35 seconds and 25 seconds, respectively. For both of these locations, it is unlikely that such short durations, as well as low accelerations, would have had an effect on mush processes. Particularly for the Landers event however, the result of the earthquake was triggered seismicity at a zone within the caldera that was undergoing active deformation and dome building at the time, and studies indicate that the effect of even a very short period of shaking may have influenced gas processes such as advective overpressure, showing that where mush is not affected, other

processes within the reservoir may be, and that triggered volcanism (or in this instance, seismicity) is still viable but by other processes. This is elaborated on in Section 5.6.1.

5.6 Applicability of melt extraction and Γ to volcanic systems

Throughout this thesis, the nature of volcanic plumbing systems and the individual chambers that form them has been described as incredibly complex. It appears that no single process occurs at a time, and that geophysical data can only go so far in aiding our understanding of chamber-wide processes, even with the addition of geochemical data. There are a myriad of processes that have been proposed when trying to define magma chamber processes, and these have been drawn into the discussion on volcanic triggering, as well as how mush forms and moves within reservoirs (as in Section 2.3). These include bubble processes, which appear removed from mush as many are modelled using purely liquid, but still have their place in the mush zone, and mush- and segregation-specific processes, where segregation of melt and solids occurs at the micro-scale. All of these processes have advantages and drawbacks, and all are likely to come under the influence of dynamic processes such as shaking in the context of a volcano put under duress by near or distant earthquake shaking.

In using Γ to define melt segregation, theorised to create bodies or 'caps' of melt (as discussed in Chapter 2) that can be erupted, the findings as outlined in the case studies have shown that seismic shaking alone, in promoting melt segregation, are unlikely to directly trigger volcanic eruptions. It is highly likely that dynamic stresses such as seismic shaking work in tandem with other mechanisms occurring within the chamber and mush zone, which leads to further processes that encourage or trigger eruptive activity. That is not to say that dynamic stresses, such as quantified by Γ, should be discarded entirely. In this section, a comparison between the Γ mechanism and other mechanisms as introduced in Chapter 1 and 2 will be made, to explore the applicability of Γ in crystal mush systems and their role in cases of seismically-triggered volcanic activity.

5.6.1 Influence of shaking on processes associated with triggered volcanism

Frequently, studies centred around seismically triggered activity will cite bubble processes as the driving force of triggered eruptions. As introduced in Chapter 1 and 2, these processes include: rectified diffusion, where bubbles expand and compress and alter the volatile content and pressure of a magma chamber; advective overpressure, where bubbles rise to the top of the chamber and increase pressure; and bubble nucleation and growth, where supersaturated magma undergoes pressure fluctuation and dissolved gases create bubbles, leading to increased pressure and volume. Bubble processes are typically attributed to explosive activity, and sometimes considered alongside the dynamic stress of passing seismic waves.

This is true for many of the case studies outlined in this chapter, such as at Mt. Merapi (Walter et al., 2007) and Barren Island (Bandopadhyay et al., 2006; Bandopadhyay et al., 2014). Furthermore, the triggered seismicity at Long Valley is also attributed to advective overpressure, where bubbles were shaken free of confining surfaces and accumulated, causing pressure changes that appeared to match the deformation found at the caldera (Linde et al., 1994). The shaking at Long Valley Caldera does not appear strong enough to trigger

a larger eruption but may have dislodged bubbles and caused an increase in the system pressure, and in turn, deformation to the area. This case study further highlights the importance of the chamber state at the point of an earthquake. The most significant window of shaking in this case study appears to be within 100 km of the source, but even weak shaking may have an impact on volcanic processes at greater distances on volcanoes that are unstable at the time.

Bubble processes are also cited for Cordon Caulle, though the correlation between both the 1960 and 2010 earthquakes and the attributed eruptions are still debated. While a link between the earthquakes and bubble accumulation leading to overpressure is noted by some, it is disregarded by others in favour of basaltic injection into the mush zone at Cordon Caulle, increasing heat and volatiles, and leading to overturn, with bubbles being released and allowed to ascend (Delgado et al., 2015; Delgado, 2020; Jay et al., 2014). It is noted however that the silicic reservoir and mush zone beneath Cordon Caulle is extensive and that melt segregation has fed both the 1960 eruption and the 2011 eruption, as well as historic eruptions such as in 1921. Intrusions below the mush complex have been inferred for periods before these eruptions, and are shown in Figure 9 of Delgado (2020), as well as much more recent intrusions that might influence eruptions in the future. Such intrusions will supply heat and volatiles, which are then influenced by the described processes.

Melt segregation processes include: compaction, where crystals compact under their own gravity after settling at the base of the chamber; and micro-settling, where crystals will sink within a melt pore and push the interstitial melt up and out (Section 1.5.1). Further included is sinking, slumping and tearing of mush plumes, where small bodies of mush and crystal aggregates sink after being shaken from their placement at the top of the chamber, displacing and forcing molten material upwards as they descend. While the case studies specifically do not describe the melt segregation process that occur under the volcano (e.g. at Cordon Caulle) at the micro scale, these processes are widely accepted to occur within those magma bodies, and so have a slightly wider, though more theoretical, application to magma chambers and mush bodies. After the introduction of these processes by Bachmann and Bergantz (2004), they have been used to explain most aspects of mush formation, crystal movement and evolution, and melt expulsion and its effect on the magma chamber as a whole. However, as remarked by Holness (2018), they have been taken as gospel, without proper evidence of their importance available. While this was not the intention upon their implementation by Bachmann and Bergantz (2004), these processes must be discussed critically.

The settling process is associated with the settling out of crystals from a body of melt, with melt being pushed upwards while the crystal sinks. And in line with the exploration of Stokes' settling in this thesis, it features heavily in melt segregation and the formation of mush. As discussed in Chapter 2, the formation of a particle pack, i.e. a mush, is from settling of dense crystals through a fluid of given viscosity. This can be applied to low-viscosity and high-viscosity systems alike (see Figure 2.2), with settling taking longer for rhyolitic systems. This process does not attribute to volcanic triggering directly, but is a stepping stone to the next process that is central to this project: compaction.

In the context presented by Bachmann and Bergantz (2004) and critiqued by Holness (2018), compaction refers to a mechanical process where crystals settle and compact under their own gravity. While settling accumulations will never form closely packed structures, compaction of the pack will over time, and in silicic systems this is complex. At around 45-50% crystallinity, the pack becomes rheologically locked, and expulsion of melt from the mush after this point is from the compaction process. When considering this for volcanic triggering, the segregation process should speed up and become more efficient as determined in the analysis of de Richter et al. (2015). However, as determined in this project, the energy induced by seismic shaking needs to be above a certain level for reorganisation and compaction of the mush to occur and for melt to be expelled from the interstitial space.

5.6.2 Comparison with other triggering mechanisms

As found when studying the experiments carried out by de Richter et al. (2015), we can say that when $\Gamma > 1$, there is enough energy produced by seismic shaking for particle reorganisation to occur. However, as shown in Figure 5.1, these experiments do not explore $\Gamma < 1$, and extrapolation of the data downwards may result in $\Gamma > 0.2$, where a higher packing fraction could be reached above the initial packing fraction.

As discussed in Section 2.4 the central issue regarding melt expulsion, for both melt segregation and for its role in causing triggered activity, is the timescale over which it functions. A timescale of 10^4-10^5 years for segregation to occur in the formation of crystal-poor rhyolites has been proposed, though other studies do find shorter timescales (Bachmann and Bergantz, 2008; Bachmann and Bergantz, 2004; Allan et al., 2013). But these idealised timescales do not consider the mush body being shaken – their estimates are from the settling and compaction process alone. By applying a shaking force to the mush, this project aimed to answer whether such motion would encourage the settling, compaction, and reorganisation process, leading to increase melt volume. As with all other aspects of the chamber, the answer to this is very complex.

As seen in Figure 5.3 (a-d), acceleration was highly variable for all case studies, referring to the variability in decay as highlighted by Edwards et al. (2011), but showed an overall negative trend that fits the attenuation expected for seismic waves. Γ only reaches 1 for three of the case studies: the 1992 Landers earthquake, the 1960 Great Chile earthquake, and the 2010 Maule earthquake. The 2004 Sumatra-Andaman earthquake comes close at $\Gamma > 0.9$. All other case studies fall between $\Gamma > 0.2$ and 1, which is a bracket of potentially significant energy as described in Section 5.1, where $\Gamma > 0.2$ indicates minor particle reorganisation, which then increases with increasing Γ. For the 1960 and 2010 Chilean earthquakes (Figure 5.3 (b)), the distance over which Γ appeared most active was within ~250 km for the 1960 event, with reduced particle remobilisation within around 300 km, and within 100 km for the 2010 event, though less significant energy may have disturbed the volcanoes involved within up to 200 km. Cordon Caulle experienced accelerations of $\Gamma = 0.9$ in 1960, on account of it's shorter distance from the rupture zone and the very high magnitude of the event, indicating that particle remobilisation and subsequent melt expulsion was a very plausible factor in the eruption only a few days later. In 2010 however, with Cordon Caulle much further from the 2010 rupture zone, the acceleration was $\Gamma < 0.1$, so melt extraction is not a likely factor for this event and for the following 2011 eruption.

Furthermore, Llaima and Villarrica also did not experience high accelerations, as $\Gamma = 0.2$ and < 0.2, respectively. While heightened fumarolic activity did occur at these volcanoes, it is unlikely to be related to mush processes. However, this case study highlights the need to consider chamber state at the time of a high-energy seismic event – as definitive and well-explored cases of triggered volcanism appear rare (Pritchard et al., 2013) – as well as previous activity or expected activity at the volcano in question. Manga and Brodsky (2006) state the overpressure of the reservoir should be within 99-99.9% of the maximum overpressure for seismicity to trigger eruptive activity. Llaima and Villarrica have histories of continuous activity, with Llaima's last eruptive cycle finishing in 2009, and Villarrica erupting last in 1985 with sustained activity above background level since then, up until the time of the 2010 earthquake (Mora-Stock et al., 2014). Therefore, these volcanoes would not build up the overpressure required for triggered volcanic activity, via melt segregation or other mechanisms, while a volcano with a more cyclic history, such as Cordon Caulle where the last eruption since 1960 was in 1990, would have a level of overpressure that may be close to the threshold of instability, so that when seismic waves pass through, an eruption may occur. This may further explain why Cordon Caulle erupted after the 1960 event and not the 2010 event, bolstered by the differences in distance between source and volcano, and the accelerations experienced.

In Figure 5.3 (c), the 2006 Java earthquake, the 1990 Luzon earthquake and the 1992 Landers earthquake are shown. The Landers earthquake produced high accelerations close to the source, which decayed quickly within 60 km. After this point, reduced remobilisation could be expected up to 150 km from source. For Java and Luzon, Γ was initially 0.4 and 0.8 respectively, but also decayed quickly, within 50 km for Java and 100 km for Luzon. While both Mt. Merapi and Mt. Pinatubo sit within this bracket, the Γ was still low at the point seismic waves would have crossed these features. At Mt. Merapi $\Gamma =< 0.2$, below the threshold of potential melt extraction by particle remobilisation, and at Mt. Pinatubo $\Gamma = 0.35$, which is close to the lower boundary of effective energy, and therefore mush-related melt expulsion is unlikely, though not impossible. Interestingly, Long Valley still had apparent, immediate activity despite being 400 km from the source. According to Linde et al. (1994), the triggered seismicity here is attributed to advective overpressure, which may indicate that even fairly weak shaking can affect bubble processes within the chamber. Due to the low Γ however, particle reorganisation is less certain.

Figure 5.3 (d) shows the Sumatra-Andaman earthquake of 2004, and the progression of waves towards Barren Island and Mt. Talang. While Γ does not reach 1, the rupture directivity is evident in this graph: the rupture propagated towards Barren Island to the north, and this can be seen in how the acceleration remains within 0.7 – 0.4 up to 1000 km from the source. However, with Mt. Talang to the southeast of the rupture zone, in the opposite direction to the rupture, acceleration fell off quicker, within 200 km. $\Gamma < 0.2$ at Mt. Talang, which indicates that shaking here was not effective, but it remains within the lower bound for Barren Island, as $\Gamma > 0.2$ up to 1050 km from source, and fell to < 0.2 at the island volcano itself, only 10 km more away. In this instance, shaking had a minimal effect due to the low acceleration, but may have encouraged very minor activity, even if not caused by mush remobilisation and compaction processes.

The rationale of applying seismic motion to a mush body, hypothetical or within a case study, is based on the hypothesis that shaking will allow crystals within the mush framework to reorganise and recompact into a more efficient structure, making for a denser mush but also expelling more melt from the interstitial space. It has been determined in the discussion of other processes (Section 5.6.1) that, as the chamber environment is complex, there is more than likely several processes occurring at once. The initial conclusion is therefore that shaking will compact a mush body and expel a volume of melt due to the reorganisation, as drawn from the findings analyses from de Richter et al. (2015) in Chapter 4. This led to the definition of the Γ parameter, where $\Gamma > 1$ means there is a significant amount of energy influencing the system, as the shaking parameters appear to control the gradual compaction phase in those experiments after the inflection point (Section 4.1). Significant energy in this stage allows an increased level of segregation. A lower bound may also be implied (Figure 5.1), where $\Gamma > 0.2$ may be enough for more minor particle reorganisation. But as seen in Figure 4.1 (a), higher viscosity tests required more time to reach a high level of compaction, even when the Γ value was high. This, alongside the studies on Stokes' settling processes (Section 4.2), leads to the assumption that, for high-viscosity i.e. silicic volcanic systems, the compaction and subsequent segregation of melt will take longer and therefore may not act quickly enough as a direct trigger for volcanic activity, despite increasing the amount of melt expelled compared to segregation occurring on its own without seismic influence. In these case studies, some eruptions occurred within a short window of time after the earthquake, such as at Mt. Merapi and Cordon Caulle in 1960. Hence, it can be concluded that in these instances, melt segregation may not have reacted fast enough to seismic shaking to affect melt storage in the shallow crust critically. Cordon Caulle, for example, is more attributed to chamber overturn via injection, though melt segregation is a key part of its magma generation. Hence there may be a small influence by seismic waves in the context of melt segregation here as the acceleration at Cordon Caulle was high ($\Gamma = 0.9$), but not on the timescale needed to be significant. In cases where an apparent eruption was delayed, the segregation via shaking mechanism may be more significant, as there is more time for segregation to occur and for pressure in the chamber to build. This may be why some eruptions after large earthquakes did not occur for several months, such as at Mt. Pinatubo, because overpressure was being encouraged by the shaking, with segregation occurring at a faster rate and providing more melt to the shallow chambers, building towards explosive eruptions. However, as the length of time between events increases, it becomes more difficult to connect the two and state that they are related for certain, and the acceleration at these volcanoes was very low at the time of the earthquake event.

The conclusions drawn from the analysis of these case studies, alongside the supporting exploration into crystal dynamics and Stokes' processes, are:

1) The extraction of melt from a mush via shaking processes, leading to the formation of molten 'caps' which then go on to produce crystal-poor rhyolite, is a viable process but is only effective close to the source of the shaking, i.e. a tectonic rupture zone, where accelerations are sufficiently strong;
2) Extraction of melt may also be latent, in the sense that melt may segregate, even if acceleration acting upon the mush is low, so long as the duration of the oscillatory force is sufficient to exacerbate the

effects upon particle movement, and that processes that occur after the segregation cause delayed eruptive activity;

3) The extraction of melt via shaking, even when the acceleration of the shaking is low or the mush body is outside of the effective zone of shaking, may act as a "primer". Processes may occur at a reduced rate, compared to if the mush body was within the effective zone or extremely close to the source, and may still therefore produce activity that is not in accordance with the typical pattern of eruption expected at a particular volcano. Any activity encouraged by the shaking (mush-related or not) may occur sooner than the next supposed window of volcanic activity expected at that volcano, even if the shaking does not produce amplified volcanic activity immediately after occurring. The alternative to this is also true for volcanoes where there is no periodic timescale of eruption, i.e. activity is virtually continuous, as discussed for Llaima and Villarrica after the 2010 Maule event;
4) Extraction is not removed from other processes, and likely runs in tandem with a myriad of mechanisms leading to increased chances of eruptive activity, as volcanic reservoirs are complex and no two are the same. Each process outlined in this thesis, including melt extraction from mush, is viable theoretically, though some processes have stronger backing than others and are much more widely cited, like gas bubble accumulation leading to overpressure and chamber rupture.

Following on from this, another conclusion that can be drawn is that, while shaking may increase the rate and efficiency of melt segregation, the increase in melt may not be substantial on its own, and that the process acts as a stepping stone for other processes to then occur. Shaking free of bubbles has already been mentioned, and is often cited as a central triggering mechanism in the various studies that have been discussed. It has also been noted that the chamber needs to be at a critical point of instability already for shaking to trigger an eruption, particularly via bubble processes, or regional tectonic alterations such as extension, where magma can ascend and vesiculate via decompression very quickly. With this in mind, dynamic stresses such as seismic shaking, by acting as a stepping stone, may encourage the build towards this critical instability, providing more melt for other processes to work within. It does not appear likely that the increased melt segregation alone will rupture a chamber and cause an eruption outright.

Chapter 6. Conclusion

In this project, the question as to whether seismic waves from high-magnitude earthquakes can trigger volcanic activity has been explored, relating in detail to the movement of crystals within crystal mush, which dominates the volcanic plumbing system. This mush, with interstitial fluids and melt between the crystalline network, was hypothesised to compact under dynamic stress (i.e. from seismic waves), resulting in the expulsion of interstitial melt and the formation of crystal-poor 'caps' above the mush column, like the source of crystal-poor rhyolitic melts and subsequently erupted ignimbrites.

Support has been drawn from macro-scale particle interactions via Stokes' Law and from the formation of magma chambers and melt 'caps' to explore whether shaking can cause sufficient internal disequilibrium, e.g. via increased overpressure, to produce a volcanic eruption. A new mechanism of disequilibrium has been composed, where melt expulsion from the crystal mush lattice occurs due to compaction initiated or encouraged by seismic waves. Other proposed mechanisms have been outlined and weighed in their plausibility against particle remobilisation and melt expulsion, particularly for gas processes where the accumulation and transport of gas bubbles causes highly unstable chamber pressures.

From this study, the following conclusions can be drawn:

1) The interaction of crystals can be envisioned using simplified particle-fluid interactions, as captured by Stokes' Law. Using real-world melt inclusion and crystal compositions, the viscosities and settling speeds of individual crystals in varying melt compositions were calculated and plotted (Figure 2.2 and Figure 4.2), showing that rhyolitic melts with high viscosities had much slower settling rates than low viscosity basaltic melts, and that crystals within either of these compositions should be large and dense in order to effectively settling to the bottom of a synthesised chamber.
2) Previous works on the movement of particles in saturated "packs" indicated that, under oscillation, the pack would compact to a more efficient structure via particle remobilisation, so that interstitial fluid could be expelled. This was combined with Stokes' Law to produce a hypothesised relationship between remobilisation/compaction and the acceleration of waves.
3) Seismic waves are highly variable in terms of their frequency and amplitude, but the acceleration, and therefore shaking energy, is quantifiable using $\Gamma = A/g$, where A is the acceleration (PGA) over the force of gravity. High Γ was indicative of high energy which could allow for particles (i.e. crystals) to remobilise in their confining fluid, and therefore resettle and compact into a more efficient lattice, expelling melt. The energy is most significant when $\Gamma > 1$, though the packing fraction of a pack (or mush) may increase marginally if below 1 ($\Gamma \geq 0.2$).
4) Using five case studies, it was found that high magnitude earthquakes are capable of causing accelerations that are close to or exceed 1g, and therefore Γ was close to or exceeded 1. However, the decay effects of seismic waves dictated that this energy (Γ) decayed linearly over distance via an inverse square law, so that accelerations recorded at a greater distance from the earthquake source were smaller, and therefore less significant.

5) This effective distance varied for each location, likely due to the attenuating effects of the regional geology and the initial magnitude of the earthquake. While certain volcanoes did sit within the determined effective distance, such as Mt. Merapi after the 2006 Java event, Mt. Pinatubo after the 1990 Luzon event, and Cordon Caulle after the 1960 Great Chilean event, these volcanoes predominantly did not experience accelerations high enough for sufficient mush remobilisation, compaction, and melt expulsion to occur to a great degree, with the exception of Cordon Caulle, where $\Gamma = 0.9$. For this volcano, the 1960 event was "strong" enough to potentially induce changes in the mush structure, although other processes such as injection and overturn have been strongly cited as the eruptive mechanism.
6) Comparison to other triggering mechanisms as proposed in the literature indicates that shaking may not trigger volcanic activity directly, as the significance of shaking on a magma chamber is dictated by the composition, duration of the shaking, initial state at the time of shaking (i.e. level of instability), and the distance of the body from the earthquake source. The triggering mechanisms, including melt expulsion, are not divorced from each other. For example, Cordon Caulle has displayed large eruptions periodically in 1921, 1960 and 1990, a separation of several decades between each event, a period of time in which the overpressure of the reservoir can increase to levels that are bordering on unstable. Attributed mechanisms may include the melt expulsion mechanisms explored in this thesis as a result of shaking, which would influence the overpressure within the system, but predominantly cited is bubble accumulation after injection below the mush zone, as supplied heat and volatiles cause reheating and overturn of the body, with melt segregation producing the eruptive supply of magma. As shown, the processes are closely interlinked.

6.1 Future applications and improvements to methodology

Throughout this thesis, the sheer complexity of the micro-scale crystal processes and the reservoir-wide processes that alter and influence volcanic plumbing systems has been repeatedly stressed. As technology has improved, new ideas have been defined concerning how the magma reservoir is constructed and how it produces the wide range of volcanic products that volcanoes eject.

Understanding how mush reacts to tectonic-scale forces such as earthquakes, and by extension how volcanoes react after high magnitude events in general, is important for future volcanic eruption forecasting. While the extent of the relationship between earthquakes and volcanoes is largely unknown and clouded by several sources of uncertainty, this thesis concludes that the key to quantifying this relationship lies within the micro-scale processes that occur with the reservoir itself, and how the reservoir contents react to oscillation, particularly when seismic forcing is intense and high-amplitude. How crystal mush, which dominates the reservoir, responds to such forcing has not been studied in great detail previously, and concluding this project shows that much work is still to be done to answer lines of enquiry such as:

- How crystals in mush move in relation to each other in more detail, including how particle shape influences this as an extension of Stokes' Law;
- Use of experimental set-up to test the effects of different particle shapes outlined, a wider range of viscosities, and also shaking durations, to find the "optimum" conditions for melt expulsion;
- Applying the calculated extraction percentage (~3%) to real mush body volumes constrained by geophysical imaging methods, though higher quality images and more accurate mush volumes would be required;
- Inclusion of more case studies in the analysis, especially if the case studies occur within the same tectonically and volcanically active region. An example would be to explore only Chilean volcanoes in relation to the Chilean subduction zone, and determine a relationship between earthquakes along the active subduction zone and local volcanoes, rather than try to define this relationship to a whole range of volcanoes in greatly variable settings, i.e. the relationship may function differently for Chilean volcanoes compared to Javanese volcanoes, due to the fluctuations in geology, volcanic structure, composition and fault/subduction activity;
- Comparing the forecasted cyclicity of a particular volcano's eruptive pattern to an eruptive pattern disturbed by high magnitude earthquakes, testing the earthquake's ability to "prime" and induce volcanic activity sooner than designated by previous forecasting.

Appendix A. Stokes' Law calculations

Volcano		Crystal sizes (m, R)[†]	Average viscosity (Pa s, μ)	Average settling velocity (m/s^2, v_s)	Average Re	References
Cascades[*]	*Belknap*	0.00025 – 0.001	4.47×10^{1}	2.21×10^{-5}	1.30×10^{-6}	Hughes (1982) Mordensky and Wallace (2018)
	Mt Washington	0.00025 – 0.002	5.12×10^{1}	7.16×10^{-5}	7.19×10^{-6}	
	North Sister	0.00025 – 0.0005	6.39×10^{1}	4.80×10^{-6}	1.04×10^{-7}	
Mount St Helens		0.00035 – 0.005	5.37×10^{3}	3.04×10^{-6}	1.18×10^{-8}	Rutherford et al. (1985) Blundy and Cashman (2005) Melson (1983)
Mount Pinatubo		0.0005 – 0.005	5.55×10^{4}	3.01×10^{-7}	7.61×10^{-11}	Borisova et al. (2005) Rutherford and Devine (1999)
Popocatepetl		0.0001 – 0.003	1.41×10^{4}	2.64×10^{-7}	5.71×10^{-10}	Atlas et al. (2006) Witter et al. (2005) Straub and Martin-Del Pozzo (2001)
Sakurajima		0.00005 – 0.00015	1.80×10^{4}	1.43×10^{-9}	3.63×10^{-14}	Araya et al. (2019) Yanagi et al. (1991)
Santorini		0.0005 – 0.002	4.47×10^{2}	1.13×10^{-5}	2.23×10^{-7}	Cadoux et al. (2014) Barton and Huijsmans (1986) Druitt et al. (2016)
			3.65×10^{2}	1.14×10^{-5}	1.91×10^{-7}	
			6.55×10^{3}	7.10×10^{-7}	4.94×10^{-9}	
Soufriere Hills		0.000005 – 0.003	7.50×10^{4}	3.11×10^{-8}	1.76×10^{-12}	Devine et al. (1998) Barclay et al. (1998) Horwell et al. (2013)
Taupo Volcanic Zone		0.001 – 0.005	1.18×10^{5}	1.14×10^{-7}	1.11×10^{-11}	Begue et al. (2014) Allen and McPhie (2003) Gelman et al. (2013) Shane et al. (2005) Cole et al. (2014)

[*] Has been split into the three volcanoes used.

[†] Crystal density (ρ_c) average values for plagioclase (2670 kg/m^3), olivine (3320 kg/m^3), quartz (2650 kg/m^3), and pyroxenes (3300 kg/m^3).

Appendix B. Case Study Shakemaps

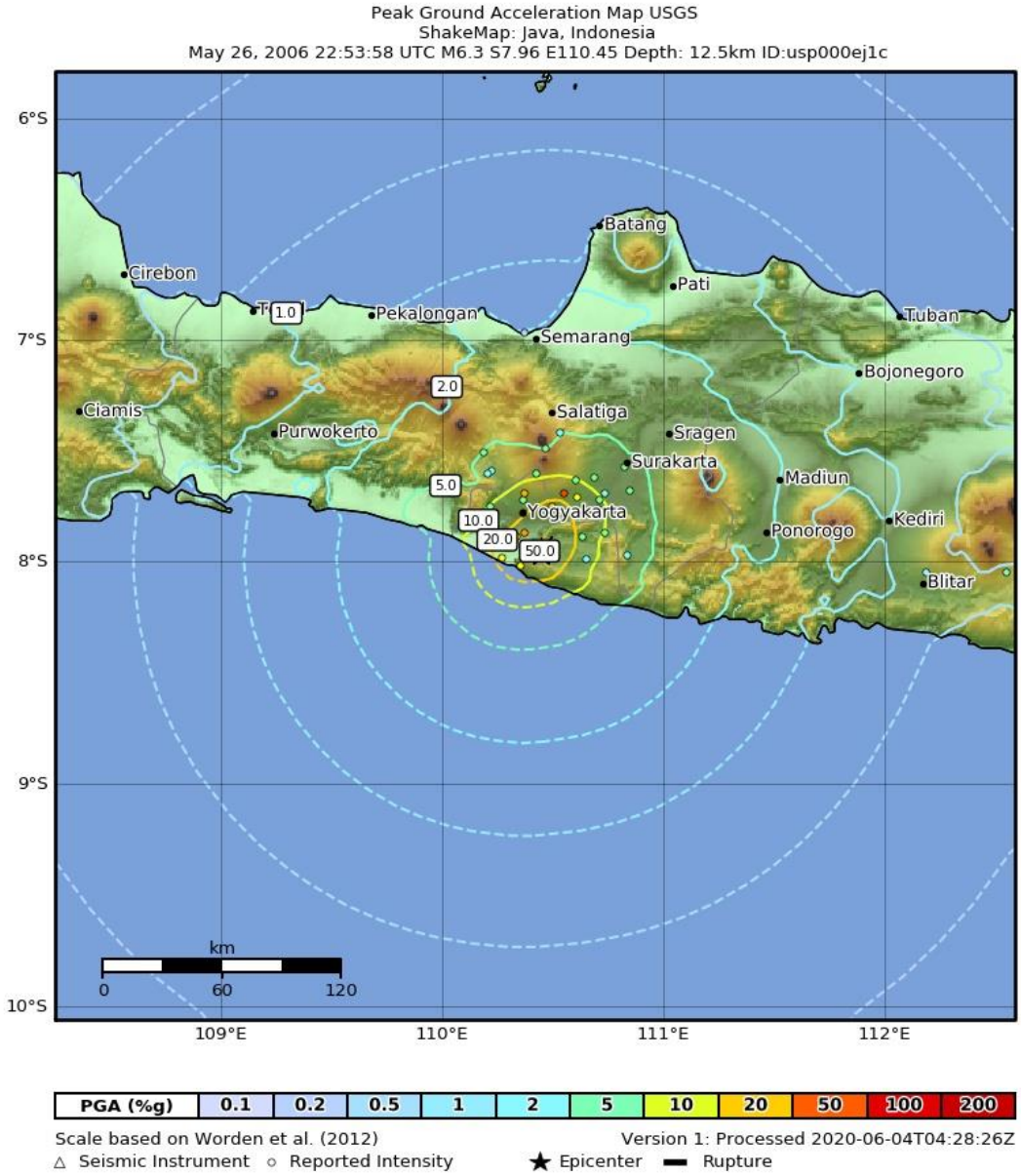

Figure B.1 - Shakemap of Java earthquake, 26/05/2006 (USGS, 2020a).

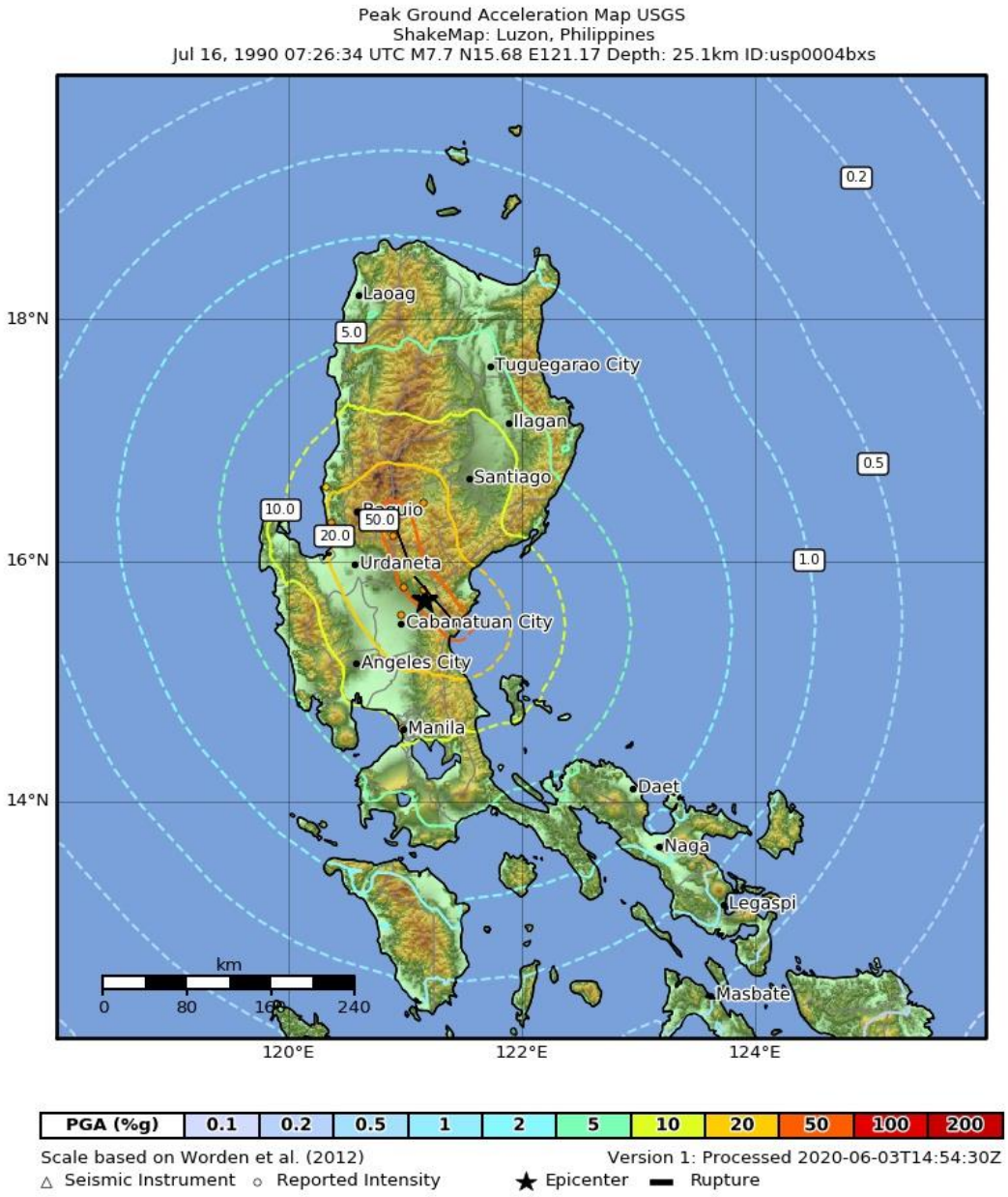

Figure B.2 - Shakemap of Luzon earthquake, 16/07/1990 (USGS, 2020c).

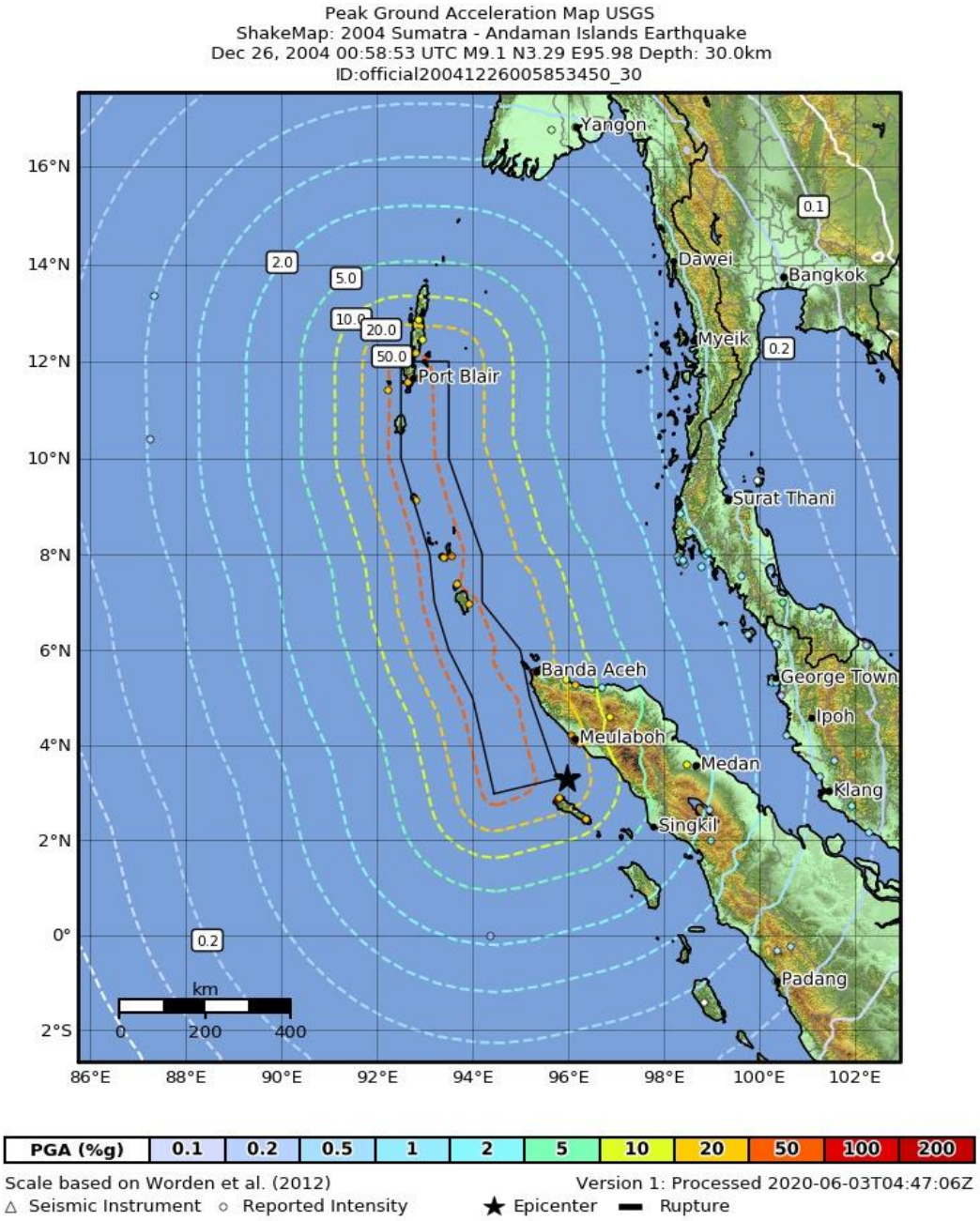

Figure B.3 - Shakemap of Sumatra-Andaman earthquake, 26/12/2004 (USGS, 2020f).

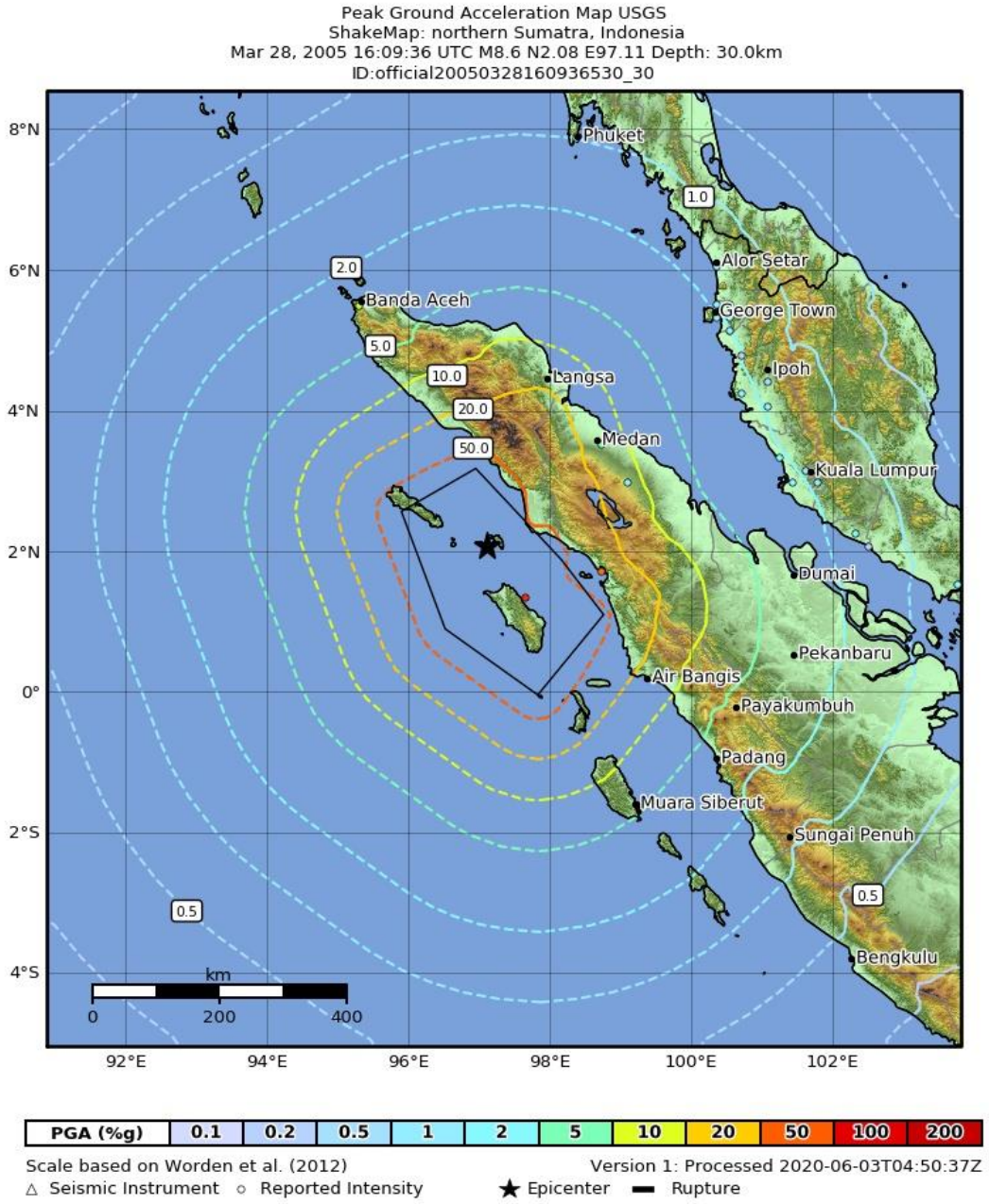

Figure B.4 - Shakemap of Nias-Simeulue earthquake, 28/03/2005 (USGS, 2020d).

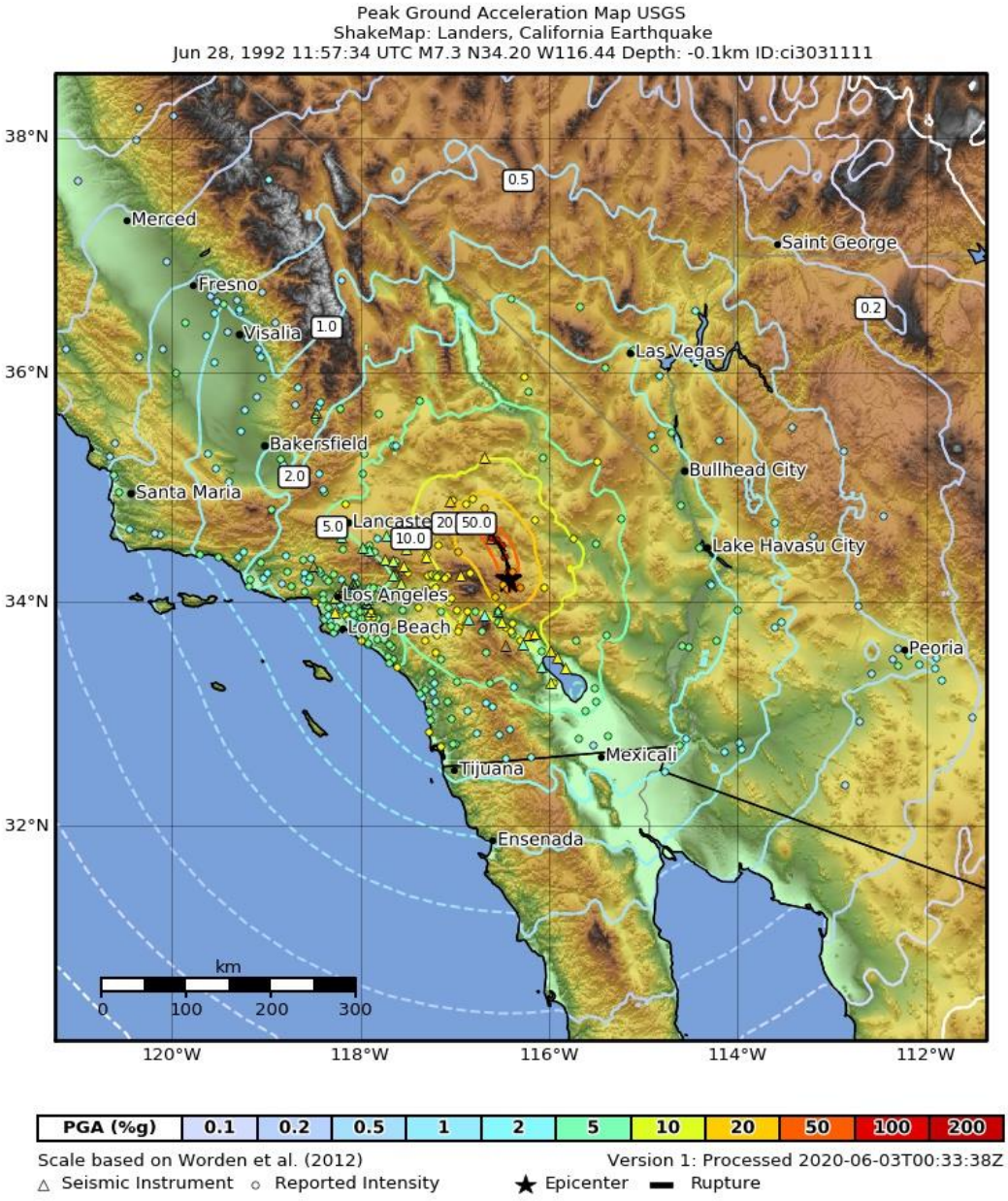

Figure B.5 - Shakemap of Landers earthquake, 28/06/1992 (USGS, 2020b).

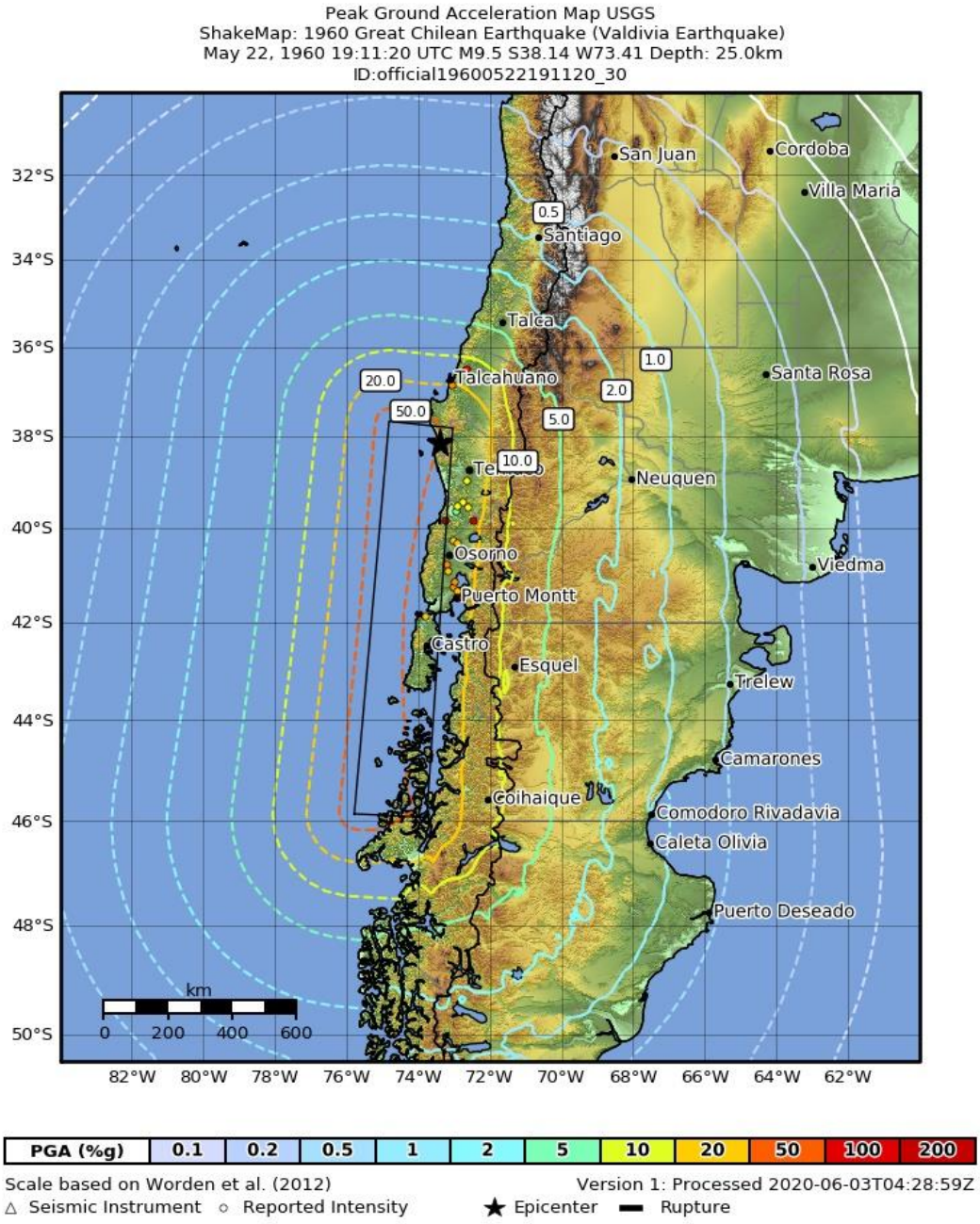

Figure B.6 - Shakemap of the Great Chile/Valdivia earthquake, 22/05/1960 (USGS, 2020g).

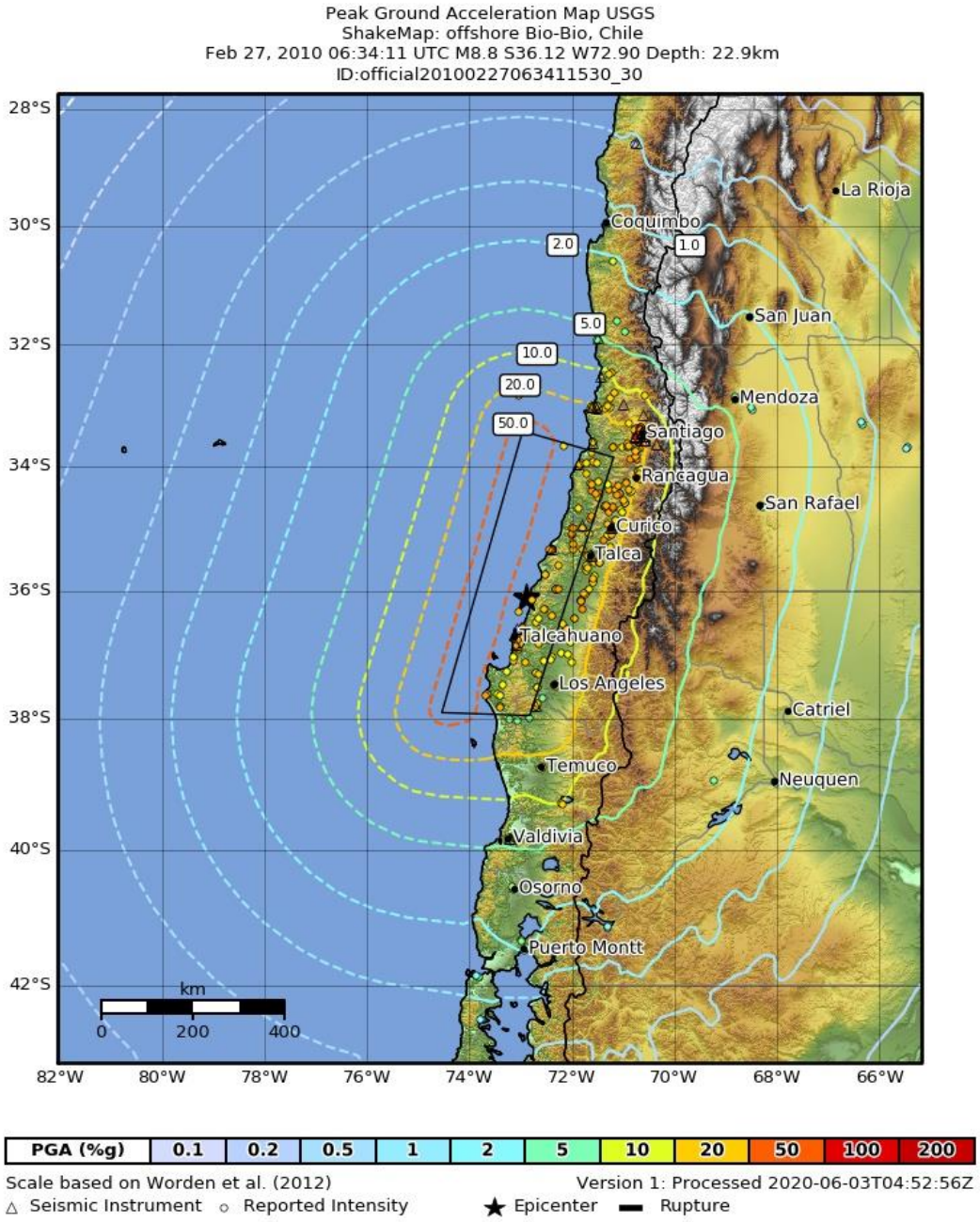

Figure B.7 - Shakemap of Maule earthquake, 27/02/2010 (USGS, 2020e).

Appendix C. Case Study Γ values summary

Earthquake event	Associated volcano	Distance from source (km) *	Γ
Java/Yogyakarta (26/05/2006)	Mt. Merapi, Java	13.45	0.383469
		15	0.37917
		22	0.17544
		24	0.345882
		28.3	0.08847
		31	0.598096
		40	0.080872
Luzon (16/07/1990)	Mt. Pinatubo, Philippines	10.3	0.809923
		23.05	0.744146
		26.3	0.583701
		26.5	0.8000726
		120.3	0.225523
Sumatra-Andaman (26/12/2004)	Barren Island, Andaman Islands	95	0.4720387
		260	0.5029282
		261	0.6895644
		584	0.6514775
		737	0.4146584
		1044	0.3718730
		1069	0.1447506
	Mt. Talang, Sumatra	46	0.2703077
		50.6	0.9321816
		95	0.4720387
		101	0.2194250
		360	0.0157946
		674	0.0157946
Nias-Simeulue (28/03/2005)	Mt. Talang, Sumatra	100.7	0.9109888
		184.9	0.5429145
Landers (28/06/1992)	Long Valley Caldera, United States	22.39	1.509084
		40.44	1.509084
		43.95	1.509084
		73.25	0.390367
		85.71	0.181138
		120.62	0.122158
		193.28	0.061379
		203.85	0.05988
		445.77	0.015795
Great Chile/Valdivia (22/05/1960)	Cordon-Caulle/Puyehue, Chile	186	1.8103816
		270	0.2717072
		307	0.2708075
Maule (27/02/2010)	Cordon-Caulle/Villarrica/Llaima, Chile	9.52	0.575104
		50.7	0.544514
		55.2	0.576903
		59.2	0.310194
		78.9	1.081531
		129.6	0.288501
		154.2	0.153048
		186.9	0.283903
		206.3	0.082772
		290.8	0.206629
		358.4	0.180338
		411.5	0.101265
		490.0	0.063878

	494.3	0.071975

* Distance between rupture zone and recording station.

References.

AKI, K. 1980. Scattering and attenuation of shear waves in the lithosphere. *Journal of Geophysical Research: Solid Earth,* 85(B11)**,** pp. 6496-6504.

ALLAN, A. S. R., MORGAN, D. J., WILSON, C. J. N. & MILLET, M.-A. 2013. From mush to eruption in centuries: assembly of the super-sized Oruanui magma body. *Contributions to Mineralogy and Petrology,* 166(1)**,** pp. 143-164.

ALLEN, R. M., GASPARINI, P., KAMIGAICHI, O. & BOSE, M. 2009. The status of earthquake early warning around the world: An introductory overview. *Seismological Research Letters,* 80(5)**,** pp. 682-693.

ALLEN, S. R. & MCPHIE, J. 2003. Phenocryst fragments in rhyolitic lavas and lava domes. *Journal of Volcanology and Geothermal Research,* 126(3)**,** pp. 263-283.

AMMON, C. J., JI, C., THIO, H.-K., ROBINSON, D., NI, S., HJORLEIFSDOTTIR, V., KANAMORI, H., LAY, T., DAS, S., HELMBERGER, D., ICHINOSE, G., POLET, J. & WALD, D. 2005. Rupture Process of the 2004 Sumatra-Andaman Earthquake. *Science,* 308(5725)**,** pp. 1133-1139.

ARAYA, N., NAKAMURA, M., YASUDA, A., OKUMURA, S., SATO, T., IGUCHI, M., MIKI, D. & GESHI, N. 2019. Shallow magma pre-charge during repeated Plinian eruptions at Sakurajima volcano. *Scientific Reports,* 9(1)**,** pp. 1979.

ARZILLI, F., LA SPINA, G., BURTON, M. R., POLACCI, M., LE GALL, N., HARTLEY, M. E., DI GENOVA, D., CAI, B., VO, N. T., BAMBER, E. C., NONNI, S., ATWOOD, R., LLEWELLIN, E. W., BROOKER, R. A., MADER, H. M. & LEE, P. D. 2019. Magma fragmentation in highly explosive basaltic eruptions induced by rapid crystallization. *Nature Geoscience,* 12(12)**,** pp. 1023-1028.

ATLAS, Z. D., DIXON, J. E., SEN, G., FINNY, M. & MARTIN-DEL POZZO, A. L. 2006. Melt inclusions from Volcán Popocatépetl and Volcán de Colima, Mexico: Melt evolution due to vapor-saturated crystallization during ascent. *Journal of Volcanology and Geothermal Research 153,* (3)**,** pp. 221-240.

BACHMANN, O. & BERGANTZ, G. 2008. The Magma Reservoirs That Feed Supereruptions. *Elements,* 4(1)**,** pp. 17-21.

BACHMANN, O. & BERGANTZ, G. W. 2004. On the Origin of Crystal-poor Rhyolites: Extracted from Batholithic Crystal Mushes. *Journal of Petrology,* 45(8)**,** pp. 1565-1582.

BACHMANN, O. & BERGANTZ, G. W. 2009. Rhyolites and their Source Mushes across Tectonic Settings. *Journal of Petrology,* 49(12)**,** pp. 2277-2285.

BACHMANN, O., DUNGAN, M. A. & LIPMAN, P. W. 2002. The Fish Canyon Magma Body, San Juan Volcanic Field, Colorado: Rejuvenation and Eruption of an Upper-Crustal Batholith. *Journal of Petrology,* 43(8)**,** pp. 1469-1503.

BACHMANN, O. & HUBER, C. 2016. Silicic magma reservoirs in the Earth's crust. *American Mineralogist,* 101(11)**,** pp. 2377-2404.

BACHMANN, O. & HUBER, C. 2019. The Inner Workings of Crustal Distillation Columns; The Physical Mechanisms and Rates Controlling Phase Separation in Silicic Magma Reservoirs. *Journal of Petrology,* 60(1)**,** pp. 3-18.

BANDOPADHYAY, P., GHOSH, B. & LIMONTA, M. 2014. A reappraisal of the eruptive history and recent (1991-2009) volcanic eruptions of the Barren Island, Andaman Sea. *Episodes,* 37(3)**,** pp. 192-205.

BANDOPADHYAY, P. C., MITRA, S. K., PAL, T. & RAGHAV, S. 2006. The 2005 eruption on Barren Island, Andaman Sea. *Current Science,* 90(5)**,** pp. 620-622.

BANERJEE, P., POLLITZ, F. F. & BÜRGMANN, R. 2005. The Size and Duration of the Sumatra-Andaman Earthquake from Far-Field Static Offsets. *Science,* 308(5729)**,** pp. 1769-1772.

BARCLAY, J., RUTHERFORD, M. J., CARROLL, M. R., MURPHY, M. D., DEVINE, J. D., GARDNER, J. & SPARKS, R. S. J. 1998. Experimental phase equilibria constraints on pre-eruptive storage conditions of the Soufriere Hills magma. *Geophysical Research Letters,* 25(18)**,** pp. 3437-3440.

BARRIENTOS, S. E. 1994. Large thrust earthquakes and volcanic eruptions. *pure and applied geophysics,* 142(1)**,** pp. 225-237.

BARRIENTOS, S. E. & WARD, S. N. 1990. The 1960 Chile earthquake: inversion for slip distribution from surface deformation. *Geophysical Journal International,* 103(3)**,** pp. 589-598.

BARTON, M. & HUIJSMANS, J. P. P. 1986. Post-caldera dacites from the Santorini volcanic complex, Aegean Sea, Greece: an example of the eruption of lavas of near-constant composition over a 2,200 year period. *Contributions to Mineralogy and Petrology,* 94(4)**,** pp. 472-495.
BAUTISTA, B. C., BAUTISTA, M. L. P., STEIN, R. S., BARCELONA, E. S., PUNONGBAYAN, R. S., LAGUERTA, E. P., RASDAS, A. R., AMBUBUYOG, G. & AMIN, E. Q. 1996. Relationship of regional and local structures to Mount Pinatubo activity. *Fire and mud: eruptions and lahars of Mount Pinatubo, Philippines,* pp. 351-370.
BEBBINGTON, M. S. & MARZOCCHI, W. 2011. Stochastic models for earthquake triggering of volcanic eruptions. *Journal of Geophysical Research,* 116(B5)**,** pp. B05204.
BEGUE, F., GRAVLEY, D. M., CHAMBEFORT, I., DEERING, C. D. & KENNEDY, B. M. 2014. Magmatic volatile distribution as recorded by rhyolitic melt inclusions in the Taupo volcanic zone, New Zealand. *Special Publication - Geological Society of London,* 410(1)**,** pp. 71-94.
BERCOVICI, D. & RICARD, Y. 2003. Energetics of a two-phase model of lithospheric damage, shear localization and plate-boundary formation. *Geophysical Journal International,* 152(3)**,** pp. 581-596.
BEST, M. G. 2003. *Igneous and Metamorphic Petrology,* Malden, MA, Blackwell Science Ltd.
BIGGS, J. & ANNEN, C. 2019. The lateral growth and coalesence of magma systems. *Philosophical Transactions of the Royal Society A,* 377(2139)**,** pp. 20180005.
BLUNDY, J. & CASHMAN, K. 2005. Rapid decompression-driven crystallization recorded by melt inclusions from Mount St. Helens volcano. *Geology,* 33(10)**,** pp. 793-796.
BOORE, D. M. 2004. Ground motion in Anchorage, Alaska, from the 2002 Denali fault earthquake: Site response and displacement pulses. *Bulletin of the Seismological Society of America,* 94(6B)**,** pp. S72-S84.
BORISOVA, A. Y., PICHAVANT, M., BENY, J.-M., ROUER, O. & PRONOST, J. 2005. Constraints on dacite magma degassing and regime of the June 15, 1991, climactic eruption of Mount Pinatubo (Philippines): New data on melt and crystal inclusions in quartz. *Journal of Volcanology and Geothermal Research,* 145(1)**,** pp. 35-67.
BOROSCHEK, R. & CONTRERAS, V. Strong ground motion from the 2010 Mw 8.8 Maule Chile earthquake and attenuation relations for Chilean subduction zone interface earthquakes. *International Symposium on Engineering Lessons Learned from the 2011 Great East Japan Earthquake,* 2012 2012, Tokyo, Japan. pp. 1722-1733.
BOROSCHEK, R. L., CONTRERAS, V., KWAK, D. Y. & STEWART, J. P. 2012. Strong Ground Motion Attributes of the 2010 Mw 8.8 Maule, Chile, Earthquake. *Earthquake Spectra,* 28(1)**,** pp. 19-38.
BRIGGS, R. W., SIEH, K., MELTZNER, A. J., NATAWIDJAJA, D., GALETZKA, J., SUWARGADI, B., HSU, Y.-J., SIMONS, M., HANANTO, N., SUPRIHANTO, I., PRAYUDI, D., AVOUAC, J.-P., PRAWIRODIRDJO, L. & BOCK, Y. 2006. Deformation and Slip Along the Sunda Megathrust in the Great 2005 Nias-Simeulue Earthquake. *Science,* 311(5769)**,** pp. 1897-1901.
BRODSKY, E. E., STURTEVANT, B. & KANAMORI, H. 1998. Earthquakes, volcanoes, and rectified diffusion. *Journal of Geophysical Research: Solid Earth,* 103(B10)**,** pp. 23827-23838.
BROMILEY, G. D. & LAW, S. 2020. Eruption of crystal mush and the formation of steep-sided volcanic domes on Venus: Insight from picritic bodies near Marki, Cyprus. *Icarus,* 337, pp. 113467.
BROXTON, D., HEIKEN, G., CHIPERA, S. & BYERS JR, F. 1995. Stratigraphy, petrography, and mineralogy of Bandelier Tuff and Cerro Toledo deposits. *Earth Science Investigations for Environmental Restoration—Los Alamos National Laboratory, Technical Area,* 21, pp. 33-63.
BULLEN, K. E. & BOLT, B. A. 1985a. The earthquake source. *An introduction to the theory of seismology.* 4th ed. Cambridge, England: Cambridge University Press, pp. 398-431.
BULLEN, K. E. & BOLT, B. A. 1985b. Strong-motion seismology. *An introduction to the theory of seismology.* 4th ed. Cambridge, England: Cambridge University Press, pp. 432-469.
BUTLER, R. 2018. High-Frequency (>100 Hz) Earthquakes North of Moloka‘i Detected on the Seafloor at the Aloha Cabled Observatory. *Bulletin of the Seismological Society of America,* 108(5A)**,** pp. 2739-2747.
CADOUX, A., SCAILLET, B., DRUITT, T. H. & DELOULE, E. 2014. Magma Storage Conditions of Large Plinian Eruptions of Santorini Volcano (Greece). *Journal of Petrology,* 55(6)**,** pp. 1129-1171.
CAMPBELL, K. W. & BOZORGNIA, Y. 2003. Updated near-source ground-motion (attenuation) relations for the horizontal and vertical components of peak ground acceleration and acceleration response spectra. *Bulletin of the Seismological Society of America,* 93(1)**,** pp. 314-331.
CARCIONE, J. M., FARINA, B., POLETTO, F., QADROUH, A. N. & CHENG, W. 2020. Seismic attenuation in partially molten rocks. *Physics of the Earth and Planetary Interiors,* pp. 106568.

CARICCHI, L., ANNEN, C., BLUNDY, J., SIMPSON, G. & PINEL, V. 2014. Frequency and magnitude of volcanic eruptions controlled by magma injection and buoyancy. *Nature Geoscience,* 7(2)**,** pp. 126-130.

CASHMAN, K. V. & GIORDANO, G. 2014. Calderas and magma reservoirs. *Journal of Volcanology and Geothermal Research,* 288(C)**,** pp. 28-45.

CASHMAN, K. V., SPARKS, R. S. J. & BLUNDY, J. D. 2017. Vertically extensive and unstable magmatic systems: A unified view of igneous processes. *Science,* 355(6331)**,** pp. eaag3055.

CASSIDY, J. F. 2015. The 2004 Sumatra Earthquake and Tsunami: Lessons Learned in Subduction Zone Science and Emergency Management for the Cascadia Subduction Zone. *Pure and Applied Geophysics,* 172(3)**,** pp. 835-847.

CHARLIER, B., BACHMANN, O., DAVIDSON, J., DUNGAN, M. & MORGAN, D. 2007. The Upper Crustal Evolution of a Large Silicic Magma Body: Evidence from Crystal-scale Rb Sr Isotopic Heterogeneities in the Fish Canyon Magmatic System, Colorado. *Journal of Petrology,* 48, pp. 1876-1894.

CHRISTENSEN, N. I. & MOONEY, W. D. 1995. Seismic velocity structure and composition of the continental crust: A global view. *Journal of Geophysical Research: Solid Earth,* 100(B6)**,** pp. 9761-9788.

CHRISTIANSEN, E. H. 2005. Contrasting processes in silicic magma chambers: evidence from very large volume ignimbrites. *Geological Magazine,* 142(6)**,** pp. 669-681.

CIMARELLI, C., COSTA, A., MUELLER, S. & MADER, H. M. 2011. Rheology of magmas with bimodal crystal size and shape distributions: Insights from analog experiments. *Geochemistry, Geophysics, Geosystems,* 12(7)**,** pp. Q07024.

CLIFT, R., GRACE, J. R. & WEBER, M. E. 2013a. Shapes of Rigid and Fluid Particles. *Bubbles, Drops, and Particles.* Mineola, New York: Dover Publications, Inc., pp. 16-29.

CLIFT, R., GRACE, J. R. & WEBER, M. E. 2013b. Slow Viscous Flow Past Nonspherical Rigid Particles. *Bubbles, Drops, and Particles.* Mineola, New York: Dover Publications, Inc., pp. 69-96.

COLE, J. W., DEERING, C. D., BURT, R. M., SEWELL, S., SHANE, P. A. R. & MATTHEWS, N. E. 2014. Okataina Volcanic Centre, Taupo Volcanic Zone, New Zealand: A review of volcanism and synchronous pluton development in an active, dominantly silicic caldera system. *Earth-Science Reviews,* 128, pp. 1-17.

COOPER, K. 2017. What Does a Magma Reservoir Look Like? The "Crystal's-Eye" View. *Elements,* 13, pp. 23-28.

COSTA, A., GOTTSMANN, J., MELNIK, O. & SPARKS, R. S. J. 2011. A stress-controlled mechanism for the intensity of very large magnitude explosive eruptions. *Earth and Planetary Science Letters,* 310(1-2)**,** pp. 161-166.

CROWELL, B. W., MELGAR, D., BOCK, Y., HAASE, J. S. & GENG, J. 2013. Earthquake magnitude scaling using seismogeodetic data. *Geophysical Research Letters,* 40(23)**,** pp. 6089-6094.

DAINES, M. J. & PEC, M. 2015. Migration of Melt. *In:* SIGURDSSON, H. (ed.) *The Encyclopedia of Volcanoes.* 2nd ed.: Elsevier Science, pp. 49-64.

DALTON, C. A. & EKSTRÖM, G. 2006. Global models of surface wave attenuation. *Journal of Geophysical Research: Solid Earth,* 111(B5)**,** pp. B05317.

DAVIS, M., KOENDERS, M. A. & PETFORD, N. 2007. Vibro-agitation of chambered magma. *Journal of Volcanology and Geothermal Research,* 167(1)**,** pp. 24-36.

DE RICHTER, S. K., HANOTIN, C., MARCHAL, P., LECLERC, S., DEMEURIE, F. & LOUVET, N. 2015. Vibration-induced compaction of granular suspensions. *The European Physical Journal E,* 38(7)**,** pp. 74.

DE RICHTER, S. K., HANOTIN, C., MARCHAL, P., LECLERC, S., DEMEURIE, F. & LOUVET, N. 2018. Compaction of granular suspension: Global and local study.

DE SAINT BLANQUAT, M., HORSMAN, E., HABERT, G., MORGAN, S., VANDERHAEGHE, O., LAW, R. & TIKOFF, B. 2011. Multiscale magmatic cyclicity, duration of pluton construction, and the paradoxical relationship between tectonism and plutonism in continental arcs. *Tectonophysics,* 500(1)**,** pp. 20-33.

DEER, W. A., HOWIE, R. A. & ZUSSMAN, J. 2013. *An Introduction to the Rock Forming Minerals,* London, The Mineralogical Society.

DEGRUYTER, W., BACHMANN, O., BURGISSER, A. & MANGA, M. 2012. The effects of outgassing on the transition between effusive and explosive silicic eruptions. *Earth and Planetary Science Letters,* 349-350, pp. 161-170.

DELGADO, F. 2020. Rhyolitic volcano dynamics in the Southern Andes: Contributions from 17 years of InSAR observations at Cordón Caulle from 2003 to 2020. *Journal of South American Earth Sciences*, pp. 102841.
DELGADO, F., PRITCHARD, M. E., COSTA, F., LARA, L. E. & BASUALTO, D. The dynamics of a tectonically controlled active silicic intrusion at Cordón Caulle volcano (Southern Andes) imaged by InSAR: building to the next eruption? *2015 AGU Fall Meeting*, 2015. AGU, pp. 237-240.
DEVINE, J. D., MURPHY, M. D., RUTHERFORD, M. J., BARCLAY, J., SPARKS, R. S. J., CARROLL, M. R., YOUNG, S. R. & GARDNER, J. E. 1998. Petrologic evidence for pre-eruptive pressure-temperature conditions, and recent reheating, of andesitic magma erupting at the Soufriere Hills Volcano, Montserrat, W.I. *Geophysical Research Letters,* 25(19)**,** pp. 3669-3672.
DOBRY, R., IDRISS, I. M. & NG, E. 1978. Duration characteristics of horizontal components of strong-motion earthquake records. *Bulletin of the Seismological Society of America,* 68(5)**,** pp. 1487-1520.
DOYLE, H. 1995. Seismic waves. *Seismology.* West Sussex, England: John Wiley & Sons Ltd, pp. 12-34.
DRUITT, T. H., MERCIER, M., FLORENTIN, L., DELOULE, E., CLUZEL, N., FLAHERTY, T., MÉDARD, E. & CADOUX, A. 2016. Magma Storage and Extraction Associated with Plinian and Interplinian Activity at Santorini Caldera (Greece). *Journal of Petrology,* 57(3)**,** pp. 461-494.
EDWARDS, B., FAEH, D. & GIARDINI, D. 2011. Attenuation of seismic shear wave energy in Switzerland. *Geophysical Journal International,* 185(2)**,** pp. 967-984.
EGGERT, S. & WALTER, T. R. 2009. Volcanic activity before and after large tectonic earthquakes: observations and statistical significance. *Tectonophysics,* 471(1-2)**,** pp. 14-26.
ELLIS, B. S., BACHMANN, O. & WOLFF, J. A. 2014. Cumulate fragments in silicic ignimbrites: The case of the Snake River Plain. *Geology,* 42(5)**,** pp. 431-434.
ELNASHAI, A., GENCTURK, B., KWON, O.-S., AL-QADI, I., HASHASH, Y., ROESLER, J., KIM, S., JEONG, S.-H., DUKES, J. & VALDIVIA, A. 2010. The Maule (Chile) Earthquake of February 27, 2010: Consequence Assessment and Case Studies. pp. 1-208.
ELNASHAI, A. S., KIM, S. J., YUN, G. J. & SIDARTA, D. 2007. The Yogyakarta Earthquake of May 27, 2006. *MAE Center CD Release 07-02,* pp. 1-57.
FIANTIS, D., NELSON, M., SHAMSHUDDIN, J., GOH, T. B. & VAN RANST, E. 2010. Determination of the geochemical weathering indices and trace elements content of new volcanic ash deposits from Mt. Talang (West Sumatra) Indonesia. *Eurasian Soil Science,* 43(13)**,** pp. 1477-1485.
FRANKEL, A. 2015. Decay of S-wave amplitudes with distance for earthquakes in the Charlevoix, Quebec, area: Effects of radiation pattern and directivity. *Bulletin of the Seismological Society of America,* 105(2A)**,** pp. 850-857.
GELMAN, S., DEERING, C., GUTIERREZ, F. & BACHMANN, O. 2013. Evolution of the Taupo Volcanic Center, New Zealand: petrological and thermal constraints from the Omega dacite. *Contributions to Mineralogy and Petrology,* 166(5)**,** pp. 1355-1374.
GHOSH, A., HUESCA-PÉREZ, E., BRODSKY, E. & ITO, Y. 2015. Very low frequency earthquakes in Cascadia migrate with tremor. *Geophysical Research Letters,* 42(9)**,** pp. 3228-3232.
GIORDANO, D., RUSSELL, J. K. & DINGWELL, D. B. 2008. Viscosity of magmatic liquids: A model. *Earth and Planetary Science Letters,* 271(1)**,** pp. 123-134.
GIRARD, G. & STIX, J. 2009. Buoyant replenishment in silicic magma reservoirs: Experimental approach and implications for magma dynamics, crystal mush remobilization, and eruption. *Journal of Geophysical Research: Solid Earth,* 114(B8)**,** pp. B08203.
GOMBERG, J., BLANPIED, M. & BEELER, N. 1997. Transient triggering of near and distant earthquakes. *Bulletin of the Seismological Society of America,* 87, pp. 294-309.
GRAIZER, V. & KALKAN, E. 2007. Ground Motion Attenuation Model for Peak Horizontal Acceleration from Shallow Crustal Earthquakes. *Earthquake Spectra,* 23(3)**,** pp. 585-613.
GROVE, T. L. & TILL, C. B. 2015. Melting the Earth's Upper Mantle. *In:* SIGURDSSON, H. (ed.) *The Encyclopedia of Volcanoes.* 2nd ed.: Elsevier Science, pp. 35-47.
GUALDA, G. A. R. & GHIORSO, M. S. 2013. The Bishop Tuff giant magma body: an alternative to the Standard Model. *Contributions to Mineralogy and Petrology,* 166(3)**,** pp. 755-775.
GUDMUNDSSON, A. 2011. Deflection of dykes into sills at discontinuities and magma-chamber formation. *Tectonophysics,* 500(1)**,** pp. 50-64.
GUDMUNDSSON, A. 2012. Magma chambers: Formation, local stresses, excess pressures, and compartments. *Journal of Volcanology and Geothermal Research,* 237-238(C)**,** pp. 19-41.
GUDMUNDSSON, A. 2020. Volcanic Earthquakes. *Volcanotectonics: Understanding the Structure, Deformation and Dynamics of Volcanoes.* Cambridge: Cambridge University Press, pp. 179-223.

HANOTIN, C., KIESGEN DE RICHTER, S., MARCHAL, P., MICHOT, L. J. & BARAVIAN, C. 2012. Vibration-induced Liquefaction of Granular Suspensions. *Physical Review Letters,* 108(19)**,** pp. 198301.
HARRIS, A. J. L. & RIPEPE, M. 2007. Regional earthquake as a trigger for enhanced volcanic activity: Evidence from MODIS thermal data. *Geophysical Research Letters,* 34(2)**,** pp. L02304.
HAUKSSON, E., JONES, L. M., HUTTON, K. & EBERHART-PHILLIPS, D. 1993. The 1992 Landers Earthquake Sequence: Seismological observations. *Journal of Geophysical Research: Solid Earth,* 98(B11)**,** pp. 19835-19858.
HICKS, S. P., RIETBROCK, A., RYDER, I. M. A., LEE, C.-S. & MILLER, M. 2014. Anatomy of a megathrust: The 2010 M8.8 Maule, Chile earthquake rupture zone imaged using seismic tomography. *Earth and Planetary Science Letters,* 405, pp. 142-155.
HILDRETH, W. 1979. The Bishop Tuff: evidence for the origin of compositional zonation in silicic magma chambers. *Geological Society of America Special Paper,* 180, pp. 43-75.
HILDRETH, W. & WILSON, C. J. 2007. Compositional zoning of the Bishop Tuff. *Journal of Petrology,* 48(5)**,** pp. 951-999.
HILL, D. P., JOHNSTON, M. J. S., LANGBEIN, J. O. & BILHAM, R. 1995. Response of Long Valley Caldera to the Mw = 7.3 Landers, California, Earthquake. *Journal of Geophysical Research: Solid Earth,* 100(B7)**,** pp. 12985-13005.
HILL, D. P., POLLITZ, F. & NEWHALL, C. 2002. Earthquake–Volcano Interactions. *Physics Today,* 55(11)**,** pp. 41-47.
HOLNESS, M. B. 2018. Melt segregation from silicic crystal mushes: a critical appraisal of possible mechanisms and their microstructural record. *Contributions to Mineralogy and Petrology,* 173(48)**.**
HOLTZMAN, B. K. & KOHLSTEDT, D. L. 2007. Stress-driven Melt Segregation and Strain Partitioning in Partially Molten Rocks: Effects of Stress and Strain. *Journal of Petrology,* 48(12)**,** pp. 2379-2406.
HORWELL, C. J., WILLIAMSON, B. J., LLEWELLIN, E. W., DAMBY, D. E. & LE BLOND, J. S. 2013. The nature and formation of cristobalite at the Soufrière Hills volcano, Montserrat: implications for the petrology and stability of silicic lava domes. *Bulletin of Volcanology,* 75(696)**.**
HUBER, C., BACHMANN, O. & DUFEK, J. 2012. Crystal-poor versus crystal-rich ignimbrites: A competition between stirring and reactivation. *Geology,* 40(2)**,** pp. 115-118.
HUBER, C., BACHMANN, O. & MANGA, M. 2009. Homogenization processes in silicic magma chambers by stirring and mushification (latent heat buffering). *Earth and Planetary Science Letters,* 283(1-4)**,** pp. 38-47.
HUBER, C., BACHMANN, O. & MANGA, M. 2010. Two competing effects of volatiles on heat transfer in crystal-rich magmas: thermal insulation vs defrosting. *Journal of Petrology,* 51(4)**,** pp. 847-867.
HUGHES, S. S. 1982. *Petrochemical evolution of High Cascade volcanic rocks in the Three Sisters region, Oregon.* Dissertation, Oregon State University.
ICHIHARA, M. & BRODSKY, E. E. 2006. A limit on the effect of rectified diffusion in volcanic systems. *Geophysical Research Letters,* 33(2)**,** pp. L02316.
ISHII, M., SHEARER, P. M., HOUSTON, H. & VIDALE, J. E. 2005. Extent, duration and speed of the 2004 Sumatra–Andaman earthquake imaged by the Hi-Net array. *Nature,* 435(7044)**,** pp. 933-936.
ISHII, M., SHEARER, P. M., HOUSTON, H. & VIDALE, J. E. 2007. Teleseismic P wave imaging of the 26 December 2004 Sumatra-Andaman and 28 March 2005 Sumatra earthquake ruptures using the Hi-net array. *Journal of Geophysical Research: Solid Earth,* 112(B11)**,** pp. B11307.
ITO, Y. & OBARA, K. 2006. Very low frequency earthquakes within accretionary prisms are very low stress-drop earthquakes. *Geophysical Research Letters,* 33(9)**,** pp. L09302.
ITTAI, K., VLADIMIR, L. & ODED, N. 2011. Bubble growth in visco-elastic magma: implications to magma fragmentation and bubble nucleation. *Bulletin of Volcanology,* 73(1)**,** pp. 39-54.
JAEGER, H. M., KNIGHT, J. B., LIU, C.-H. & NAGEL, S. R. 1994. What Is Shaking in the Sandbox? *MRS Bulletin,* 19(5)**,** pp. 25-31.
JAEGER, H. M. & NAGEL, S. R. 1992. Physics of the Granular State. *Science,* 255(5051)**,** pp. 1523-1531.
JAUPART, C. & MARESCHAL, J.-C. 2010. Magmatic and Volcanic Systems. *Heat Generation and Transport in the Earth.* Cambridge: Cambridge University Press, pp. 317-356.
JAUPART, C. & TAIT, S. 1995. Dynamics of differentiation in magma reservoirs. *Journal of Geophysical Research: Solid Earth,* 100(B9)**,** pp. 17615-17636.
JAY, J., COSTA, F., PRITCHARD, M., LARA, L., SINGER, B. & HERRIN, J. 2014. Locating magma reservoirs using InSAR and petrology before and during the 2011–2012 Cordón Caulle silicic eruption. *Earth and Planetary Science Letters,* 395, pp. 254-266.

JELLINEK, A. M. & DEPAOLO, D. J. 2003. A model for the origin of large silicic magma chambers: precursors of caldera-forming eruptions. *Bulletin of Volcanology,* 65(5)**,** pp. 363-381.
JOHNSTON, M. 1995. Transient deformation during triggered seismicity from the June 28, 1992, M,=7.3 Landers earthquake at Long Valley Volcanic Caldera, California. *Bulletin of the Seismological Society of America,* 85, pp. 787-795.
KAMESH RAJU, K. A., RAY, D., MUDHOLKAR, A., MURTY, G. P. S., GAHALAUT, V. K., SAMUDRALA, K., PAROPKARI, A. L., RAMACHANDRAN, R. & SURYA PRAKASH, L. 2012. Tectonic and volcanic implications of a cratered seamount off Nicobar Island, Andaman Sea. *Journal of Asian Earth Sciences,* 56, pp. 42-53.
KAWAZOE, Y. & KOKETSU, K. Source Fault and Rupture Process of the 2006 Yogyakarta Earthquake. *AGU Fall Meeting Abstracts*, 2010, San Francisco, CA. pp. S43A-2030.
KENNETT, B. L. N. 2001. Seismic Waves I - Plane Waves. *The Seismic Wavefield: Volume 1: Introduction and Theoretical Development.* Cambridge: Cambridge University Press, pp. 136-151.
KHAZAN, Y. 2010. Melt segregation and matrix compaction: the mush continuity equation, compaction/segregation time, implications. *Geophysical Journal International,* 183(2)**,** pp. 601-610.
KLEIN, C. & PHILPOTTS, A. 2017. How Do Igenous Rocks Form? *Earth Materials.* 2nd ed. Cambridge, United Kingdom: Cambridge University Press, pp. 241-277.
KNIGHT, J. B., FANDRICH, C. G., LAU, C. N., JAEGER, H. M. & NAGEL, S. R. 1995. Density relaxation in a vibrated granular material. pp. 3957-3963.
KONCA, A. O., HJORLEIFSDOTTIR, V., SONG, T.-R. A., AVOUAC, J.-P., HELMBERGER, D. V., JI, C., SIEH, K., BRIGGS, R. & MELTZNER, A. 2007. Rupture Kinematics of the 2005 Mw 8.6 Nias–Simeulue Earthquake from the Joint Inversion of Seismic and Geodetic Data. *Bulletin of the Seismological Society of America,* 97(1A)**,** pp. S307-S322.
LAFEMINA, P. C. 2015. Plate Tectonics and Volcanism. *In:* SIGURDSSON, H. (ed.) *The Encyclopedia of Volcanoes.* 2nd ed.: Elsevier Science, pp. 65-92.
LALURAJ, C., BALACHANDRAN, K., SABU, P. & PANAMPUNNAYIL, S. 2006. Persistent volcanic signature observed around Barren Island, Andaman Sea, India. *Marine Geophysical Researches,* 27(4)**,** pp. 283-288.
LARA, L. E., NARANJO, J. A. & MORENO, H. 2004. Rhyodacitic fissure eruption in Southern Andes (Cordón Caulle; 40.5°S) after the 1960 (Mw:9.5) Chilean earthquake: a structural interpretation. *Journal of Volcanology and Geothermal Research,* 138(1)**,** pp. 127-138.
LAVALLÉE, Y., HESS, K.-U., CORDONNIER, B. & BRUCE DINGWELL, D. 2007. Non-Newtonian rheological law for highly crystalline dome lavas. *Geology,* 35(9)**,** pp. 843-846.
LAY, T., KANAMORI, H., AMMON, C. J., NETTLES, M., WARD, S. N., ASTER, R. C., BECK, S. L., BILEK, S. L., BRUDZINSKI, M. R., BUTLER, R., DESHON, H. R., EKSTRÖM, G., SATAKE, K. & SIPKIN, S. 2005. The Great Sumatra-Andaman Earthquake of 26 December 2004. *Science,* 308(5725)**,** pp. 1127-1133.
LAY, T. & WALLACE, T. C. 1995a. Body waves and ray theory. *Modern Global Seismology.* London: Academic Press Limited, pp. 70-115.
LAY, T. & WALLACE, T. C. 1995b. Determination of Earth Structure. *Modern Global Seismology.* London: Academic Press Limited, pp. 236-309.
LAY, T. & WALLACE, T. C. 1995c. Elasticity and seismic waves. *Modern Global Seismology.* London: Academic Press Limited, pp. 34-69.
LAY, T. & WALLACE, T. C. 1995d. Seismometry. *Modern Global Seismology.* London: Academic Press Limited, pp. 173-199.
LEES, J. M. 2007. Seismic tomography of magmatic systems. *Journal of Volcanology and Geothermal Research,* 167(1)**,** pp. 37-56.
LEES, J. M. & CROSSON, R. S. 1989. Tomographic inversion for three-dimensional velocity structure at Mount St. Helens using earthquake data. *Journal of Geophysical Research: Solid Earth,* 94(B5)**,** pp. 5716-5728.
LEMARCHAND, N. & GRASSO, J.-R. 2007. Interactions between earthquakes and volcano activity. *Geophysical Research Letters,* 34(24)**,** pp. L24303.
LESAFFRE, C., MINEAU, V., PICART, D. & VAN DAMME, H. 2000. Densification under vibration of a saturated granular packing. *Comptes Rendus de l'Académie des Sciences - Series IV - Physics,* 1(5)**,** pp. 647-653.

LESHER, C. E. & SPERA, F. J. 2015. Thermodynamic and Transport Properties of Silicate Melts and Magma. *In:* SIGURDSSON, H. (ed.) *The Encyclopedia of Volcanoes.* 2nd ed.: Elsevier Science, pp. 113-141.
LIAO, Y., SOULE, S. A. & JONES, M. 2018. On the Mechanical Effects of Poroelastic Crystal Mush in Classical Magma Chamber Models. *Journal of Geophysical Research: Solid Earth,* 123(11)**,** pp. 9376-9406.
LINDE, A., T., SACKS, I. S., JOHNSTONE, M., J. S., HILLT, D., P. & BILHAM, R., G. 1994. Increased pressure from rising bubbles as a mechanism for remotely triggered seismicity. *Nature,* 371(6496)**,** pp. 408-410.
LINDE, A. T. & SACKS, I. S. 1998. Triggering of volcanic eruptions. *Nature,* 395(6705)**,** pp. 888-890.
LIPMAN, P., DUNGAN, M. & BACHMANN, O. 1997. Comagmatic granophyric granite in the Fish Canyon Tuff, Colorado: Implications for magma-chamber processes during a large ash-flow eruption. *Geology,* 25(10)**,** pp. 915-918.
LLEWELLIN, E. W., MADER, H. M. & WILSON, S. D. R. 2002. The constitutive equation and flow dynamics of bubbly magmas. *Geophysical Research Letters,* 29(24)**,** pp. 23-1-23-4.
LOCHMANN, K., ANIKEENKO, A., ELSNER, A., MEDVEDEV, N. & STOYAN, D. 2006. Statistical verification of crystallization in hard sphere packings under densification. *The European Physical Journal B-Condensed Matter and Complex Systems,* 53(1)**,** pp. 67-76.
LOCKWOOD, O. G. & KANAMORI, H. 2006. Wavelet analysis of the seismograms of the 2004 Sumatra-Andaman earthquake and its application to tsunami early warning. *Geochemistry, Geophysics, Geosystems,* 7(9)**,** pp. Q09013.
MACCAFERRI, F., BONAFEDE, M. & RIVALTA, E. 2011. A quantitative study of the mechanisms governing dike propagation, dike arrest and sill formation. *Journal of Volcanology and Geothermal Research,* 208(1)**,** pp. 39-50.
MANGA, M. & BRODSKY, E. 2006. Seismic Triggering of Eruptions in the Far Field: Volcanoes and Geysers. *Annual Review of Earth and Planetary Sciences,* 34(1)**,** pp. 263-291.
MARSH, B. 1996. Solidification Fronts and Magmatic Evolution. *Mineralogical Magazine - MINER MAG,* 60, pp. 5-40.
MARSH, B. D. 2015. Magma Chambers. *In:* SIGURDSSON, H. (ed.) *The Encyclopedia of Volcanoes.* 2nd ed.: Elsevier Science, pp. 185-201.
MASUDA, K., IDE, S., OHTA, K. & MATSUZAWA, T. 2020. Bridging the gap between low-frequency and very-low-frequency earthquakes. *Earth, Planets and Space,* 72(47)**.**
MAUGHAN, L. L., CHRISTIANSEN, E. H., BEST, M. G., GROMME, C. S., DEINO, A. L. & TINGEY, D. G. 2002. The Oligocene Lund Tuff, Great Basin, USA: a very large volume monotonous intermediate. *Journal of Volcanology and Geothermal Research,* 113(1-2)**,** pp. 129-157.
MCGEARY, R. K. 1961. Mechanical Packing of Spherical Particles. *Journal of the American Ceramic Society,* 44(10)**,** pp. 513-522.
MCKENZIE, D. 1984. The Generation and Compaction of Partially Molten Rock. *Journal of Petrology,* 25(3)**,** pp. 713-765.
MCNUTT, S. R. & ROMAN, D. C. 2015. Volcanic Seismicity. *In:* SIGURDSSON, H. (ed.) *The Encyclopedia of Volcanoes.* 2nd ed.: Elsevier Science, pp. 1011-1034.
MELSON, W. G. 1983. Monitoring the 1980-1982 Eruptions of Mount St. Helens: Compositions and Abundances of Glass. *Science,* 221(4618)**,** pp. 1387-1391.
MENAND, T. 2011. Physical controls and depth of emplacement of igneous bodies: A review. *Tectonophysics,* 500(1)**,** pp. 11-19.
MENAND, T., DE SAINT-BLANQUAT, M. & ANNEN, C. 2011. Emplacement of magma pulses and growth of magma bodies. *Tectonophysics,* 500(1)**,** pp. 1-2.
MIDORIKAWA, S. 1993. Semi-empirical estimation of peak ground acceleration from large earthquakes. *Tectonophysics,* 218(1-3)**,** pp. 287-295.
MILLER, C. A., WILLIAMS-JONES, G., FOURNIER, D. & WITTER, J. 2017. 3D gravity inversion and thermodynamic modelling reveal properties of shallow silicic magma reservoir beneath Laguna del Maule, Chile. *Earth and Planetary Science Letters,* 459(C)**,** pp. 14-27.
MISHRA, O. P., KAYAL, J. R., CHAKRABORTTY, G. K., SINGH, O. P. & GHOSH, D. 2007. Aftershock Investigation in the Andaman–Nicobar Islands of India and Its Seismotectonic Implications. *Bulletin of the Seismological Society of America,* 97(1A)**,** pp. S71-S85.

MORA-STOCK, C., THORWART, M., WUNDERLICH, T., BREDEMEYER, S., HANSTEEN, T. H. & RABBEL, W. 2014. Comparison of seismic activity for Llaima and Villarrica volcanoes prior to and after the Maule 2010 earthquake. *International Journal of Earth Sciences,* 103(7)**,** pp. 2015-2028.

MORAN, S. C., LEES, J. M. & MALONE, S. D. 1999. P wave crustal velocity structure in the greater Mount Rainier area from local earthquake tomography. *Journal of Geophysical Research: Solid Earth,* 104(B5)**,** pp. 10775-10786.

MORDENSKY, S. P. & WALLACE, P. J. 2018. Magma storage below Cascades shield volcanoes as inferred from melt inclusion data: A comparison of long-lived and short-lived magma plumbing systems. *Journal of Volcanology and Geothermal Research,* 368, pp. 1-12.

MORI, J., EBERHART-PHILLIPS, D. & HARLOW, D. H. 1996. *Three-Dimensional Velocity Structure at Mount Pinatubo: Resolving Magma Bodies and Earthquake Hypocenters* [Online]. Available: https://pubs.usgs.gov/pinatubo/mori2/ [Accessed 21 October 2020].

MUELLER, S., LLEWELLIN, E. W. & MADER, H. M. 2011. The effect of particle shape on suspension viscosity and implications for magmatic flows. *Geophysical Research Letters,* 38(13)**,** pp. L13316.

MURPHY, J. R. & O'BRIEN, L. J. 1977. The correlation of peak ground acceleration amplitude with seismic intensity and other physical parameters. *Bulletin of the Seismological Society of America,* 67(3)**,** pp. 877-915.

NAKAMURA, K. 2006. Textures of plagioclase microlite and vesicles within volcanic products of the 1914-1915 eruption of Sakurajima Volcano, Kyushu, Japan. *Journal of Mineralogical and Petrological Sciences,* 101(4)**,** pp. 178-198.

NOWAK, E. R., KNIGHT, J. B., POVINELLI, M. L., JAEGER, H. M. & NAGEL, S. R. 1997. Reversibility and irreversibility in the packing of vibrated granular material. *Powder Technology,* 94(1)**,** pp. 79-83.

NUNZIATA, C. 2004. Seismic Ground Motion in Napoli for the 1980 Irpinia Earthquake. *In:* PANZA, G. F., PASKALEVA, I. & NUNZIATA, C. (eds.) *Seismic Ground Motion in Large Urban Areas.* Basel: Birkhäuser Basel, pp. 1239-1264.

ONODA, G. Y. & LINIGER, E. G. 1990. Random loose packings of uniform spheres and the dilatancy onset. *Physical Review Letters,* 64, pp. 2727-2730.

PARAT, F., HOLTZ, F. & FEIG, S. 2008. Pre-eruptive Conditions of the Huerto Andesite (Fish Canyon System, San Juan Volcanic Field, Colorado): Influence of Volatiles (C–O–H–S) on Phase Equilibria and Mineral Composition. *Journal of Petrology,* 49(5)**,** pp. 911-935.

PARK, J., SONG, T.-R. A., TROMP, J., OKAL, E., STEIN, S., ROULT, G., CLEVEDE, E., LASKE, G., KANAMORI, H. & DAVIS, P. 2005. Earth's free oscillations excited by the 26 December 2004 Sumatra-Andaman earthquake. *Science,* 308(5725)**,** pp. 1139-1144.

PARVEZ, I. A., GUSEV, A. A., PANZA, G. F. & PETUKHIN, A. G. 2001. Preliminary determination of the interdependence among strong-motion amplitude, earthquake magnitude and hypocentral distance for the Himalayan region. *Geophysical Journal International,* 144(3)**,** pp. 577-596.

PAULATTO, M., ANNEN, C., HENSTOCK, T. J., KIDDLE, E., MINSHULL, T. A., SPARKS, R. S. J. & VOIGHT, B. 2012. Magma chamber properties from integrated seismic tomography and thermal modeling at Montserrat. *Geochemistry, Geophysics, Geosystems,* 13(1)**,** pp. Q01014.

PHILPOTTS, A. R. & AGUE, J. J. 2009. Phase equilibria in igneous systems. *Principles of Igneous and Metamorphic Petrology.* 2nd ed. Cambridge, United Kingdom: Cambridge University Press, pp. 194-242.

PICA CIAMARRA, M., NICODEMI, M. & CONIGLIO, A. 2007. Granular packs under vertical tapping: Structure evolution, grain motion, and dynamical heterogeneities. *Physical review. E, Statistical, nonlinear, and soft matter physics,* 75, pp. 021303.

PLAFKER, G. & SAVAGE, J. C. 1970. Mechanism of the Chilean Earthquakes of May 21 and 22, 1960. *GSA Bulletin,* 81(4)**,** pp. 1001-1030.

PRITCHARD, M. E., JAY, J. A., ARON, F., HENDERSON, S. T. & LARA, L. E. 2013. Subsidence at southern Andes volcanoes induced by the 2010 Maule, Chile earthquake. *Nature Geoscience,* 6(8)**,** pp. 632-636.

PYLE, D. M. & PYLE, D. L. 1995. Bubble migration and the initiation of volcanic eruptions. *Journal of Volcanology and Geothermal Research,* 67(4)**,** pp. 227-232.

RICHTER, G., WASSERMANN, J., ZIMMER, M. & OHRNBERGER, M. 2004. Correlation of seismic activity and fumarole temperature at the Mt. Merapi volcano (Indonesia) in 2000. *Journal of Volcanology and Geothermal Research,* 135(4)**,** pp. 331-342.

RIPEPE, M. & GORDEEV, E. 1999. Gas bubble dynamics model for shallow volcanic tremor at Stromboli. *Journal of Geophysical Research: Solid Earth,* 104(B5)**,** pp. 10639-10654.
ROBERGE, J., WALLACE, P. & KENT, A. 2013. Magmatic processes in the Bishop Tuff rhyolitic magma based on trace elements in melt inclusions and pumice matrix glass. *Contributions to Mineralogy and Petrology,* 165(2)**,** pp. 237-257.
RUTHERFORD, M. J. & DEVINE, J. D. 1999. *Preeruption Pressure-Temperature Condition and Volatiles in the 1991 Dacitic Magma of Mount Pinatubo* [Online]. USGS Publications. Available: https://pubs.usgs.gov/pinatubo/ruth/ [Accessed 11 November 2019].
RUTHERFORD, M. J., SIGURDSSON, H., CAREY, S. & DAVIS, A. 1985. The May 18, 1980, eruption of Mount St. Helens: 1. Melt composition and experimental phase equilibria. *Journal of Geophysical Research: Solid Earth,* 90(B4)**,** pp. 2929-2947.
SAHAGIAN, D. L. & PROUSSEVITCH, A. A. 1992. Bubbles in volcanic systems. *Nature,* 359(6395)**,** pp. 485.
SANDERS, C. O., PONKO, S. C., NIXON, L. D. & SCHWARTZ, E. A. 1995. Seismological evidence for magmatic and hydrothermal structure in Long Valley Caldera from local earthquake attenuation and velocity tomography. *Journal of Geophysical Research: Solid Earth,* 100(B5)**,** pp. 8311-8326.
SARAGONI, G. R., LEW, M., NAEIM, F., CARPENTER, L. D., YOUSSEF, N. F., ROJAS, F. & ADAROS, M. S. 2010. Accelerographic measurements of the 27 February 2010 offshore Maule, Chile earthquake. *The Structural Design of Tall and Special Buildings,* 19(8)**,** pp. 866-875.
SCOTT, D. R. & STEVENSON, D. J. 1986. Magma ascent by porous flow. *Journal of Geophysical Research: Solid Earth,* 91(B9)**,** pp. 9283-9296.
SCOTT, G. D. 1960. Packing of Spheres: Packing of Equal Spheres. *Nature,* 188(4754)**,** pp. 908-909.
SHANE, P., NAIRN, I. A. & SMITH, V. C. 2005. Magma mingling in the ~50 ka Rotoiti eruption from Okataina Volcanic Centre: implications for geochemical diversity and chronology of large volume rhyolites. *Journal of Volcanology and Geothermal Research,* 139(3)**,** pp. 295-313.
SHEARER, P. M. 2009. Ray theory: Amplitude and phase. *Introduction to Seismology.* 2nd ed. Cambridge, United Kingdom: Cambridge University Press Textbooks, pp. 139-180.
SHETH, H. 2014. What drives centuries-long polygenetic scoria cone activity at Barren Island volcano? *Journal of Volcanology and Geothermal Research,* 289, pp. 64-80.
SHIBANO, Y., NAMIKI, A. & SUMITA, I. 2012. Experiments on upward migration of a liquid-rich layer in a granular medium: Implications for a crystalline magma chamber. *Geochemistry, Geophysics, Geosystems,* 13(3)**,** pp. Q03007.
SIEH, K., JONES, L., HAUKSSON, E., HUDNUT, K., EBERHART-PHILLIPS, D., HEATON, T., HOUGH, S., HUTTON, K., KANAMORI, H., LILJE, A., LINDVALL, S., MCGILL, S. F., MORI, J., RUBIN, C., SPOTILA, J. A., STOCK, J., THIO, H. K., TREIMAN, J., WERNICKE, B. & ZACHARIASEN, J. 1993. Near-Field Investigations of the Landers Earthquake Sequence, April to July 1992. *Science,* 260(5105)**,** pp. 171-176.
SIGURDSSON, H. 2015. Origin and Transport of Magma. *In:* SIGURDSSON, H. (ed.) *The Encyclopedia of Volcanoes.* 2nd ed.: Elsevier Science, pp. 33-34.
SINGER, B. S., LE MÉVEL, H., LICCIARDI, J. M., CÓRDOVA, L., TIKOFF, B., GARIBALDI, N., ANDERSEN, N. L., DIEFENBACH, A. K. & FEIGL, K. L. 2018. Geomorphic expression of rapid Holocene silicic magma reservoir growth beneath Laguna del Maule, Chile. *Science Advances,* 4(6)**,** pp. eaat1513.
SLIWINSKI, J. T., BACHMANN, O., ELLIS, B. S., DÁVILA-HARRIS, P., NELSON, B. K. & DUFEK, J. 2015. Eruption of Shallow Crystal Cumulates during Explosive Phonolitic Eruptions on Tenerife, Canary Islands. *Journal of Petrology,* 56(11)**,** pp. 2173-2194.
SMITH, V. C., SHANE, P. & NAIRN, I. A. 2005. Trends in rhyolite geochemistry, mineralogy, and magma storage during the last 50 kyr at Okataina and Taupo volcanic centres, Taupo Volcanic Zone, New Zealand. *Journal of Volcanology and Geothermal Research,* 148(3)**,** pp. 372-406.
SOMMER, M. A. 1977. Volatiles H2O, CO2, and CO in silicate melt inclusions in quartz phenocrysts from the rhyolitic Bandelier air-fall and ash-flow tuff, New Mexico. *The Journal of Geology,* 85(4)**,** pp. 423-432.
SØRENSEN, M., ATAKAN, K. & PULIDO, N. 2007. Simulated strong ground motions for the great M 9.3 Sumatra–Andaman earthquake of 26 December 2004. *Bulletin of the Seismological Society of America,* 97(1A)**,** pp. S139-S151.
SORIA-HOYO, C., VALVERDE, J. M. & CASTELLANOS, A. 2008. Effect of vibration on flow properties of fine glass beads. *AIChE Journal,* 54(4)**,** pp. 886-896.

SPARKS, R. S. J., ANNEN, C., BLUNDY, J. D., CASHMAN, K. V., RUST, A. C. & JACKSON, M. D. 2019. Formation and dynamics of magma reservoirs. *Philosophical Transactions of the Royal Society A: Mathematical, Physical and Engineering Sciences,* 377(2139)**,** pp. 20180019.
STRAUB, S. M. & MARTIN-DEL POZZO, A. L. 2001. The significance of phenocryst diversity in tephra from recent eruptions at Popocatepetl volcano (central Mexico). *Contributions to Mineralogy and Petrology,* 140(4)**,** pp. 487-510.
STRECK, M. J. 2014. Evaluation of crystal mush extraction models to explain crystal-poor rhyolites. *Journal of Volcanology and Geothermal Research,* 284, pp. 79.
TRIFUNAC, M. D. & BRADY, A. G. 1975. A study on the duration of strong earthquake ground motion. *Bulletin of the Seismological Society of America,* 65(3)**,** pp. 581-626.
TRYGGVASON, A., RÖGNVALDSSON, S. T. & FLÓVENZ, Ó. G. 2002. Three-dimensional imaging of the P- and S-wave velocity structure and earthquake locations beneath Southwest Iceland. *Geophysical Journal International,* 151(3)**,** pp. 848-866.
TSUJI, T., YAMAMOTO, K., MATSUOKA, T., YAMADA, Y., ONISHI, K., BAHAR, A., MEILANO, I. & ABIDIN, H. Z. 2009. Earthquake fault of the 26 May 2006 Yogyakarta earthquake observed by SAR interferometry. *Earth, Planets and Space,* 61(7)**,** pp. e29-e32.
UDÍAS, A. 2000a. Models of fracture. *In:* UDÍAS, A. (ed.) *Principles of Seismology.* Cambridge: Cambridge University Press, pp. 337-358.
UDÍAS, A. 2000b. Seismographs and seismograms. *In:* UDÍAS, A. (ed.) *Principles of Seismology.* Cambridge: Cambridge University Press, pp. 402-422.
USGS. 2020a. *M 6.3 - Java, Indonesia* [Online]. Available: https://earthquake.usgs.gov/earthquakes/eventpage/usp000ej1c/shakemap/pga [Accessed 3 October 2020].
USGS. 2020b. *M 7.3 - Landers, California Earthquake* [Online]. Available: https://earthquake.usgs.gov/earthquakes/eventpage/ci3031111/shakemap/pga [Accessed 29 October 2020].
USGS. 2020c. *M 7.7 - Luzon, Philippines* [Online]. Available: https://earthquake.usgs.gov/earthquakes/eventpage/usp0004bxs/shakemap/pga?source=atlas [Accessed 7 October 2020].
USGS. 2020d. *M 8.6 - northern Sumatra, Indonesia* [Online]. Available: https://earthquake.usgs.gov/earthquakes/eventpage/official20050328160936530_30/shakemap/pga?source=atlas [Accessed 30 October 2020].
USGS. 2020e. *M 8.8 - offshore Bio-Bio (Maule), Chile* [Online]. Available: https://earthquake.usgs.gov/earthquakes/eventpage/official20100227063411530_30/shakemap/pga [Accessed 4 October 2020].
USGS. 2020f. *M 9.1 - 2004 Sumatra - Andaman Islands Earthquake* [Online]. Available: https://earthquake.usgs.gov/earthquakes/eventpage/official20041226005853450_30/shakemap/pga [Accessed 4 October 2020].
USGS. 2020g. *M 9.5 - 1960 Great Chilean Earthquake (Valdivia Earthquake)* [Online]. Available: https://earthquake.usgs.gov/earthquakes/eventpage/official19600522191120_30/shakemap/pga [Accessed 3 October 2020].
UTHE, R. E. 2004. Shedding LIGHT on the Inverse-Square Law: Students demonstrate the quantitative relationship between light intensity and distance. *The Science Teacher,* 71(8)**,** pp. 44-47.
VACCARI, F., SUHADOLC, P. & PANZA, G. F. 1990. Irpinia, Italy, 1980 earthquake: Waveform modelling of strong motion data. *Geophysical Journal International,* 101(3)**,** pp. 631-647.
VELASCO, A. A., AMMON, C. J. & LAY, T. 1994. Empirical green function deconvolution of broadband surface waves: Rupture directivity of the 1992 Landers, California (Mw = 7.3), earthquake. *Bulletin of the Seismological Society of America,* 84(3)**,** pp. 735-750.
VELASCO, A. A., AMMON, C. J., LAY, T. & HAGERTY, M. 1996. Rupture process of the 1990 Luzon, Philippines (Mw= 7.7), earthquake. *Journal of Geophysical Research: Solid Earth,* 101(B10)**,** pp. 22419-22434.
VIGNY, C., SOCQUET, A., PEYRAT, S., RUEGG, J. C., MÉTOIS, M., MADARIAGA, R., MORVAN, S., LANCIERI, M., LACASSIN, R., CAMPOS, J., CARRIZO, D., BEJAR-PIZARRO, M., BARRIENTOS, S., ARMIJO, R., ARANDA, C., VALDERAS-BERMEJO, M. C., ORTEGA, I., BONDOUX, F., BAIZE, S., LYON-CAEN, H., PAVEZ, A., VILOTTE, J. P., BEVIS, M., BROOKS, B., SMALLEY, R., PARRA, H., BAEZ, J. C., BLANCO, M., CIMBARO, S. &

KENDRICK, E. 2011. The 2010 Mw 8.8 Maule Megathrust Earthquake of Central Chile, Monitored by GPS. *Science,* 332(6036)**,** pp. 1417-1421.
VOIGHT, B., CONSTANTINE, E. K., SISWOWIDJOYO, S. & TORLEY, R. 2000. Historical eruptions of Merapi Volcano, Central Java, Indonesia, 1768–1998. *Journal of Volcanology and Geothermal Research,* 100(1)**,** pp. 69-138.
VOUDOUKIS, N. 2017. Inverse square law for light and radiation: A unifying educational approach. *European Journal of Engineering Research and Science,* 2(11)**,** pp. 23-27.
WALD, D. J. & HEATON, T. H. 1994. Spatial and temporal distribution of slip for the 1992 Landers, California, earthquake. *Bulletin of the Seismological Society of America,* 84(3)**,** pp. 668-691.
WALTER, T. R. & AMELUNG, F. 2007. Volcanic eruptions following M ≥ 9 megathrust earthquakes: Implications for the Sumatra-Andaman volcanoes. *Geology,* 35(6)**,** pp. 539-542.
WALTER, T. R., WANG, R., ACOCELLA, V., NERI, M., GROSSER, H. & ZSCHAU, J. 2009. Simultaneous magma and gas eruptions at three volcanoes in southern Italy: An earthquake trigger? *Geology,* 37(3)**,** pp. 251-254.
WALTER, T. R., WANG, R., ZIMMER, M., GROSSER, H., LÜHR, B. & RATDOMOPURBO, A. 2007. Volcanic activity influenced by tectonic earthquakes: Static and dynamic stress triggering at Mt. Merapi. *Geophysical Research Letters,* 34(5)**,** pp. L05304.
WATT, S. F. L., PYLE, D. M. & MATHER, T. A. 2009. The influence of great earthquakes on volcanic eruption rate along the Chilean subduction zone. *Earth and Planetary Science Letters,* 277(3)**,** pp. 399-407.
WEI, S., CHEN, M., WANG, X., GRAVES, R., LINDSEY, E., WANG, T., KARAKAŞ, Ç. & HELMBERGER, D. 2018. The 2015 Gorkha (Nepal) earthquake sequence: I. Source modeling and deterministic 3D ground shaking. *Tectonophysics,* 722, pp. 447-461.
WESPESTAD, C. E., THURBER, C. H., ANDERSEN, N. L., SINGER, B. S., CARDONA, C., ZENG, X., BENNINGTON, N. L., KERANEN, K., PETERSON, D. E., CORDELL, D., UNSWORTH, M., MILLER, C. & WILLIAMS-JONES, G. 2019. Magma Reservoir Below Laguna del Maule Volcanic Field, Chile, Imaged With Surface-Wave Tomography. *Journal of Geophysical Research: Solid Earth,* 124(3)**,** pp. 2858-2872.
WITTER, J. B., KRESS, V. C. & NEWHALL, C. G. 2005. Volcán Popocatépetl, Mexico. Petrology, Magma Mixing, and Immediate Sources of Volatiles for the 1994–Present Eruption. *Journal of Petrology,* 46(11)**,** pp. 2337-2366.
WOLFF, J. & RAMOS, F. 2014. Processes in caldera-forming high-silica rhyolite magma: Rb–Sr and Pb isotope systematics of the Otowi Member of the Bandelier Tuff, Valles Caldera, New Mexico, USA. *Journal of Petrology,* 55(2)**,** pp. 345-375.
WU, Y.-M. & KANAMORI, H. 2005. Experiment on an onsite early warning method for the Taiwan early warning system. *Bulletin of the Seismological Society of America,* 95(1)**,** pp. 347-353.
WU, Y.-M., KANAMORI, H., ALLEN, R. M. & HAUKSSON, E. 2007. Determination of earthquake early warning parameters, τc and Pd, for southern California. *Geophysical Journal International,* 170(2)**,** pp. 711-717.
YAMADA, M., MORI, J. & HEATON, T. 2009. The slapdown phase in high-acceleration records of large earthquakes. *Seismological Research Letters,* 80(4)**,** pp. 559-564.
YANAGI, T., ICHIMARU, Y. & HIRAHARA, S. 1991. Petrochemical evidence for coupled magma chambers beneath the Sakurajima volcano, Kyushu, Japan. *GEOCHEMICAL JOURNAL,* 25(1)**,** pp. 17-30.
YOSHIDA, Y. & ABE, K. 1992. Source mechanism of the Luzon, Philippines earthquake of July 16, 1990. *Geophysical Research Letters,* 19(6)**,** pp. 545-548.